

# Cryptophanes and Their Complexes—Present and Future

Thierry Brotin\* and Jean-Pierre Dutasta\*

Laboratoire de Chimie, CNRS, École Normale Supérieure de Lyon, 46 Allée d'Italie, F-69364 Lyon 07, France

Received June 5, 2007

## Contents

1. Introduction	88	9.4. Laser-Polarized Xenon and Cryptophanes	116
2. Syntheses of Cryptophanes	90	9.4.1. Laser-Polarized Xenon in Cryptophane Complexes	117
2.1. The “Direct (Two-Step) Method”	90	9.4.2. Probing the Molecular Cavity of Cryptophane	117
2.2. The “Template Method”	92	9.4.3. “Functionalized” Xenon	118
2.3. Coupling of CTVs	95	10. Syntheses and Chiroptical Properties of Optically Pure Cryptophanes	120
3. Syntheses of New Cryptophanes Using the Template Method	95	10.1. Optical Resolution of CTVs and Cryptophanes	120
3.1. Deuterium Labeled Cryptophanes	95	10.1.1. Optical Resolution Using Chiral HPLC	120
3.2. Methylthio Containing Cryptophanes	96	10.1.2. Resolution of CTVs	121
3.3. Amphipathic Cryptophanes	96	10.2. Syntheses of Optically Pure Cryptophanes	122
3.4. Syntheses of $C_2$ -Symmetrical Cryptophanes	97	10.2.1. From Enantiopure CTVs	122
4. Transformation and Functionalization of Cryptophanes	97	10.2.2. From Cryptophanol	123
4.1. Water-Soluble Cryptophanes: Hexacarboxylic Acid Cryptophanes	98	10.3. Electronic Circular Dichroism (ECD) Spectra of Resolved Cryptophanes	124
4.2. Monofunctionalized Cryptophanes: Cryptophanol	98	10.3.1. ECD of CTVs	124
4.3. Cryptophanes as Biosensors	99	10.3.2. ECD of $D_3$ -Symmetrical Cryptophanes	125
4.4. Bis-cryptophanes	100	10.3.3. ECD of $C_1$ -Symmetrical Cryptophanes	126
5. Structural Aspects and Characterization of Cryptophanes	100	10.4. VCD of Cryptophane Hosts	126
5.1. Some Peculiarities in the Characterization of Cryptophane Hosts	101	11. Conclusion—The Future of Cryptophanes	127
5.2. Inverted and Imploded Cryptophanes	102	12. Dedication	128
5.3. Molecular Structures of Cryptophane-A 1 and Related Ones	103	13. Acknowledgments	128
5.4. Some Aspects of Cryptophanes in the Crystalline State	104	14. Note Added in Proof	128
6. Binding Properties of Cryptophanes	105	15. References	128
6.1. Complexation of Small Neutral Molecules	106		
6.2. Complexation of Ammonium Guests	107		
6.3. Complexation of Metal Cations	109		
6.4. Complexation of Anion Guests	109		
7. Dynamics of the Guest in the Cryptophane Cavity	109		
7.1. Investigations by NMR Spectroscopy	109		
7.2. Computational Investigations	111		
7.3. Host–Guest Complexes in the Solid: Raman Microspectrometry	111		
7.4. Studies in Mesophases	112		
8. Chiral Discrimination	113		
8.1. CHFCIBr	113		
8.2. CHFCII	114		
9. Xenon in the Cryptophane Cavity	114		
9.1. Xe@cryptophane Complexes	114		
9.2. $^{129}\text{Xe}$ NMR Spectroscopy of Xe@Cryptophane Complexes	115		
9.3. Dynamics of Xenon Encapsulation	116		

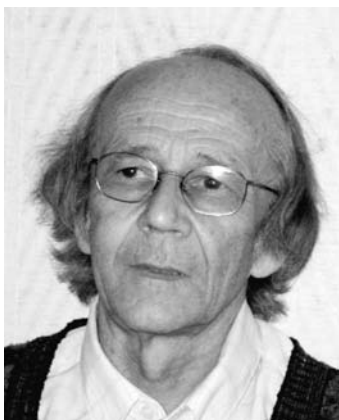
## 1. Introduction

The encapsulation of charged or neutral species in the inner cavity of organic hosts is a fascinating field of research and represents an important challenge for many research laboratories all over the world. The outstanding success of this topic arises mainly from the imagination of the chemists in designing and synthesizing organic hosts with recognition functionality. Since the origin of the concept of host–guest chemistry, a wide variety of synthetic organic compounds have been prepared as molecular receptors, which can form self-organized systems with various degrees of complexity, and have possible applications, including molecular recognition,<sup>1</sup> drug delivery,<sup>2</sup> separation and storage,<sup>3</sup> biosensing, and catalysis (chemical reaction inside the confined space of a molecular nanoreactor).<sup>4–6</sup> Although, in terms of publications, this field is largely dominated by the supramolecular chemistry of calixarene and cavitand hosts, the synthesis by A. Collet in the early 1980s of original molecules called *cryptophanes*<sup>7</sup> introduced a new source of inspiration for designing molecular cavities.<sup>8</sup> The pioneering work of Collet’s group at the Collège de France and after 1988 at the École Normale Supérieure in Lyon concerned the synthesis of cryptophanes and the study of their binding properties with charged or neutral small molecules (Chart

\* E-mail: thierry.brotin@ens-lyon.fr; jean-pierre.dutasta@ens-lyon.fr.



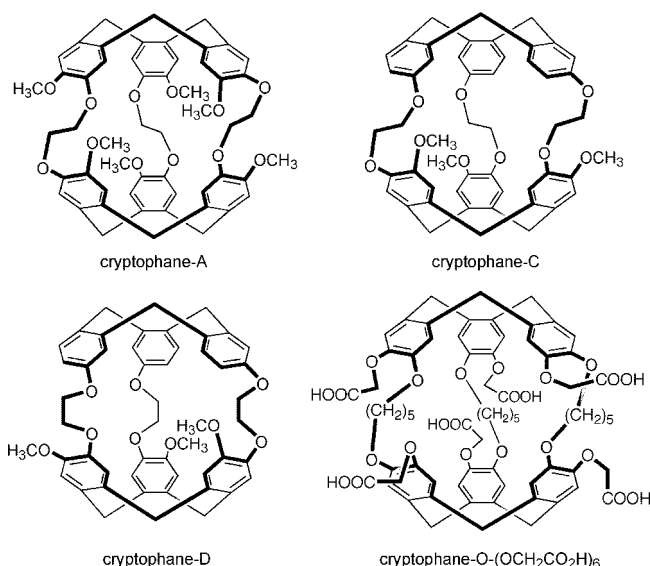
Thierry Brotin graduated in chemistry at the University of Bordeaux, France, where he received his Doctorat degree in chemistry in 1990 for work on low molecular weight organogelators under the supervision of Prof. H. Bouas-Laurent and Dr. J.-P. Desvergne. He joined the Centre National de la Recherche Scientifique (CNRS) in 1992 at the Laboratory of Chemistry of the École Normale Supérieure de Lyon with Prof. A. Collet. He did postdoctoral work in 1997 with Prof. J. Michl at the University of Colorado at Boulder, working on organometallic chemistry. He returned to the ENS in Lyon, where he obtained a higher doctorate (HDR) in 2006. Since 1998 his main topic of interest has focused on the chemistry and optical resolution of cryptophane derivatives and their binding properties, in particular with xenon.



Jean-Pierre Dutasta gained his Doctorat d'Etat es-Sciences Physiques from the University of Grenoble, France, in 1980 for studies on the synthesis, conformational analysis, and NMR investigations of organophosphorus compounds with Prof. J.-B. Robert. He joined the Centre National de la Recherche Scientifique (CNRS) in 1979 and did postdoctoral work in 1980–1982 at the University of California at Los Angeles under the supervision of Prof. D. J. Cram. His interest in supramolecular chemistry research began when he was a postdoctoral fellow at UCLA. He was then appointed to the University Joseph Fourier in Grenoble, where he started research on macrocyclic phosphorus compounds and phosphonate cavitands. He joined the Laboratory of Chemistry of the École Normale Supérieure de Lyon in 1988 with Prof. André Collet, where he was appointed Research Director. He heads a research group in the Laboratory of Chemistry of the ENS-Lyon, and his research activities include stereochemistry, NMR, and supramolecular chemistry, including cryptophanes, hemicyptophanes, and phosphonate cavitands chemistry.

1). Among the most important results published at that time were the complexation of methane by cryptophane-A,<sup>9</sup> the recognition of acetylcholine by cryptophane-O,<sup>10</sup> the chiral discrimination of CHFCIBr by enantioenriched cryptophane-C,<sup>11</sup> and the formation of the highly stable Xe@cryptophane-A complex.<sup>12</sup> Reviews on this subject appeared in 1987,<sup>13</sup> 1993,<sup>14,15</sup> and 1996.<sup>16</sup> The continuing interest in cryptophane hosts has been emphasized again recently by Holman in 2004.<sup>17</sup>

Chart 1



In this review article we wish to recall the important steps that allowed the progress in the chemistry of cryptophanes and to focus on recent developments originating from new synthetic strategies which open the route to possible applications in the fields of molecular recognition and sensor devices. We thus exclude an exhaustive description of the whole family of cryptophanes of the first generation that have been widely described in the former review articles mentioned above. So far, cryptophane molecules have been used mainly to investigate the binding properties of a large variety of guests and to model guest binding in more complex biological macromolecules. More recently, there is increasing interest in these molecules, particularly to physical chemists and spectroscopists. A main interest concerns the physical behavior of the guest molecule in the confined space of the molecular cavity of the cryptophanes compared to that of the guest in solvent. Cryptophanes are indeed considered among the first molecular hosts able to isolate a substrate from the neighboring environment, thus defining certain properties related to the inner phase.<sup>18</sup> This property is also shared by other molecular receptors such as the carcerand hosts first developed by Cram,<sup>1,19</sup> hydrogen-bond molecular capsules developed more recently by Rebek,<sup>20</sup> and self-assembled coordination clusters.<sup>21,22</sup>

Since the first synthesis of cryptophane-A in 1981, considerable progress has been made in designing cryptophanes that exhibit selective encapsulation properties toward organic and inorganic guests. In this review, we devote particular attention to studies of their binding properties that use various spectroscopic techniques. Among these techniques, NMR occupies an important role. Recently, Raman microspectrometry has proved to be particularly well suited for studies in the solid state. Additionally, developments in the preparation of optically pure cryptophanes allowed the investigation of their chiroptical properties by means of electronic circular dichroism (ECD) and vibrational circular dichroism (VCD). These different aspects will be reported and discussed, introducing recent results obtained by using these newly developing techniques associated with *ab initio* calculations at the DFT level.

Cryptophanes can bind reversibly to a variety of guests; we will examine a series of examples including halomethanes and ammonium salts, and particular attention will be devoted

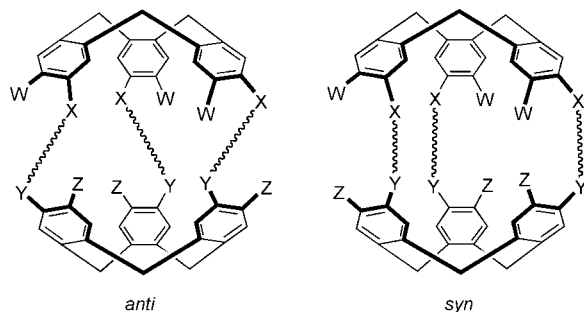


**Figure 1.** Schematic view of *anti* and *syn* cryptophane isomers.

to the encapsulation of xenon. This noble gas *guest* occupies a special place due to its important role in biomedical applications and magnetic resonance imaging (MRI).<sup>23–25</sup> In fact, cryptophanes are by far the best molecular hosts for xenon, making this host–guest assembly one of the most valuable for future developments in biosensing. This is easily seen by the recent growth in interest for this system shown by several research groups. As we shall see later, this holds particularly true for <sup>129</sup>Xe NMR studies of xenon@cryptophane complexes using laser-polarized xenon.

The originality of the cryptophanes is characterized by their spherical structure defining an internal lipophilic molecular cavity. However, these hollow molecules have a well-defined structure only for the smallest representatives, i.e. the hosts with short bridging chains, which also define the size of the cavity. It seems useful to point out here briefly the different possible forms of the cryptophane molecules. A widely known description of a cryptophane molecule is that of a hollow sphere enclosed by two cyclotriphenylene caps and the three linkers: the *syn* and *anti* structures are defined in Figure 1 (not considering any dissymmetry of the linkers, which can be different). Furthermore, the chirality of the cyclotriphenylene units makes the *anti* cryptophane chiral ( $D_3$  or  $C_3$  symmetry). If the cyclotriphenylene units or the linkers are different ( $X \neq Y$  and/or  $W \neq Z$ ), then all of these *anti* and *syn* cryptophanes are chiral molecules ( $C_1$ ,  $C_2$ , or  $C_3$  symmetry).

However, it is known that cyclotriphenylene moieties are flexible and can invert or adopt a saddle–twist conformation even at temperatures close to ambient.<sup>26,27</sup> As a consequence, for the cryptophane structure, it is necessary to consider the existence of the *out–out*, *in–out*, *in–in*, and *out–saddle* conformers, as defined in Figure 2. The existence of these conformational isomers not only can be due to greater flexibility of the molecules but also is dependent on the environment and particularly on the presence or absence of a guest species inside the cavity.

The IUPAC nomenclature of cryptophanes is rather complicated, and after 1985 Collet used a terminology based on the chronology of their discovery, which is still used for the most popularly studied molecules.<sup>28</sup> For example, cryptophane-A (*anti*) was the first characterized (its *syn* isomer cryptophane-B has not been detected so far) and was followed by the discovery of the *anti/syn* pair of the cryptophanes-C and D (Chart 1). Nowadays, the multiplicity and the variability of the cryptophane molecules make this nomenclature inadequate and other more well-adapted terminologies exist. In this review we will preserve the nomenclature of Collet for the best-known species. In addition, a number, which excludes any ambiguity, identifies each compound in this article. Formally, the general nomenclature for the  $C_3$  symmetrically substituted cyclotriphenylene

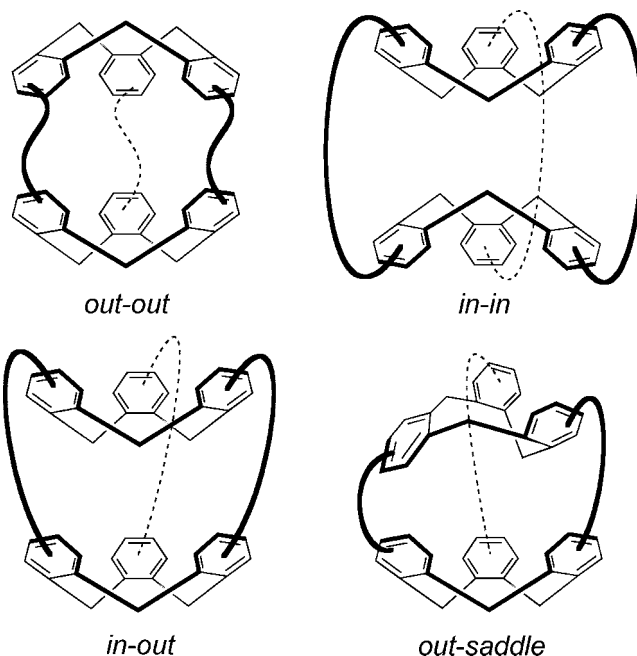
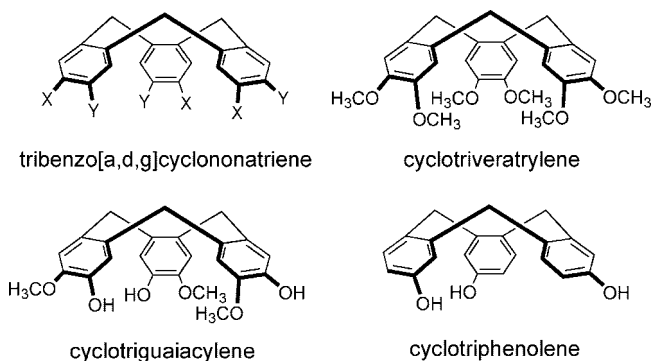


**Figure 2.** Conformers of cryptophanes.

**Chart 2**



derivatives that constitute the backbone of the cryptophane molecules is tribenzo[*a,d,g*]cyclononatriene. Some are derivatives of *cyclotrimeratrylene* (CTV), *cyclotriguaiacylene*, or *cyclotriphenolene*, and so forth (Chart 2). To avoid the use of complex nomenclature and also in agreement with current practice, during this review, we will use the abbreviation “CTV” for moieties that are constructed on the cyclotrimeratrylene framework (formally a cyclic trimer of veratrole). For the sake of clarity, when unnecessary for the understanding, chiral compounds in racemates will be described and represented in schemes and figures, under one configuration.

## 2. Syntheses of Cryptophanes

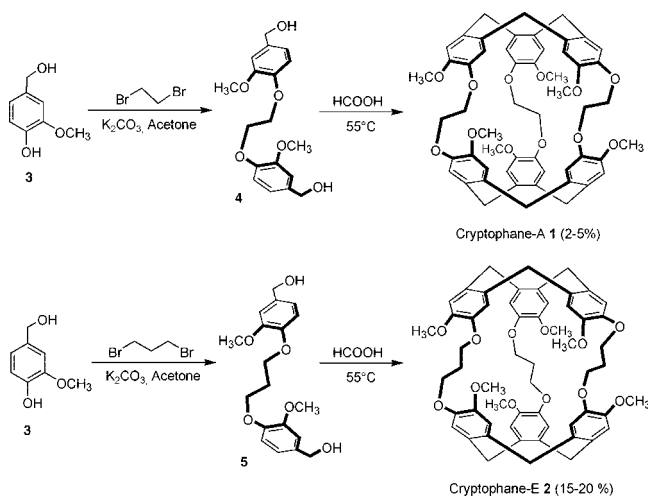
The lipophilic cavity of the ball-shaped cryptophane molecules is constructed from two cyclotrimeratrylene (CTV) moieties connected by three linkers of variable length and constitution. So far, two main approaches have been reported for the preparation of cryptophane hosts: the *direct method* (or two-step method) and the *template method*.

### 2.1. The “Direct (Two-Step) Method”

The direct method presented in Scheme 1 for the synthesis of *anti*-cryptophane-A (**1**) and *anti*-cryptophane-E (**2**) is simple and fast but has been restricted so far to the formation



## Scheme 1

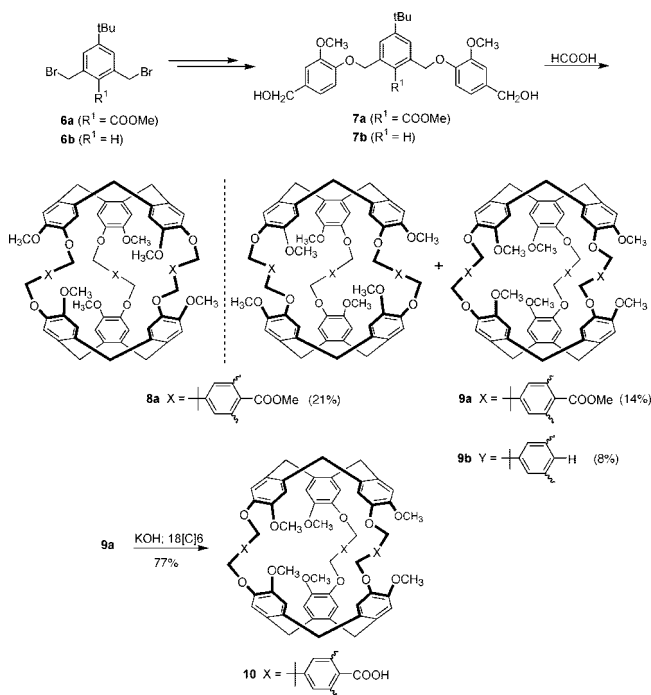


of  $D_3$  or  $C_{3h}$ -symmetrical compounds.<sup>29</sup> In addition, yields are usually low (2–5% for cryptophane-A (1), although cryptophane-E (2) and larger cryptophanes have been obtained with 15–20% yields). This method requires the preparation, from vanillyl alcohol 3, of bis(vanillyl alcohol) derivatives, e.g. 4 and 5, which are then treated in formic acid ( $\sim 10^{-2}$  M solution) to give rise to the desired cryptophanes. The cryptophanes are isolated by column chromatography from the polymeric materials that are formed predominantly. The procedure was successfully applied for compounds with linkers up to  $-(\text{CH}_2)_7\text{O}-$  and with linkers containing olefinic and acetylenic units.<sup>14–16</sup>

It is important to note that the reaction requires strong electron-donating groups on the benzylic alcohol; thus, the substituents in the *meta* and *para* positions are of importance. For this reason, vanillyl alcohol derivatives have been widely used as the starting material for the preparation of cryptophane molecules. Although this limits the synthetic possibilities of the direct method and affords cryptophanes with low or moderate yields, the simplicity of this approach is still very attractive. For instance, Weber and co-workers applied this method to the synthesis of new cryptophane receptors for the encapsulation of alkaline and alkaline-earth metal ions.<sup>30</sup> Starting respectively from the derivatives 6a and 6b, the diols 7a and 7b were prepared in two steps and were then allowed to react in formic acid for several days to give the corresponding cryptophanes 8a and 9a,b (Scheme 2). *anti*-Cryptophane 8a, obtained in 21% yield, is chiral ( $D_3$  symmetry) whereas the corresponding *syn*-isomer 9a, obtained in 14% yield, is achiral ( $C_{3h}$  symmetry). The separation of the two species was achieved easily by column chromatography on silica gel. From 7b, only compound 9b ( $C_{3h}$  symmetry) was isolated in 8% yield. Compound 9a, treated under basic conditions, yielded cryptophane 10 (77%) after recrystallization from acetone. The binding properties of cryptophane 10 will be discussed in section 6.3.

Holman and co-workers followed the same strategy to prepare *anti*-cryptophane 11 with ester-substituted *m*-xylylene bridges (10–12% yield).<sup>31</sup> Host *anti*-11 encapsulated one THF molecule, which filled the molecular cavity. Under heating at temperatures above 100 °C, the complex lost THF to give free *anti*-11 (Figure 3). Remarkably, the authors observed conformational flexibility of the CTV units in the empty host. This behavior was known for large-cavity containing cryptophanes but has seldom been reported (see section 5.1).<sup>32</sup> In the present case, <sup>1</sup>H NMR and single-crystal

## Scheme 2



structure determination showed an “imploded” empty cryptophane, where one of the CTVs exists in a flexible saddle–twist conformation, whereas the other adopts the usual cone shape structure. The loss of the solvent guest molecule forces the host to self-rearrange to fill its cavity. The resulting imploded cryptophane is able to restore its original rigid  $D_3$  symmetry upon encapsulation of a solvent guest, following a conversion pathway with an energy barrier of  $99 \text{ kJ mol}^{-1}$ .<sup>31</sup>

Akabori and co-workers, using the direct method, obtained cryptophanes with an assortment of bridges. For instance, from the bis-vanillyl alcohol 12, cryptophane 13 with *p*-xylylene bridges was obtained in 3% yield. Similarly, from the bis-vanillyl alcohol 14, cryptophane 15 with *o*-xylylene bridges was obtained with comparable yields (Scheme 3). The reactions run in formic acid at room temperature appeared to be stereospecific, as the *anti* isomers were exclusively recovered.<sup>33</sup> A new type of cryptophane with diethyleneoxy bridges was prepared from the precursor 16 heated at 55–60 °C in formic acid (Scheme 3). The *anti* (17) and *syn* (18) isomers were isolated in low yields (1.9% and 2.9%, respectively).<sup>34</sup> Because of the relative importance of these compounds for alkali metal or alkylammonium cation complexation,<sup>33,34</sup> as well as alkane recognition,<sup>35</sup> it is worth noting that they have been prepared with much better yields following the template procedure described in the next section (see Schemes 8 and 9).

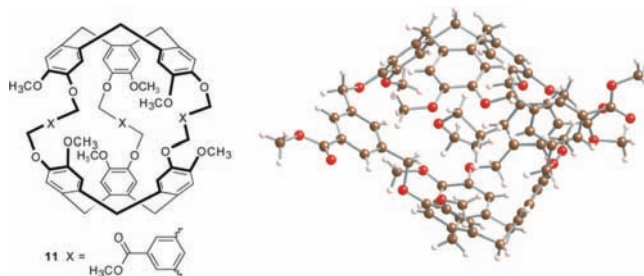
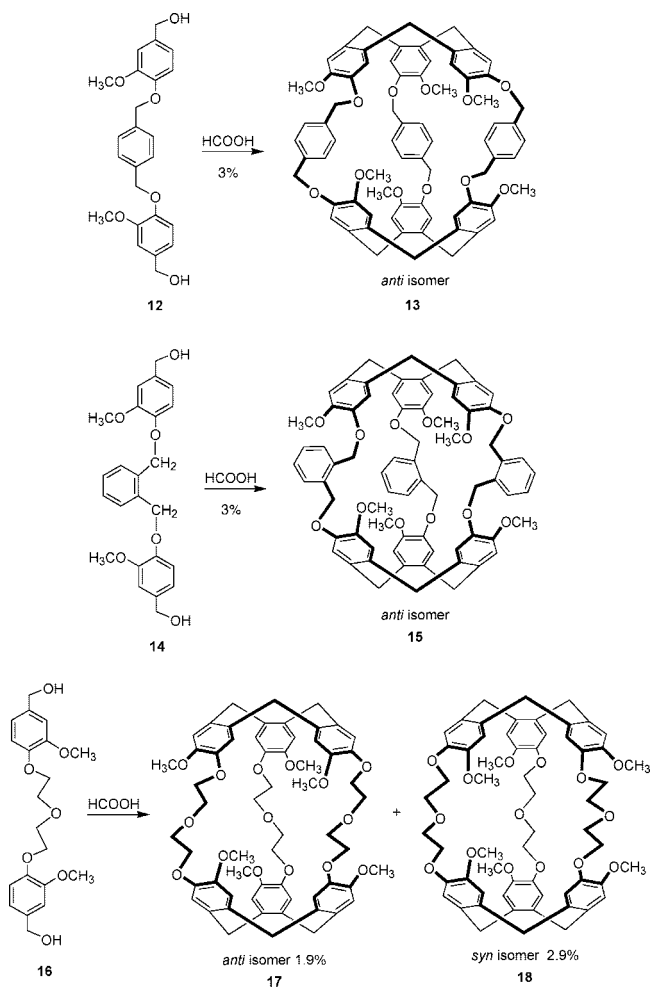


Figure 3. *Anti*-cryptophane 11, and X-ray crystal structure of THF@11.

## Scheme 3

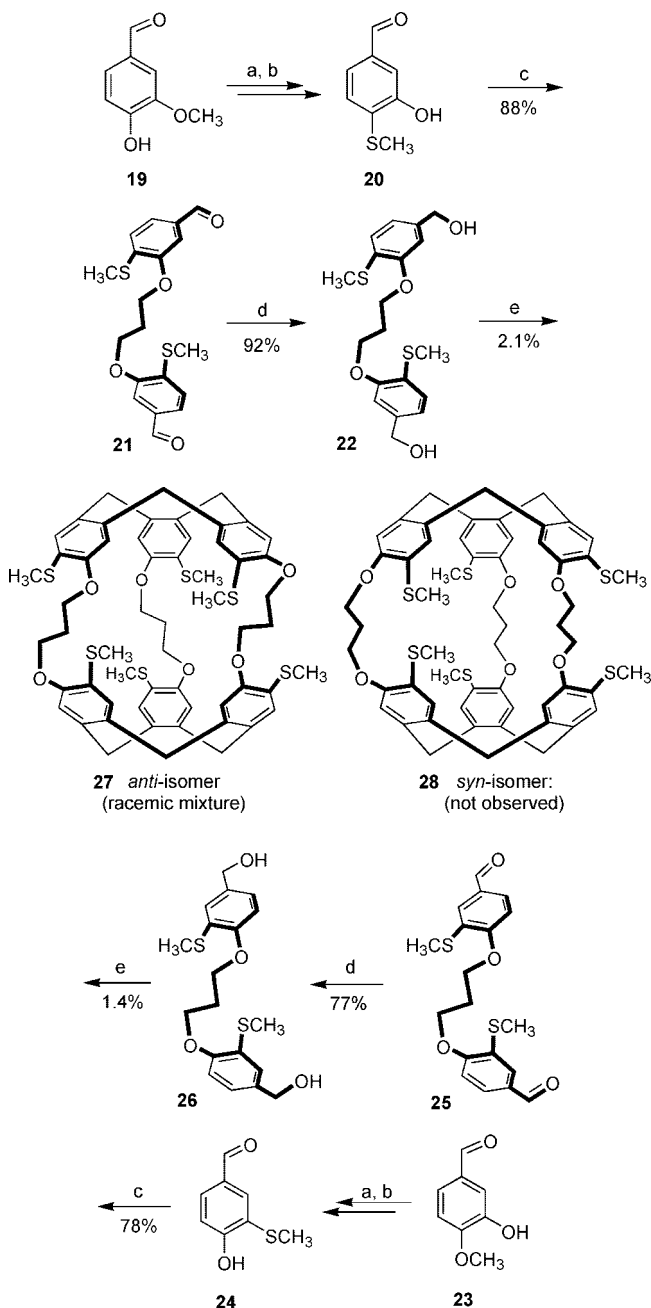


Garcia et al. also applied the direct method to design  $D_3$ -symmetrical sulfur containing cryptophanes. Starting from vanillin (**19**), 3-hydroxy-4-methylthiobenzaldehyde (**20**) was obtained in five steps. The coupling reaction of **20** with 1,3 dibromopropane led to the formation of compound **21**, which was reduced with  $\text{NaBH}_4$  to give the bis-benzylic alcohol derivative **22**. Similarly, starting from isovanillin (**23**), 4-hydroxy-3-methylthiobenzaldehyde (**24**), a regioisomer of **20**, was formed and reacted with 1,3 dibromopropane to afford **25**, which was reduced to **26** with  $\text{NaBH}_4$ . Compounds **22** and **26** were treated in pure formic acid to afford the *anti*-cryptophane isomer **27** with low yields (2.1% from **22** and 1.4% from **26**); the formation of the *syn* isomer **28** was not observed (Scheme 4).<sup>36</sup>

The introduction of sulfur atoms in the structure of cryptophanes is particularly interesting for the preparation of new derivatives that cannot be prepared directly from the corresponding CTV units. Later, compounds **27** and **28** were obtained with better yields, following the multistep procedure described in the next section, and the desulfurization reaction of these compounds easily led to new cryptophanes (see section 3.2).

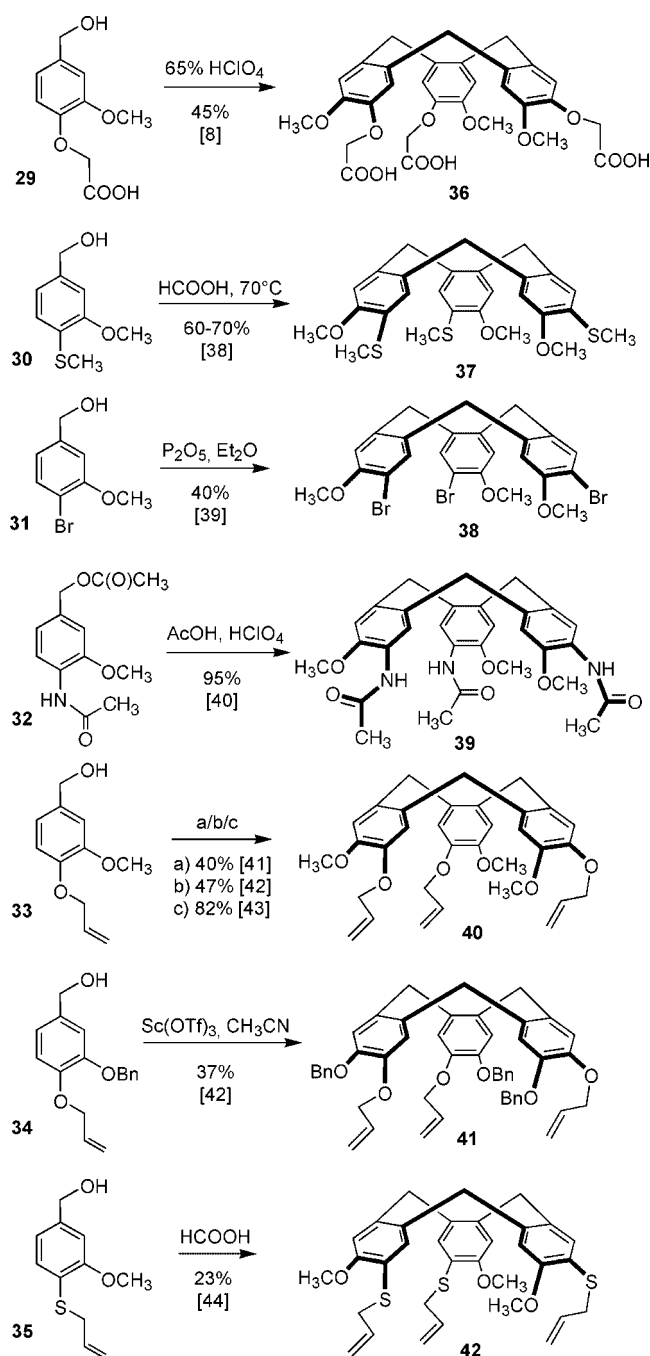
## 2.2. The "Template Method"

The second approach, called the *template method*, requires the formation of the two cyclotrimeratrylene units at different stages of the synthesis. The template term is related to the CTV precursor with the three linkers bearing the benzyl

Scheme 4<sup>a</sup>

<sup>a</sup> Conditions and reagents: (a) Newman–Kwart reaction,<sup>37</sup> four steps. (b)  $\text{CH}_2\text{Cl}_2$ ,  $\text{BBR}_3$ ,  $-78^\circ\text{C}$ . (c)  $\text{C}_3\text{H}_6\text{Br}_2$ ,  $\text{K}_2\text{CO}_3$ ,  $\text{CH}_3\text{CN}$ . (d)  $\text{NaBH}_4$ ,  $\text{CH}_3\text{OH}$ . (e)  $\text{HCOOH}$ ,  $60^\circ\text{C}$ , 6 h.

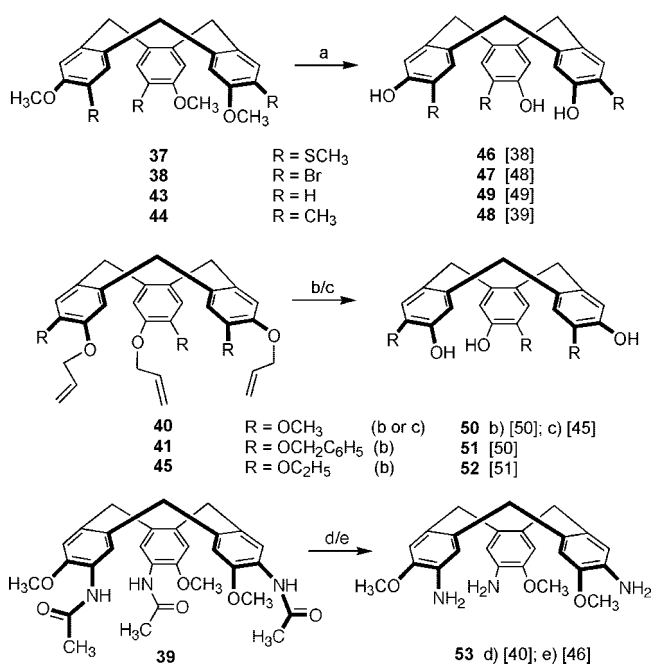
alcohol groups, which will give rise to the second CTV unit of the cryptophane structure. This precursor is thus *preorganized*—acting as a template—for the last intramolecular ring closure reaction, which is therefore not diffusion controlled, in contrast to the direct approach. Generally, the reaction conditions require  $10^{-3}$  M concentrations to reduce the formation of polymeric materials. However, this method strongly depends on the preparation of selectively protected cyclotrimeratrylene derivatives. In addition, as mentioned for the *direct method*, the efficient cyclization of benzyl alcohol moieties requires electron-donating substituents in the *meta*-position of the alcoholic function. This restricts the possibilities to the preparation of CTVs with  $-\text{OR}$ ,  $-\text{NRR}'$ , or  $-\text{SR}$  substituents. Different reagents have been used to promote the trimerization reaction of the benzylic derivatives

Scheme 5<sup>a</sup>

<sup>a</sup> Conditions and reagents: (a)  $\text{HClO}_4$ ,  $\text{CH}_3\text{OH}$ . (b)  $\text{Sc}(\text{OTf})_3$ ,  $\text{CH}_3\text{CN}$ . (c) ionic solvent. References are in square brackets.

into the corresponding cyclotrimeratrylene compounds (Scheme 5). The reagents vary in nature; organic or inorganic acids, Lewis acids, and even an ionic solvent have been used.<sup>43</sup> For instance, starting from the benzylic alcohol derivatives **29**–**35**, the corresponding CTVs **36**–**42** were easily prepared. CTV **40** is particularly important for the synthesis of cryptophanes and can be obtained in good yields either in perchloric acid and methanol or in an ionic solvent (tributylhexylammonium bis(trifluoromethyl-sulfonyl)amide).

Recently, scandium triflate  $\text{Sc}(\text{OTf})_3$  in acetonitrile was demonstrated to efficiently promote the intermolecular cyclization reaction of the benzylic alcohol **33** in 47% yield.<sup>42</sup> The use of catalytic amounts of  $\text{Sc}(\text{OTf})_3$  (~1%) in  $\text{CH}_3\text{CN}$  or  $\text{CH}_2\text{Cl}_2$  under mild conditions was found to be efficient

Scheme 6<sup>a</sup>

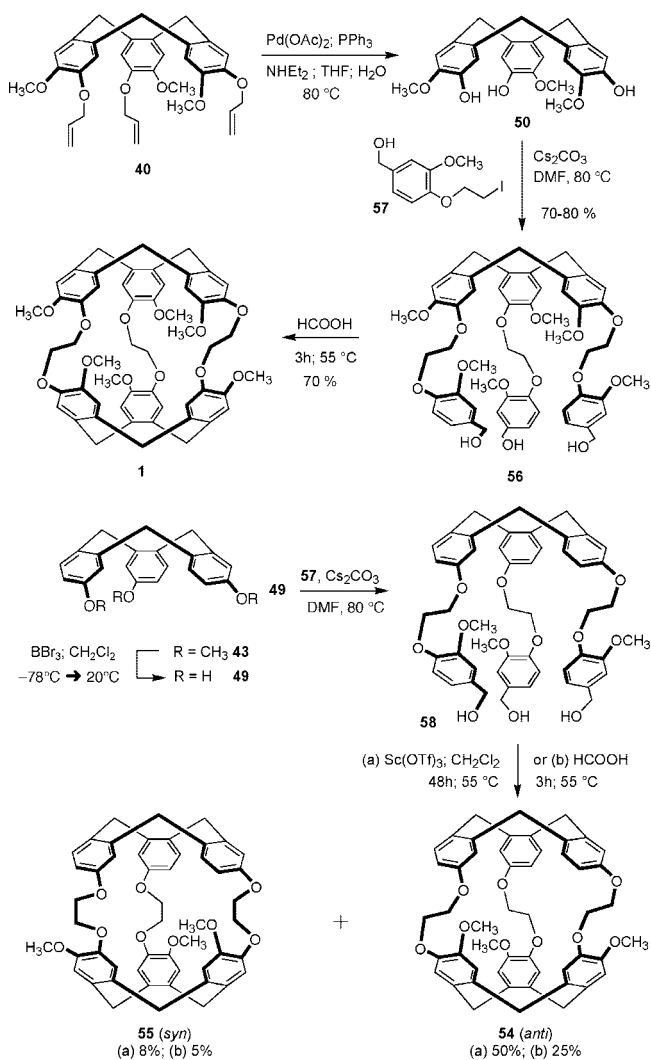
<sup>a</sup> Conditions and reagents: (a)  $\text{BBr}_3$ ,  $\text{CH}_2\text{Cl}_2$ ,  $-78^\circ\text{C}$ ; (b)  $\text{Pd}(\text{OAc})_2$ ,  $\text{NH}(\text{C}_2\text{H}_5)_2$ ,  $\text{THF}$ ,  $\text{H}_2\text{O}$ ,  $\text{P}(\text{C}_6\text{H}_5)_3$ ,  $80^\circ\text{C}$ ; (c)  $\text{NaBH}_4$ ,  $\text{I}_2$ ; (d)  $\text{Na}_2\text{O}_2$ ,  $\text{HOCH}_2\text{CH}_2\text{OH}$ ,  $180^\circ\text{C}$ ; (e)  $\text{C}_2\text{H}_5\text{OH}$ ,  $\text{HCl}$ ,  $95^\circ\text{C}$ . References are in square brackets.

for the condensation reaction of many benzylic alcohol derivatives and presents some advantages over the other previous reagents. In many cases, comparable or even better yields are obtained, and the purification steps are made easier. An example is given with compound **41**, which was prepared in 37% yield from **34**. It could not be easily obtained and isolated by other approaches. This molecule is of high interest, as it bears different protecting groups that allow the preparation of multifunctionalized cryptophane hosts. Moreover, the nontoxic  $\text{Sc}(\text{OTf})_3$  catalyst can be recovered easily by extraction and reused for subsequent experiments. There is no doubt that, in the future,  $\text{Sc}(\text{OTf})_3$  will be a catalyst of prime importance for the elaboration of new CTV derivatives that could not be prepared or purified so far. Presently, CTV derivatives **36**–**41** in Scheme 5 are commonly used for the design of cryptophane hosts.

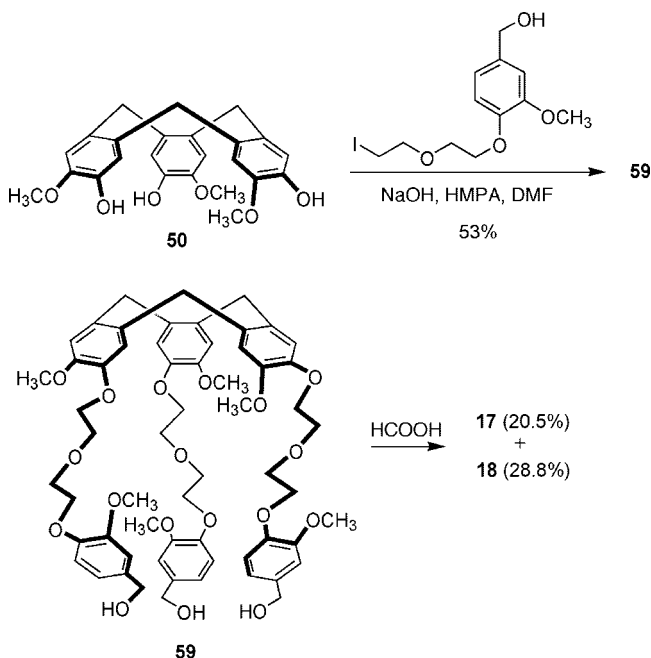
Deprotection of the methyl or allyl ether moieties of the cyclotrimeratrylene derivatives **37**, **38**, **40**, **41**, and **43**–**45**, using boron tribromide, a palladium catalyst, or sodium borohydride/ $\text{I}_2$ ,<sup>45</sup> gave rise to new functionalized CTVs **46**–**52** bearing three phenol groups (Scheme 6). The tris-amino CTV **53** was obtained by treating **39** with  $\text{Na}_2\text{O}_2$  in ethylene glycol at high temperature<sup>40</sup> or, more conveniently, by acid hydrolysis of **39** in ethanol (Scheme 6).<sup>46</sup> Compound **53** is a potential precursor of cyclotriamisylylene **43**, which can be used for the construction of cryptophane molecules. Likewise, Hardie and co-workers started from **53** to build metallo-supramolecular cages and coordination polymers.<sup>47</sup> Compounds **46**–**52** are key compounds in the template approach, for the elaboration of cryptophanes, which are not accessible through the *two-step* method.

The two examples in Scheme 7 demonstrate the possibilities of the template method to design cryptophane-A (**1**), *anti*-cryptophane-C (**54**), and its *syn* isomer cryptophane-D (**55**). Cryptophane-A (**1**) was obtained from precursor **56**, which in turn was obtained in two steps from CTV **40**.

## Scheme 7

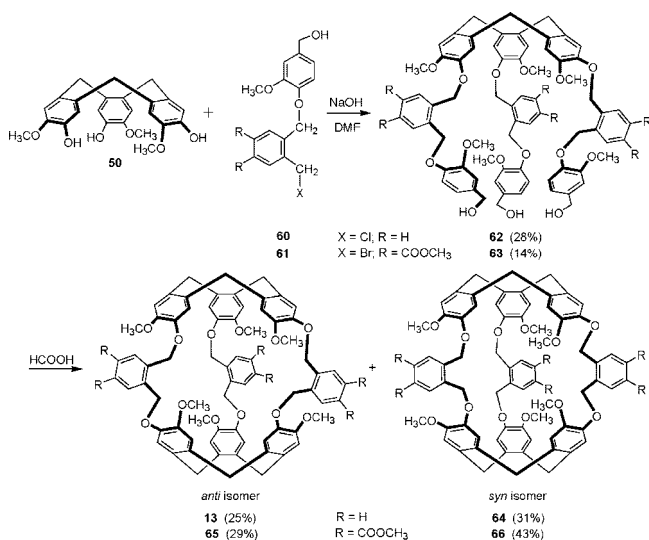


## Scheme 8



Cryptophanes **54** and **55**, which cannot be prepared by the direct method, were obtained from a multistep procedure:

## Scheme 9



CTV **49**, obtained by demethylation of CTV **43** with  $\text{BBr}_3$ , was allowed to react with compound **57** to yield cryptophane precursor **58**, which in turn was allowed to react under acidic conditions to give the *anti*- and *syn*-cryptophanes **54** (25%) and **55** (5%), respectively.<sup>52</sup> Cryptophane **54** discriminates between the two enantiomers of  $\text{CHFClBr}$  (see section 8). Additionally, an approach that would allow for the design of enantioenriched **54** has been proposed and will be discussed in more detail in section 10.2. Recently, the ring closure reaction leading to cryptophanes **54** and **55** was performed in  $\text{CH}_2\text{Cl}_2$  in the presence of  $\text{Sc(OTf)}_3$ , with 50% and 8% yields, respectively.<sup>42</sup>

The *template method* offers more possibilities than the direct method, as it is possible to affix a variety of linkers on the cyclotrimeratrylene precursor. Most often,  $D_3$ - and  $C_{3h}$ -symmetrical cryptophanes were thus prepared, such as cryptophane-A (**1**), cryptophane-E (**2**), or *syn*-cryptophanes **18** and **28**, but compounds with other symmetries have also been synthesized such as cryptophane-C (**54**) with  $C_3$  symmetry. sections 3 and 4 of this review will consider the synthesis of  $C_2$ -symmetrical and  $C_1$ -symmetrical cryptophanes as well as monofunctionalized analogues. The success of the template method depends on the synthesis of the appropriate cyclotrimeratrylene precursors; the cyclization of the second CTV unit is usually performed in pure formic acid or in a mixture of chloroform and formic acid ( $10^{-3}$  M in substrate) at moderate temperatures ( $50$ – $60^\circ\text{C}$ ). Following this strategy, yields for the ring closure reaction are usually higher (for cryptophanes of  $D_3$  or  $C_{3h}$  symmetry) than those obtained with the direct method, as the reaction is no longer diffusion limited. For instance, cryptophane-A (**1**, *anti* isomer) is obtained with a 70–80% yield from its CTV precursor, whereas the direct method gives very low yields (2–5%). However, it was observed that the efficiency of the cyclization step is highly dependent on the nature and the length of the linkers between the two CTV units. For example, cryptophane-E (**2**) is obtained with a lower yield than cryptophane-A (**1**) under the same experimental conditions. In addition, a large difference is also observed between the two methods concerning the formation of the *syn*-isomer with respect to the *anti*-isomer. The *syn/anti* ratio depends on the nature and the length of the linkers and the groups attached on the CTV units.



A further example was reported by Akabori and co-workers, who followed the route shown in Scheme 8 to synthesize cryptophanes **17** and **18** for the complexation of alkanes and ammonium salts.<sup>34</sup> From the precursor **59**, they obtained a mixture of the two cryptophanes **17** (*anti*, racemic) and **18** (*syn*, achiral) in 20.5% and 28.8% yields, respectively. In contrast, use of the direct method provided a mixture of **17** and **18** in 1.9% and 2.9% yields, respectively (see section 2.1). The *anti* and *syn* isomers were characterized by chromatography on a chiral stationary phase (Chiralpak OT<sup>+</sup>). The binding properties of **17** and **18** will be discussed in section 6.1.

Again using the template method, the same authors reported the synthesis of cryptophanes possessing xylylene bridges.<sup>33,35</sup> The reaction of CTV **50** with benzyl alcohol derivatives **60** and **61** afforded compounds **62** and **63**, respectively, in good yields. The *anti/syn* cryptophanes **13/64** and **65/66** with  $D_3/C_{3h}$  symmetry were obtained in moderate yields by treating compounds **62** and **63**, respectively, in formic acid at room temperature (Scheme 9).

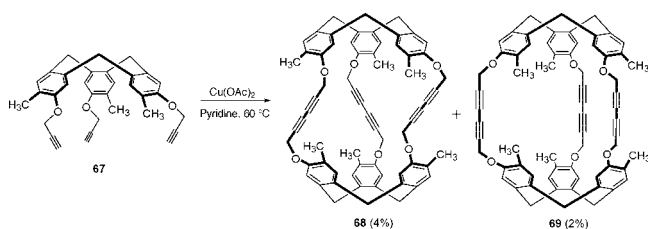
### 2.3. Coupling of CTVs

A third synthetic route, first described by Cram and co-workers, was used to synthesize cryptophanes with linkers containing acetylenic units. This approach involves the coupling, in the presence of copper acetate, of two identical tris[propargyl-ether]-CTVs **67**, to give the *anti*-cryptophane **68** ( $D_3$  symmetry) (4%) and the *syn*-cryptophane **69** ( $C_{3h}$  symmetry) (2%) (Scheme 10).<sup>39</sup> This strategy has been seldom developed, as it needs the preparation of suitably functionalized CTV precursors, and yields are particularly low.

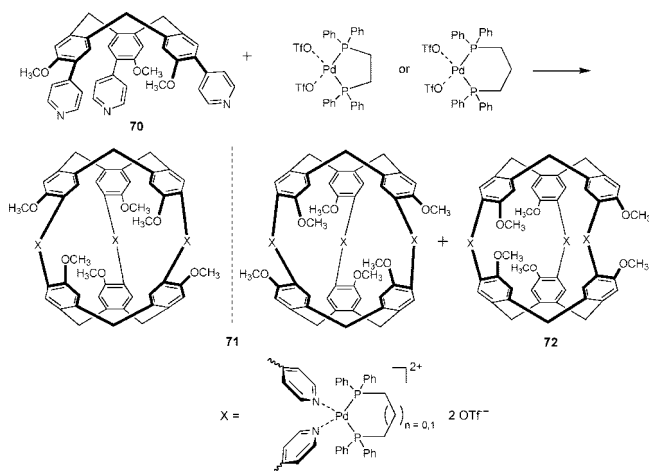
Recently, Zhong et al. extended this procedure to design cryptophanes by connecting two CTV units through coordination to metal atoms. Each pyridyl residue in CTV **70** self-assembles with a palladium complex to give quantitatively a mixture of *anti*-cryptophane **71** ( $D_3$  symmetry) and *syn*-cryptophane **72** ( $C_{3h}$  symmetry) (Scheme 11). Interestingly, both compounds exchange in solution to give the thermodynamically more stable *syn* compound **72**. The identification and absolute configuration of each enantiomer of **71** were achieved by combining electronic circular dichroism (ECD) spectroscopy and chiral phase HPLC.<sup>53</sup>

A similar strategy was developed by Hardie and co-workers to construct cryptophane-like cavitands through silver coordination of two tris(pyridyl)-CTV derivatives obtained from the triamino-CTV **53**. In this case, the formation of the cryptophane dimeric capsule competes with the formation of 3D-coordination polymers depending on the experimental conditions.<sup>47</sup> The reversible binding of the two caps was in this case based on the coordination to metal ions. Another compound was reported by Hong and co-workers, who self-assembled two complementary CTVs with car-

Scheme 10



Scheme 11



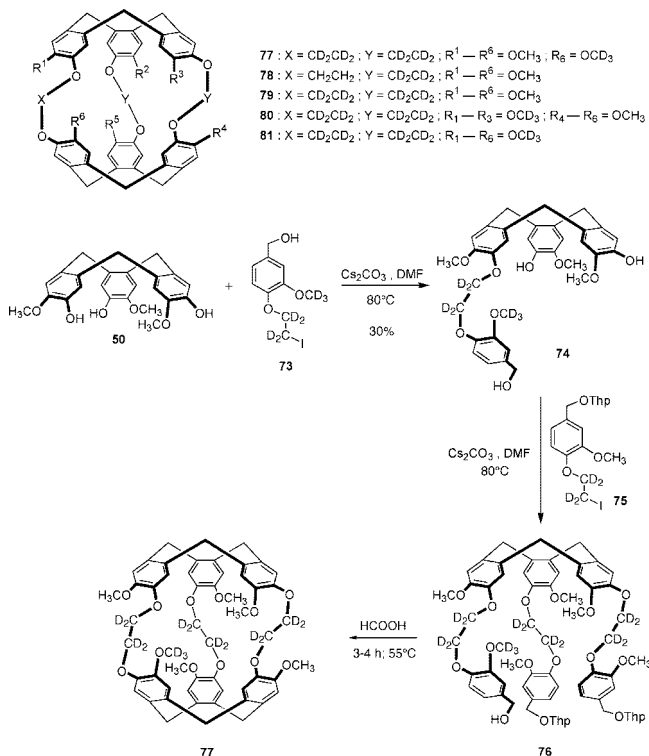
boxylic acid/amine functions to form a cryptophane structure through charged hydrogen-bonding interactions.<sup>54</sup>

## 3. Syntheses of New Cryptophanes Using the Template Method

### 3.1. Deuterium Labeled Cryptophanes

The stepwise approach of the *template method* allowed Brotin and co-workers to synthesize deuterium labeled cryptophanes (Scheme 12), in order to investigate environmental effects on xenon chemical shift using <sup>129</sup>Xe NMR spectroscopy (see section 9). The synthesis of the selectively deuterated cryptophane may require the preparation of monosubstituted CTVs. For instance, the reaction of **50** with the deuterium labeled benzyl alcohol **73** in DMF in the presence of an excess of cesium carbonate afforded the monosubstituted CTV **74**. This procedure allowed the introduction of a single deuterated linker bearing an OCD<sub>3</sub> group. The

Scheme 12





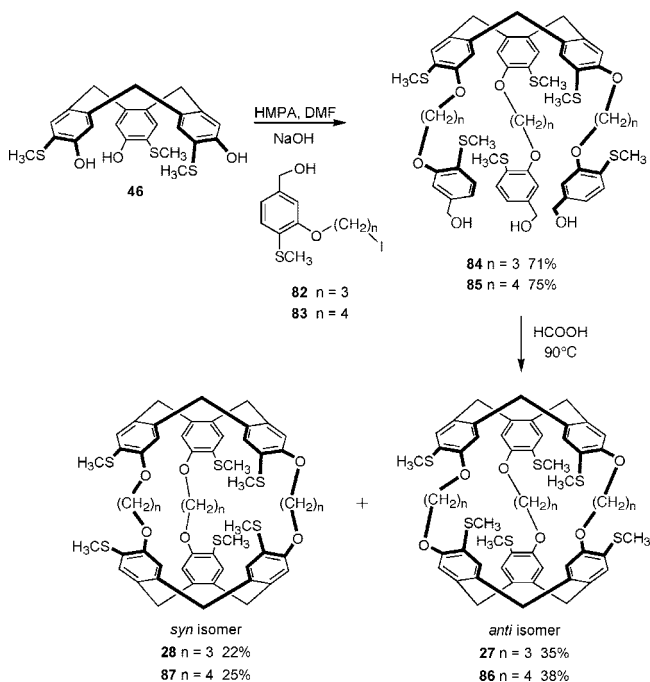
main difficulty lies in the separation of the monosubstituted derivatives from the side-products, mainly the di- and trisubstituted compounds. This can be readily achieved by column chromatography, and the desired compound was obtained in moderate yield (30%) due to the statistical distribution of the “tentacles” on the CTV unit. The next step involves the condensation of **74** with the protected benzylic alcohol derivative **75** to give the cryptophane precursor **76** in 78% yield. In the latter, THP groups were introduced to increase the solubility of the cryptophane precursor, simplifying the separation by chromatography on silica gel. Following this procedure, selectively deuterated cryptophanes **77–81** were thus obtained in 60–74% yields after treatment of the cryptophane precursors in formic acid (Scheme 12).<sup>50</sup>

### 3.2. Methylthio Containing Cryptophanes

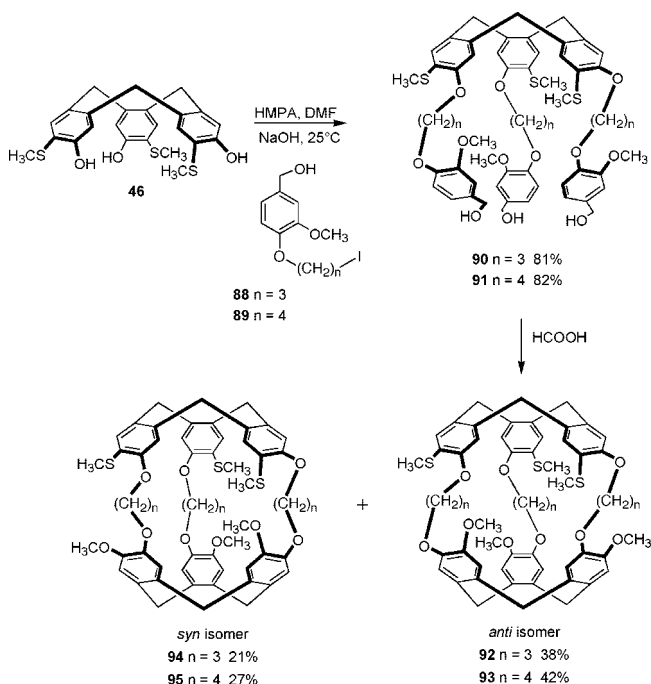
The cryptophanes **27** and **28** bearing six methylthio groups, which can be obtained through the two-step route (see section 2.1), were also synthesized by the *template method*. Similarly, the related sulfur containing cryptophanes bearing three butanedioxy bridges were also reported by Humilière, following the strategy reported above for cryptophane-A (**1**) and cryptophane-E (**2**).<sup>44</sup> The trihydroxy CTV **46** obtained in 95% yield from the parent compound **37** (70% yield from the thiovanillyl alcohol derivative **30**) upon reaction with three identical tentacles **82** or **83** gives the cryptophane precursors **84** and **85** in 71% and 75% yields, respectively. The last ring closure reaction was performed in formic acid to afford a mixture of cryptophanes **27/28** and **86/87** [*anti/syn* mixtures: 57% ( $n = 3$ ) and 63% ( $n = 4$ )] (Scheme 13).

For comparison, by using the two-step method, compound **86** was obtained with very low yield (1–3%).<sup>44</sup> The separation of the two isomers was then successfully achieved by column chromatography on silica gel, and the identification of each compound was performed by using chiral phase HPLC. It is interesting to note that enantioenriched **27** was also prepared following the same procedure starting with

Scheme 13



Scheme 14



enantiopure CTV **46** (see section 10.2 for the preparation of optically active cryptophanes).<sup>55</sup>

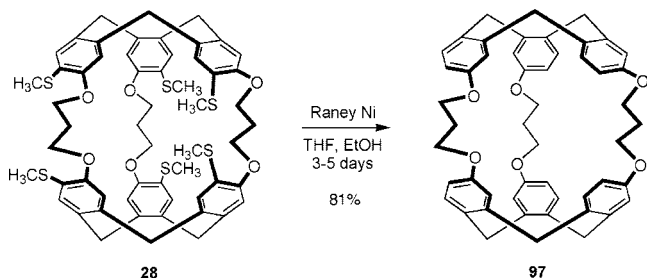
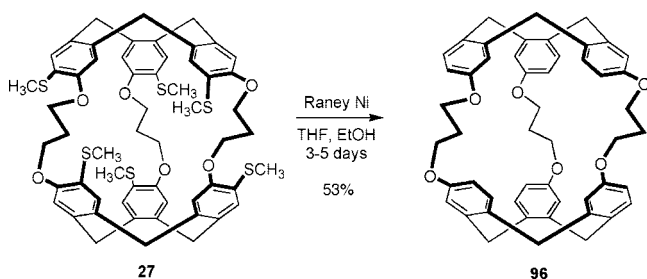
A similar strategy can then be applied to design cryptophanes with  $C_3$  symmetry, in which the two CTVs bear OCH<sub>3</sub> or SCH<sub>3</sub> groups (Scheme 14). For instance, CTV **46** reacts with 3 equiv of benzyl alcohol derivatives **88** or **89** under basic conditions to give rise to the cryptophane precursors **90** and **91**, respectively. Then cyclization of the second CTV cap in formic acid affords mixtures of the *anti* (**92**, 38%  $n = 3$ ; **93**, 42%  $n = 4$ ) and *syn* (**94**, 21%  $n = 3$ ; **95**, 27%  $n = 4$ ) cryptophane isomers. Separation of the isomers can be achieved easily by column chromatography on silica gel. Unlike the *syn* cryptophanes **28** and **87** bearing six methylthio groups, the new compounds **94** and **95** are chiral compounds.

The presence of SCH<sub>3</sub> instead of OCH<sub>3</sub> groups on the cryptophane backbone not only modifies significantly the binding properties of these new derivatives by modifying the accessibility to the cryptophane cavity<sup>36</sup> but also gives the opportunity to design new cryptophanes whose synthesis cannot be achieved directly using the *template method*. For instance, Humilière et al. successfully reduced the methylthio groups in **27** and **28**, in the presence of Raney nickel, giving rise to the new derivatives **96** and **97** in good yields (Scheme 15).<sup>44</sup> So far, the binding properties of cryptophanes **96** and **97** have not been reported.

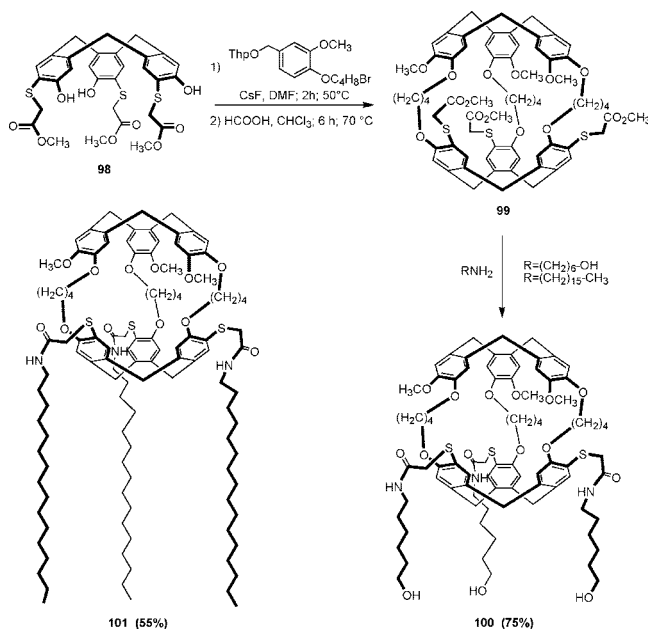
### 3.3. Amphipathic Cryptophanes

Although they do not possess a conventional amphiphilic structure, cryptophanes are good candidates for the construction of organized 2D assemblies. Indeed, it has been shown that they can form reversible monomolecular layers at the air–water interface, albeit with a rather limited stable surface domain.<sup>56</sup> Introduction of long alkyl chains on the periphery of these bowl-shaped molecules enhances their amphipathic character and consequently leads to a significant improvement of the stability of the corresponding interfacial films. Starting from the tris-thioester substituted CTV **98**, the key

Scheme 15



Scheme 16

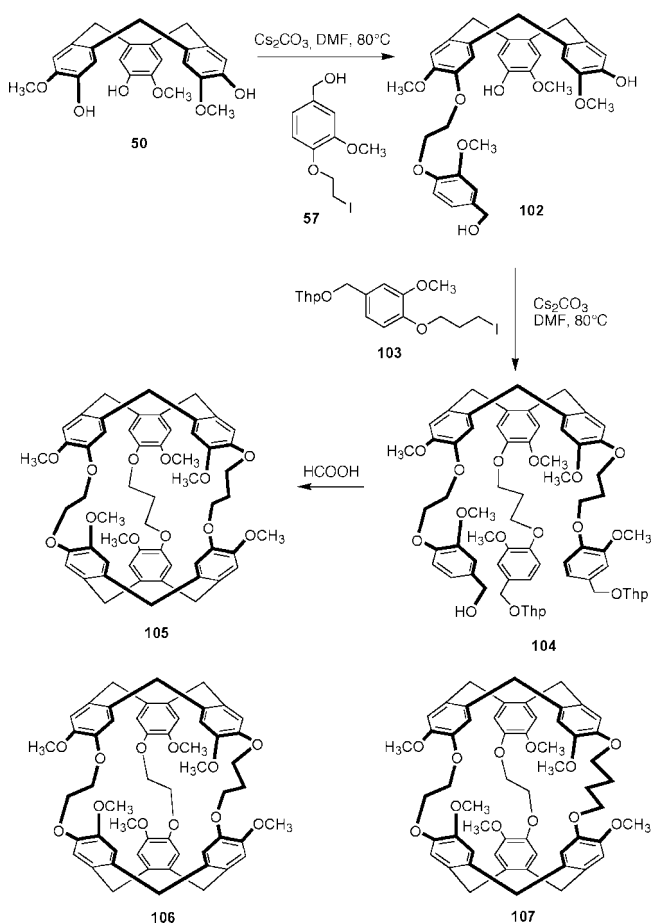


cryptophane molecule **99** was synthesized in two steps (22% overall yield) according to the template method. From **99**, the preparation of the amphipathic cryptophanes **100** and **101** was quite straightforward and was based on the reaction between the ester functions in **99** and a primary amine (Scheme 16).<sup>57</sup>

### 3.4. Syntheses of $C_2$ -Symmetrical Cryptophanes

A modified approach of the template method in which linkers of differing nature were introduced in separate steps has been used for the design of  $C_2$ -symmetrical cryptophanes (Scheme 17) and monofunctionalized cryptophanes (see section 4.2). For example, the reaction of CTV **50** with 1 equiv of benzyl alcohol derivative **57** gave CTV **102** in 30% yield. Subsequent reaction of CTV **102** with protected benzyl alcohol derivative **103** led to the cryptophane precursor **104** in 74% yield. Treatment of **104** in formic acid afforded *anti*-cryptophane-233 (**105**) (37% yields). Cryptophanes **106** and

Scheme 17

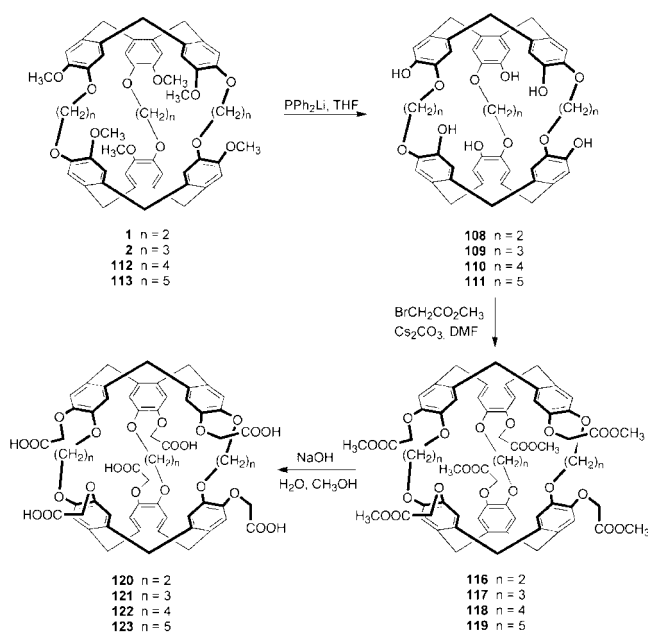


**107** have been obtained in 35% and 38% yields, respectively, by reaction of the corresponding precursors in pure formic acid (Scheme 17). A similar yield was obtained for cryptophane-223 (**106**) (33%) when a stoichiometric amount of Sc(OTf)<sub>3</sub> is used instead of formic acid.<sup>42</sup> On the whole, yields are lower than those reported for cryptophane-A (**1**), suggesting that dissymmetry enhances the formation of side-products during the cyclization step.  $C_2$ -Symmetrical cryptophanes-233 (**105**), -223 (**106**), and -224 (**107**) were prepared in order to study their Xe@cryptophane complexes in organic solution.<sup>58,59</sup>

## 4. Transformation and Functionalization of Cryptophanes

Most of the known cryptophanes with  $C_3$  and  $D_3$  symmetry, which have been designed in the past two decades, are indeed nearly ideal models to investigate the binding of various guests inside a molecular cavity. The past few years have seen an increasing interest in developing the chemistry of these fascinating molecular cages. However, there was little hope to build up novel systems with possible applications, if only the known synthetic procedures were applied. There was a lack of synthetic approaches to modify and functionalize these hosts, and little information has been reported in the literature concerning position-dependent chemical transformations involving cryptophane molecules. This situation originates from the high symmetry of the cryptophanes and the difficulties to control the reactivity of a particular site with respect to other equivalent sites. Nevertheless, the situation has changed drastically during the last few years as a result of two main events. The first

Scheme 18



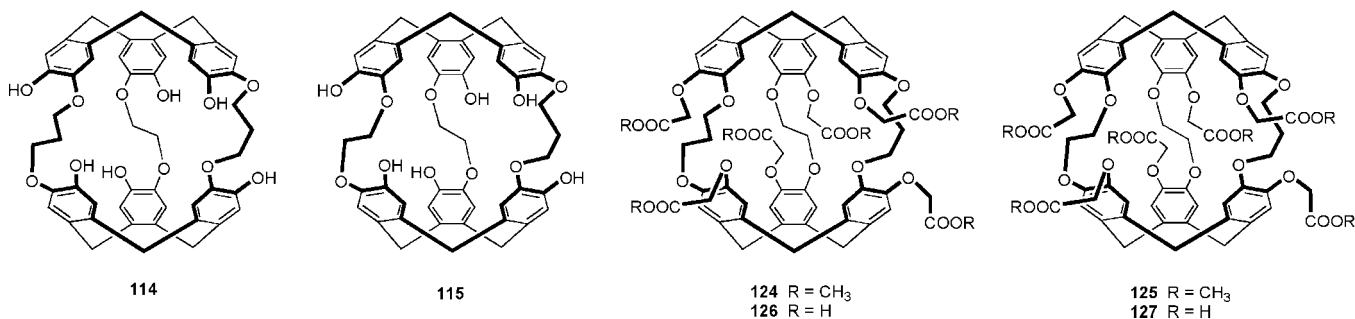
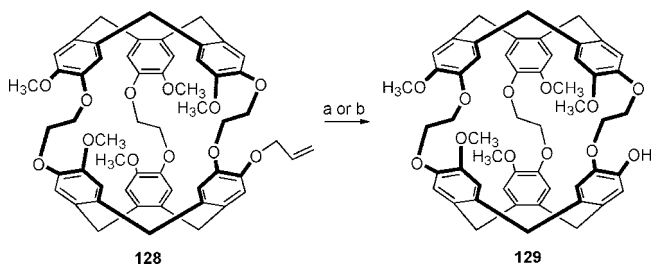
event was the discovery of the complexation of xenon by cryptophane-A (**1**), which prompted several research groups to design more complex cryptophanes for the encapsulation of the xenon guest. The second one has been the efforts made by our group and the Pines group at the University of Berkeley to conceive and propose new synthetic routes for synthesizing functionalized cryptophanes.

#### 4.1. Water-Soluble Cryptophanes: Hexacarboxylic Acid Cryptophanes

The first chemical transformation of cryptophanes was reported by Collet and co-workers, who selectively demethylated the six methoxy groups in cryptophane-A (**1**) by using lithium diphenylphosphide ( $\text{PPh}_2\text{Li}$ ) in THF.<sup>60</sup> This reagent is highly selective for the dealkylation of methoxy groups and does not affect the  $\text{O}-(\text{CH}_2)_n-\text{O}$  bridges.<sup>61</sup> Hexahydroxy cryptophane-A( $\text{OH}$ )<sub>6</sub> (**108**),<sup>62</sup> -E( $\text{OH}$ )<sub>6</sub> (**109**),<sup>62</sup> -M( $\text{OH}$ )<sub>6</sub> (**110**),<sup>63</sup> and -O( $\text{OH}$ )<sub>6</sub> (**111**)<sup>10</sup> have thus been obtained with good yields from cryptophanes-A (**1**), -E (**2**), -M (**112**), and -O (**113**), respectively (Scheme 18).

Huber et al. applied a slightly modified procedure to cryptophanes-233 (**105**) and -223 (**106**), to prepare the corresponding hexa-OH compounds **114** and **115**, with lower yields than those reported for **108–111**. The reaction of cryptophanes **108–111** with methyl bromoacetate led to the hexaester derivatives **116–119**, respectively. Subsequent hydrolysis of the ester groups in basic conditions generated

Chart 3

Scheme 19<sup>a</sup>

<sup>a</sup> Conditions and reagents: (a)  $\text{Bu}_3\text{SnH}$ ,  $\text{Pd}[\text{P}(\text{C}_6\text{H}_5)_3]_4$ . (b)  $\text{Pd}(\text{OAc})_2$ ,  $\text{P}(\text{C}_6\text{H}_5)_3$ ,  $\text{NH}_2\text{C}_2\text{H}_5$ , THF,  $\text{H}_2\text{O}$ .

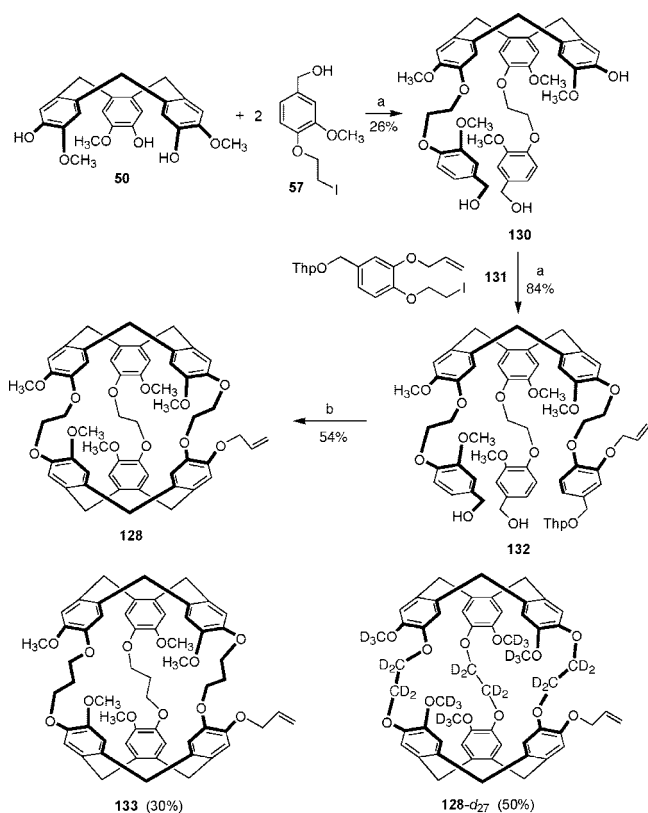
the new sparingly water-soluble hexaacid cryptophanes **120–123** (Scheme 18). Similarly, this approach was extended to the synthesis of the hexaester cryptophanes-233 (**124**) and -223 (**125**) and their water-soluble counterparts **126** and **127** (Chart 3).<sup>64</sup>

The synthesis of hexacarboxylic acid cryptophanes constituted significant progress in the chemistry of cryptophanes. It thus made possible the development and exploration of the complexation properties of water-soluble hosts in polar media (see section 6). These investigations have been extended to important topics of molecular recognition of biological targets. Nevertheless, this synthetic approach seems inappropriate for a selective and controlled deprotection of the methoxy groups, as  $\text{PPh}_2\text{Li}$  is used in large excess. Only recently, however, two groups have independently developed new strategies to synthesize functionalized cryptophanes, focusing on the preparation of the monohydroxy cryptophanol.

#### 4.2. Monofunctionalized Cryptophanes: Cryptophanol

The key step in obtaining monohydroxy cryptophanol is the synthesis of the monoprotected cryptophane **128**, which can be easily cleaved to give the cryptophanol-A molecule **129** (Scheme 19).

Compound **129** is an important target molecule for the elaboration of complex systems such as biosensors (section 4.3), bis-cryptophanes (section 4.4), and enantiopure cryptophanes (section 10.2). So far, two different approaches have been proposed to synthesize cryptophane **128**. Darzac et al. developed a strategy based on the monofunctionalization or the bis-functionalization of CTV **50**.<sup>65,66</sup> Compound **50** was first treated with 2 equiv of benzyl alcohol **57** to give rise to the disubstituted derivative **130** with moderate yield (26%). Then, the condensation of the protected vanillyl alcohol derivative **131**, prepared in several steps from 3,4-dihydroxy benzaldehyde, with CTV **130**, afforded cryptophane precur-

Scheme 20<sup>a</sup>

<sup>a</sup> Conditions and reagents: (a)  $\text{Cs}_2\text{CO}_3$ , DMF, 80 °C. (b)  $\text{HCOOH}$ ,  $\text{CHCl}_3$ , 55 °C.

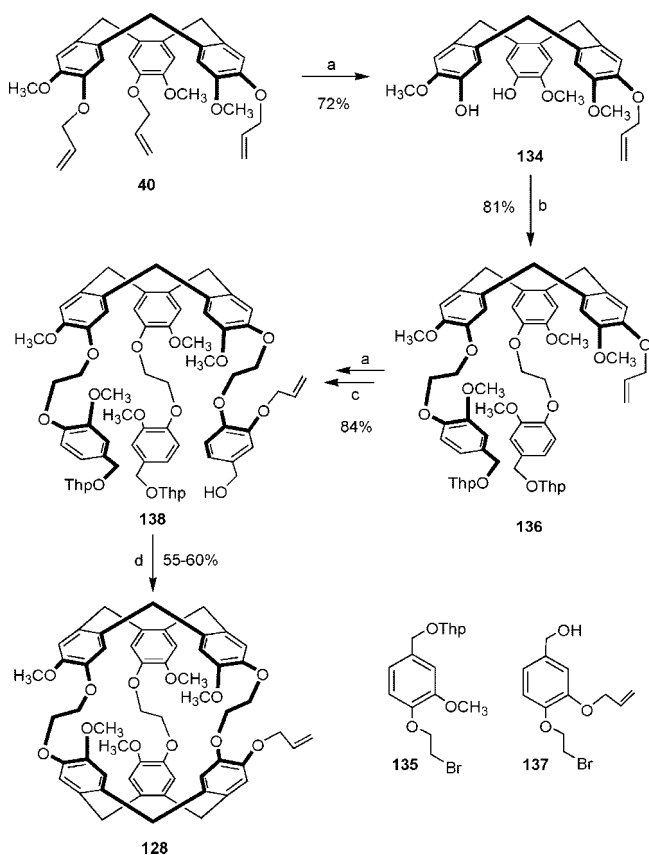
or **132** with good yields (84%). The final cyclization step was conducted in a 1:1 mixture of chloroform and formic acid to give cryptophane **128** in 54% yield (Scheme 20).

The experimental conditions reported for the last step reduce significantly the formation of side-products and the degradation of the starting material. However, as previously observed with cryptophanes **105–107**, the yield for compound **128** was lower than that for cryptophane-A (**1**), possibly due to the partial removal of the protecting group under the experimental conditions. Under the milder conditions of  $\text{Sc}(\text{OTf})_3$  in  $\text{CH}_3\text{CN}$  at 30 °C, cryptophane **128** was obtained in poor yield (10%, nonoptimized condition). Analogous procedures were used to produce cryptophane **133** or partially deuterated cryptophane **128-d<sub>27</sub>** (Scheme 20).

The procedure developed by Spence et al. for the synthesis of cryptophane **128** involved the selective deprotection of CTV **40** using  $\text{Pd}[\text{P}(\text{C}_6\text{H}_5)_3]_4$  as a catalyst and  $\text{Bu}_3\text{SnH}$ .<sup>67</sup> The monoprotected CTV **134** was obtained in 72% yield and was then allowed to react with 2 equiv of protected vanillyl ether **135** to give the bis-functionalized CTV **136**. A second deprotection step followed by the condensation with the allylic containing derivative **137** afforded the cryptophane precursor **138** in good yield (65% over two steps). The last cyclization reaction was conducted in pure formic acid to yield cryptophane **128** in 55–60% yield (Scheme 21).<sup>68</sup>

Unlike the previous route reported by Darzac et al., the authors do not report any degradation of the starting compound or a decrease in the yield when pure formic acid is used in the final ring closure reaction. Thus, this synthetic route gives better yields for the formation of the cryptophane precursors but requires several additional steps.

From **128**, the deallylation reaction easily leads to cryptophanol **129** (Scheme 19). By the same route, cryptophanol-

Scheme 21<sup>a</sup>

<sup>a</sup> Conditions and reagents: (a)  $\text{Bu}_3\text{SnH}$ ,  $\text{Pd}[\text{P}(\text{C}_6\text{H}_5)_3]_4$ . (b)  $\text{K}_2\text{CO}_3$ ,  $\text{Bu}_4\text{NI}$ , **135**. (c)  $\text{K}_2\text{CO}_3$ ,  $\text{Bu}_4\text{NI}$ , **137**. (d)  $\text{HCOOH}$ .

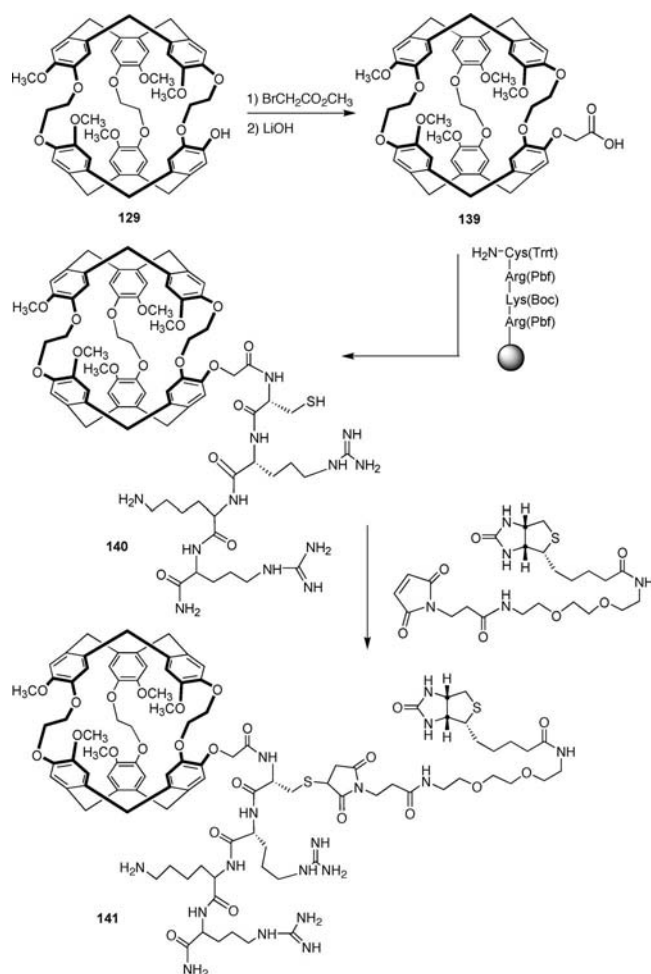
**E(OH)** and partially deuterated cryptophanol-A(OH)-*d<sub>27</sub>* were obtained from cryptophanes **133** and **128-d<sub>27</sub>**, respectively (section 4.4). This result was significant for the chemistry of the cryptophane hosts, since it opened the door to the development of the cryptophane-complex-based biosensors (section 4.3) and to a new strategy allowing access to enantiopure cryptophanes (section 10.2.2). Furthermore, other functionalized cryptophanes can now be prepared from the cryptophanols, and active investigations in this field are presently underway in several laboratories.

### 4.3. Cryptophanes as Biosensors

Pines and co-workers started from cryptophanol **129** and attached a molecular antenna (biotin) able to selectively recognize a protein (avidin) (see section 9.4.2).<sup>68</sup> The synthesis requires a multistep procedure in order to first attach a water-soluble substituent (amino acid) and then the biotin moiety (Scheme 22). Cryptophanol **128** was first alkylated with methyl bromoacetate followed by  $\text{LiOH}$  saponification to give rise to the corresponding carboxylic acid derivative **139**. A short polypeptide chain was then condensed with the acid function to allow the partial solubilization of the final product in water. A solid-phase synthesis was used to introduce the polypeptide, and the resulting cryptophane-peptide conjugate **140** was then released in solution. The next step was the coupling reaction between the thiol function of the cysteine residue in the cryptophane-peptide conjugate and the maleimide linked to the biotin ligand. The desired functionalized water-soluble cryptophane **141** was purified by reversed phase HPLC.



Scheme 22

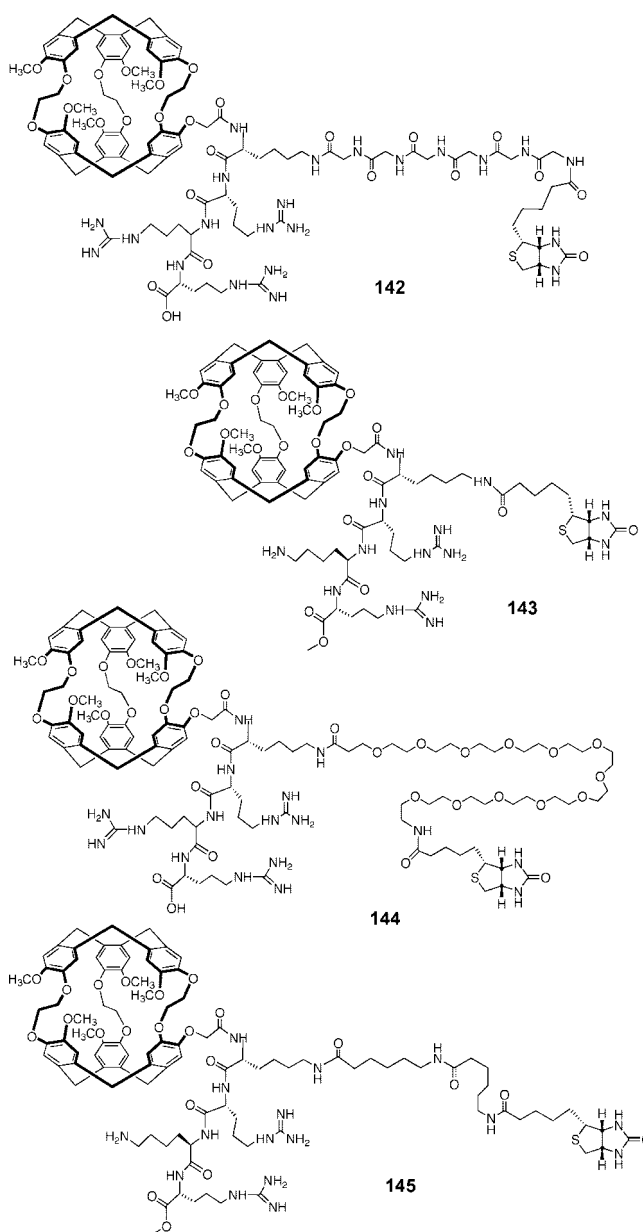


Lowery et al. reported recently the preparation and biosensing properties of several functionalized Xe@cryptophane complexes in order to study the different molecular parameters, which affect the resolution of the  $^{129}\text{Xe}$  NMR signals.<sup>69</sup> The new biosensors **142–145** were designed for the detection of protein interactions and possess different linkers, of various lengths and flexibility, that connect the cryptophane moiety to the biotin ligand (Chart 4). Compounds **142–145** were prepared according to the experimental procedure described for compound **141**, and the effect of the deuteration of the cryptophane subunit has also been investigated. The influence of the nature of the linker on the recognition process and xenon NMR spectra will be discussed in detail in section 9.4.

#### 4.4. Bis-cryptophanes

The substitution at the phenol group of cryptophanol-A(OH) (**129**) and cryptophanol-E(OH) (**146**) with 1,10-diiododecane was investigated by Darzac et al. to synthesize bis-cryptophanes in order to study the guest exchange between closely bonded molecular cavities.<sup>66</sup> These simple molecules were also designed to demonstrate the feasibility of more complex molecular systems, such as cryptophane-based polymers and dendrimers. Monosubstituted derivatives **147** and **148** were prepared from the parent cryptophanols **129** and **146**, respectively, and 1,10-diiododecane, by use of cesium carbonate in DMF. Bis-cryptophanes **149** and **150** were then obtained by condensation of **147** and **148** with cryptophanols **129-d<sub>27</sub>** (obtained by deallylation of **128-d<sub>27</sub>**)

Chart 4. Structures of the Cryptophane-Based Biosensors 142–145

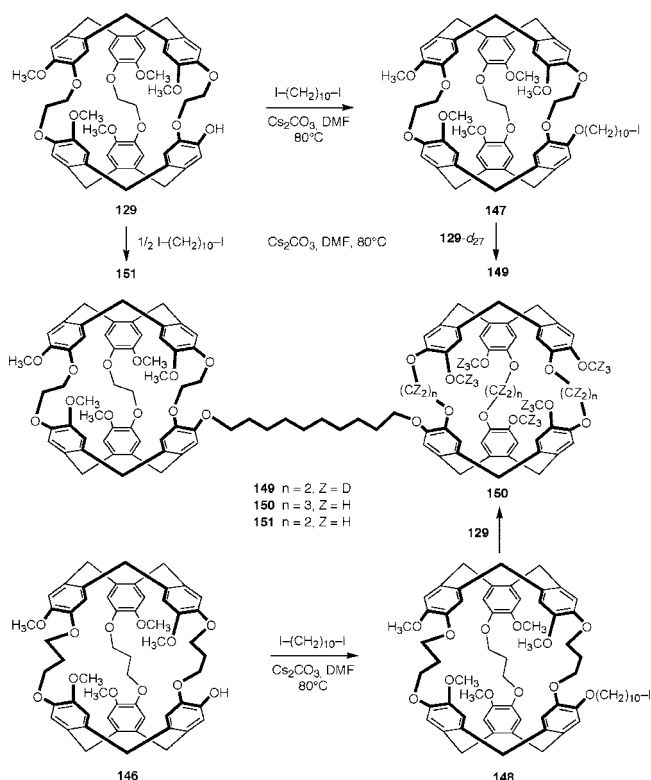


and **129**, respectively. Bis-cryptophane **151** was obtained in a one-step synthesis by coupling two cryptophanol molecules **129** with 1,10-diiododecane in DMF (Scheme 23).<sup>65</sup> Compounds **149–151** were isolated as a mixture of diastereomers due to the possible coupling of two cryptophanes with identical or opposite configurations. These molecules are interesting because of their enhanced solubility in various solvents, thus providing the possibility to study cryptophane complexation properties in a wider range of solvents (for example, see section 7.4).

#### 5. Structural Aspects and Characterization of Cryptophanes

From a general point of view, the *anti*- and *syn*-cryptophane isomers are quasi-spherical molecules presenting only a few conformational fluctuations, at least when one considers the smallest representatives. However, these fluctuations are of great importance for guest encapsulation, as they modulate the size of the different openings that allow

Scheme 23



substrates to enter and leave the molecular cavity. These conformational modifications are mainly related to the variations of the torsion angles along the C–C and C–O bonds of the linkers between the two CTV units. CTV units having an *out* cone conformation are essential to ensure the formation of the cavity and should be sufficiently rigid to preserve the spherical structure of the molecule. In addition to the *syn–anti* isomerism, other conformational parameters affect the molecular structure. The *out–out*, *in–in*, and *in–out* conformations are defined relative to the orientation of the CTV cone in the molecule, as described in section 1. Although the cone structure of the CTV units is dominant in the cryptophanes (*out–out* conformer), one must still consider their relative flexibility (see Figure 4).<sup>27,70</sup> For instance, *saddle–twist* conformations have been observed in the solid state and in solution with some *anti*-cryptophanes (*out–saddle* conformer) and especially with water-soluble cryptophanes where hydrophobic forces have dramatic effects on the molecular structure.

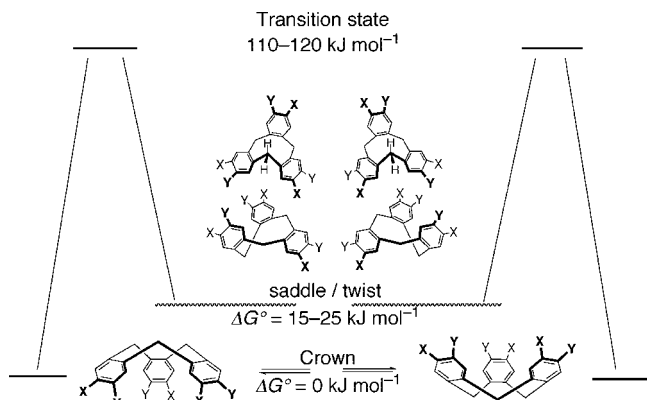


**Figure 4.** Energy profile for the inversion of the crown forms of CTVs leading to the enantiomerization through saddle–twist exchanges (Reprinted from ref 16, Copyright 1996, with permission from Elsevier).

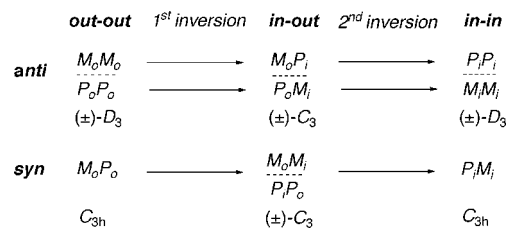


**Figure 5.** How the configuration of the CTVs defines the stereochemistry of the cryptophane molecules (Reprinted from ref 16, Copyright 1996, with permission from Elsevier).

Consequently, this conformational mobility has a direct effect on the chirality of the CTV caps specified by the *P* and *M* descriptors.<sup>71</sup> The inversion of either cap in the enantiomers of an *out–out* (*o,o*) *anti*-cryptophane ( $D_3$  symmetry) with  $P_oP_o$  and  $M_oM_o$  configuration leads to the corresponding (*i,o*)  $M_iP_o$  and its (*i,o*)  $P_iM_o$  mirror image, respectively. From an achiral (*o,o*) *syn*-cryptophane ( $C_{3h}$  symmetry) with  $M_oP_o$  configuration, inversion of one CTV cap leads to a racemic mixture of the corresponding  $P_iP_o$  and  $M_oM_i$  isomers. Figure 5 summarizes how subsequent CTV inversions change the stereochemistry of the cryptophane molecule.<sup>16</sup>

Here, we wish to point out the work of Kuck and co-workers, who synthesized tribenzotriquinacene derivatives with a CTV-like structure.<sup>72</sup> Interestingly, such molecules possess a strictly rigid skeleton that cannot invert and are therefore potentially attractive for building cryptophane-like hosts. Although they are out of the scope of this review, these compounds could possibly be functionalized to form new rigid cryptophane-like structures.<sup>73</sup>

The peripheral substituents of the cryptophanes are also important for the dynamics of guest encapsulation, as they influence the size of the portals, allowing access to the molecular cavity. The formation of host–guest complexes is dependent on the accessibility of the molecular cavity, and upon complexation, the conformational populations of the host may change. We will report below on different structural aspects that have appeared in the literature.

## 5.1. Some Peculiarities in the Characterization of Cryptophane Hosts

Like other cage compounds, cryptophanes are seldom isolated free from guest molecules, and they frequently form poorly defined solvates. Consequently, the elemental analysis often leads to nonreproducible results, and the compounds merely decompose over a large temperature range before melting. Additionally, crystals of cryptophanes are frequently of low quality, often losing trapped solvent molecules rapidly. The crystals exhibit disorder and high thermal agitation, a situation which has to be attributed to their spherical shape, their complexation properties, and the flexibility and conformation of the linkers.

Mass spectrometry (MS) and NMR spectroscopy are reliable techniques for characterization of cryptophane molecules and for investigation of their remarkable host–guest properties. Mass spectrometry, in the absence of reliable elemental analysis, appears to be very useful to characterize cryptophane derivatives by detecting the expected molecular ion. Indeed, soft ionization such as fast atom bombardment (FAB), liquid secondary ion mass spectrometry (LSIMS), and related techniques (electrospray and matrix-assisted laser desorption/ionization (MALDI)) are particularly suited to

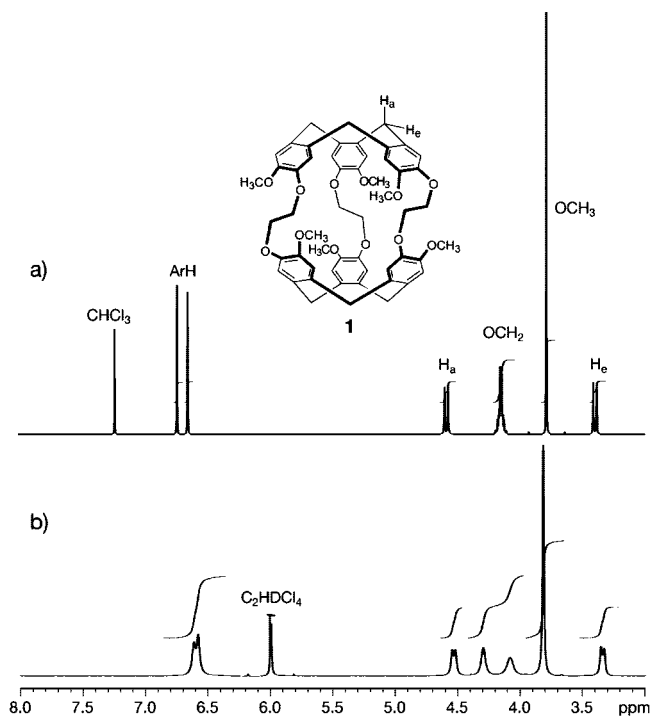


**Figure 6.** 500 MHz  $^1\text{H}$  NMR spectra of cryptophane-A (**1**) recorded at 293 K in (a)  $\text{CDCl}_3$  or (b)  $\text{C}_2\text{D}_2\text{Cl}_4$ .

study host molecules and their complexes.<sup>74</sup> In addition, liquid secondary ion mass spectrometry presents the possibility to predict the formation of cryptophanes from their precursors prior to any synthetic work. Thus, it was possible to rapidly investigate qualitatively the possibility of preparing new cryptophanes.<sup>75</sup>

Among the large range of spectroscopic techniques available to the chemist, NMR still remains the principle tool to characterize the cryptophanes and to study their binding properties. Indeed, the presence of easily distinguishable signals for the hosts leads to their unambiguous identification. In addition, the change of the environment experienced by the guest molecule upon complexation leads to dramatic shifts of the guest signals that are in general easily detected. The identification of the cryptophanes is supported by the presence in the  $^1\text{H}$  NMR spectrum of a characteristic AB pattern ( $J_{\text{AB}} \approx 13.5$  Hz) for the axial ( $\text{H}_a$ ) and equatorial ( $\text{H}_e$ ) protons of the cone shape CTV moieties (Figure 6). Moreover,  $^1\text{H}$  and  $^{13}\text{C}$  NMR spectra of cryptophanes are obviously dependent on factors such as guest encapsulation, dynamics, temperature, and solvent. For instance, the bandwidths of the  $^1\text{H}$  signals of **1** increase in  $\text{C}_2\text{D}_2\text{Cl}_4$ , a solvent that cannot enter into the molecular cavity of **1** when compared to **1** in  $\text{CDCl}_3$  (Figure 6). In the former case, the line broadening appears as a consequence of the different conformations of the three bridges.<sup>76</sup> In contrast, the presence of a solvent molecule inside the cavity rigidifies the structure of the host by reducing the number of conformational degrees of freedom.

Generally,  $^1\text{H}$  NMR spectra of  $D_3$  or  $C_{3h}$  symmetry cryptophanes are quite easy to analyze and allow differentiation of the *syn* and *anti* isomers. Cryptophane-E (**2**) and related cryptophanes such as cryptophane **27** display characteristic signals that allow differentiation of each compound according to symmetry (*anti-2* vs *syn-152*) and substitution (**2** vs **27**) (Figure 7).

In the examples of Figure 7, *anti*-cryptophane-E (**2**) and its isomer *syn*-cryptophane-F (**152**) are unambiguously

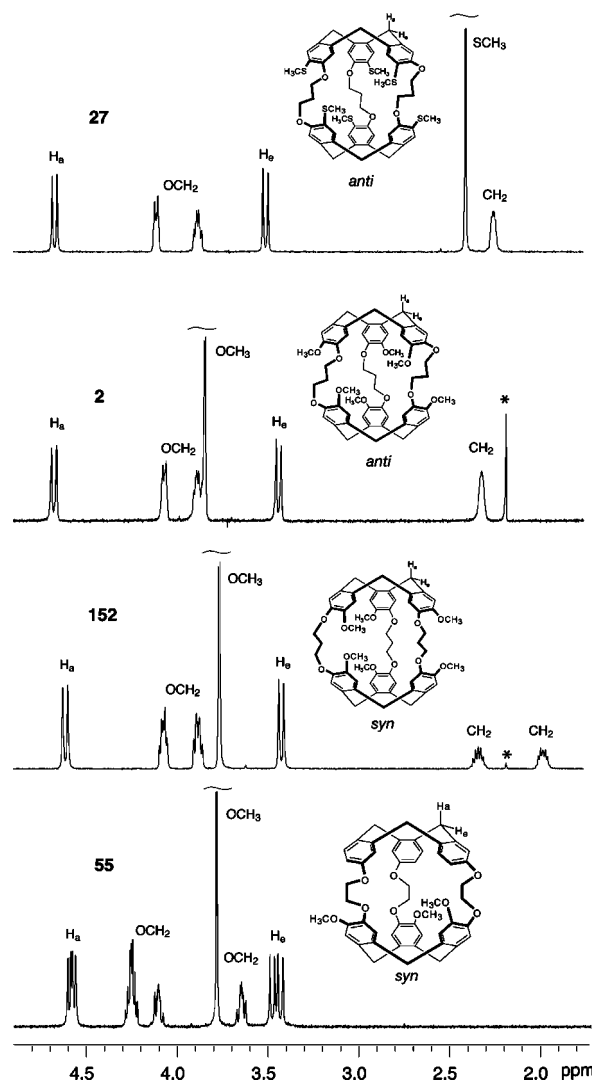


**Figure 7.** Differentiation by 500 MHz  $^1\text{H}$  NMR spectroscopy of *anti-27* ( $D_3$ ), *anti-2* ( $D_3$ ), *syn-152* ( $C_{3h}$ ), and *syn-55* ( $C_3$ ) cryptophanes at 293 K (\* residual solvent).

differentiated by the  $-\text{CH}_2\text{CH}_2\text{CH}_2-$   $^1\text{H}$  NMR signals, where the two central protons are homotopic in **2** and diastereotopic in **152** and give, as expected, one broad multiplet or two multiplets, respectively. Cryptophane-D (**55**) possesses two different CTV caps ( $C_3$  symmetry) and shows two sets of AB systems for the  $\text{H}_a$  and  $\text{H}_e$  protons and a pattern for the  $\text{CH}_2$  linker protons. Indeed, lower-symmetry compounds exhibit more complicated spectra due to the nonequivalence of the protons in the molecule. The increased complexity of the  $^1\text{H}$  NMR spectra is exemplified in the spectrum of the  $C_1$  symmetrical cryptophanol **129**, which is different from those of the  $D_3$ - and  $C_{3h}$ -cryptophanes (Figure 8).

## 5.2. Inverted and Imploded Cryptophanes

The first evidence of the inversion of a CTV unit in a cryptophane was reported by Collet and co-workers for compounds with long  $-\text{O}(\text{CH}_2)_n\text{O}-$  ( $n \geq 5$ ) spacer bridges.<sup>32</sup> Cryptophane-O (**113**) can invert at 523 K to give the inverted *in-out* cryptophane *inv-113*, for which a molecular modeling view is given in Figure 9.<sup>77</sup> The compound was characterized by  $^1\text{H}$  NMR spectroscopy in freshly prepared  $\text{CHCl}_3$  solution; as a function of time, the *out-out* compound **113** was totally recovered. An activation energy  $E_a = 88.3 \pm 4.2$   $\text{kJ mol}^{-1}$  was determined from  $^1\text{H}$  NMR experiments at different



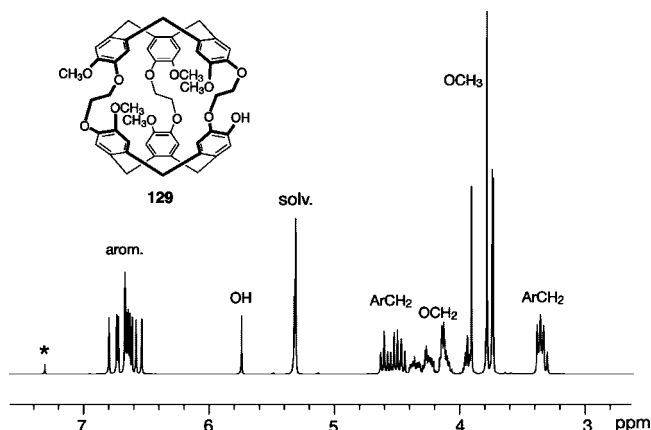


**Figure 8.** 500 MHz  $^1\text{H}$  NMR spectrum of cryptophanol **129** in  $\text{CD}_2\text{Cl}_2$  at 293 K; an example for an *anti*- $C_1$ -symmetrical cryptophane (\* residual  $\text{CHCl}_3$ ).

temperatures for the *in-out*  $\rightleftharpoons$  *out-out* exchange process, thus leading to an activation enthalpy  $\Delta H^\ddagger = 85.7 \text{ kJ mol}^{-1}$  and an activation entropy  $\Delta S^\ddagger = -35.9 \text{ J K}^{-1} \text{ mol}^{-1}$  (Figure 9).<sup>78</sup>

Holman and co-workers studied CTV inversion in cryptophane **11** and showed by  $^1\text{H}$  NMR in solution that, when the cavity was void, one CTV cap was in the cone (*out*) conformation and the other adopted a flexible saddle conformation (see section 2.1).<sup>31</sup> This led to an imploded cryptophane that can recover its usual *out-out* conformation in the presence of a suitable guest (Figure 10). The energy barrier for the cone-saddle/cone-cone conversion was  $99 \text{ kJ mol}^{-1}$  ( $\Delta H^\ddagger = 70 \text{ kJ mol}^{-1}$  and  $\Delta S^\ddagger = -98 \text{ J K}^{-1} \text{ mol}^{-1}$ ).

This conformational mobility has only been reported for a few examples; however, it can also occur in small cryptophanes and is particularly active in water-soluble compounds, free from guest molecules, where hydrophobic forces prevail. Huber et al. demonstrated that, under degassed conditions, cryptophane **120** in water exhibited  $^1\text{H}$  NMR signals in the aromatic region characteristic of a CTV in the saddle conformation.<sup>64</sup> Because of steric hindrance, the

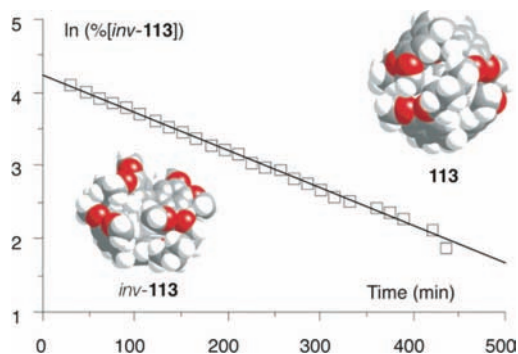


**Figure 9.** Evolution of a  $\text{CHCl}_3$  solution of *inv*-**113**, and CPK models of the MM-calculated structures of **113** and *inv*-**113**.

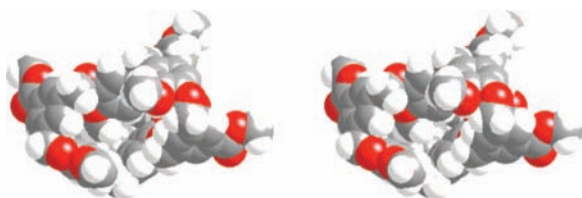


**Figure 10.** Stereoview of the X-ray molecular structure of the imploded cryptophane **11**.

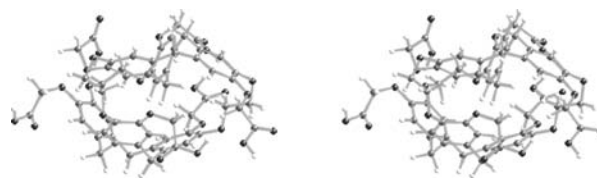


**Figure 11.** Stereoview of the calculated structure of cryptophane **120** in the cone-saddle conformation.

complete inversion of one CTV unit is unlikely, and the CTV is restrained to partial inversion, leading to the cone-saddle conformation of the cryptophane (Figure 11). The authors reported a half-life time of 5 days at 293 K for the cone-saddle/cone-cone isomerization process.

### 5.3. Molecular Structures of Cryptophane-A 1 and Related Ones

From NMR experiments in solution, an average conformation of the molecule is usually observed. Nevertheless, an X-ray crystal structure determination can be essential to examine precise conformational aspects of the host-guest system. Unfortunately, because of their spherical structure and the presence of one or more substrates in the molecular cavity (even small guests such as  $\text{N}_2$ ,  $\text{O}_2$ , or  $\text{H}_2\text{O}$  might be present), the cryptophanes very often give crystals of poor quality for X-ray diffraction analysis. To our knowledge, less than a dozen X-ray crystal structures of cryptophanes are currently reported in the literature. A significant point, often proposed to discuss the properties of complexation, is the size of the cavity and the size of the openings accessible to the substrate. For this purpose, solid-state structures determination can be very useful. Unfortunately, the size of the windows varies as a function of the conformation of the linkers and the other substituent, and any assertion on the size of the openings in the hosts must be considered with precaution; computational investigations are thus helpful complementary tools.

The structures of the cryptophane-A family are interesting, as they precisely present all the possible cases in terms of conformation of the linkers. Cryptophane-A (**1**) and related cryptophanes **153–155**, whose structures are presented in Figure 12, possess the same skeleton and differ only in their peripheral substituents. Cryptophanes **153–155** were synthesized with low yields using the *template method* described in section 2.2.<sup>79</sup>

Typically, the  $\text{CHCl}_3@1$  complex exists in three different crystalline forms (see section 7.3).<sup>80</sup> The crystals differ in the number of interstitial solvent molecules and the conformations of the  $-\text{OCH}_2\text{CH}_2\text{O}-$  linkers of the host (Figure 13). These solvates suggest that conformational changes around C-C bonds are close in energy, and it is difficult to establish that bound and free host can be simply described by a single conformation. It is interesting to note that in all three forms the C-H bond of the encapsulated  $\text{CHCl}_3$  is aligned with the  $C_3$  axis of the host. The orientation and the dynamics of the  $\text{CHCl}_3$  guest inside the cavity of cryptophanes have been investigated further by the groups of Kowalewski and Goodson by means of NMR experiments and by Cavagnat and co-workers using Raman microspectrometry (see section 7).

In the solid state, cryptophane complexes  $\text{CH}_2\text{Cl}_2@153$ ,  $\text{CHCl}_3@154$ , and  $\text{CHCl}_3@155$  display, respectively, *aga* (*anti, gauche, anti*), *aaa* (*anti, anti, anti*), and *gag* (*gauche, anti, gauche*) conformations for their ethylenedioxy bridges





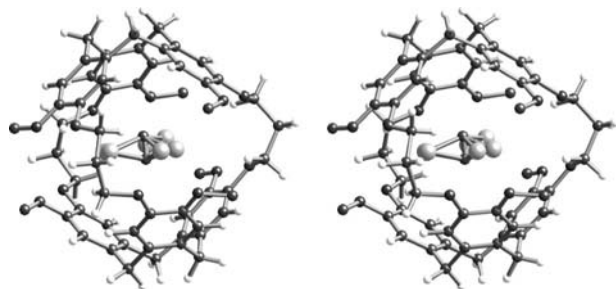


**Figure 16.** Stereoview of the X-ray molecular structure of the  $\text{CHCl}_3$ @cryptophane-E (**2**) complex showing the two equivalent orientations of the  $\text{CHCl}_3$  guest molecule.

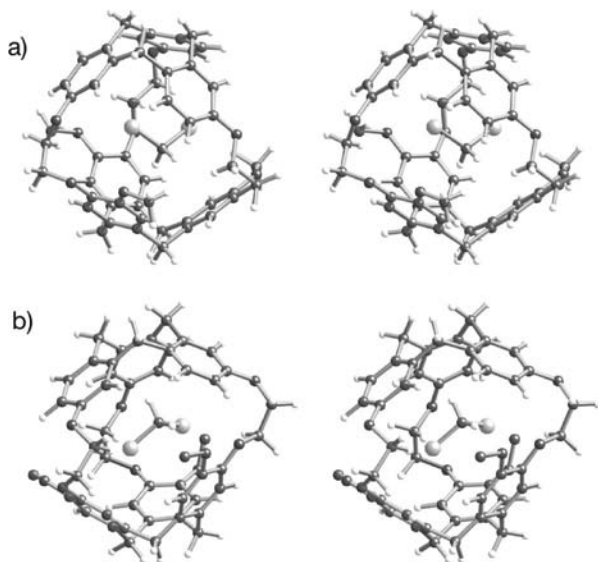


**Figure 17.** Stereoviews of the X-ray molecular structure of (a)  $\text{CH}_2\text{Cl}_2$ @cryptophane-C (**54**) (*anti*) and (b)  $\text{CH}_2\text{Cl}_2$ @cryptophane-D ((+)-**55**) (*syn*) complexes.

chlorine atoms of the guest are located in the central equatorial plane (Figure 16).<sup>81</sup> From cryptophane-E (**2**) in a  $\text{CH}_2\text{Cl}_2/\text{CHCl}_3$  mixture, the radical cation  $\text{CHCl}_3@2^{+\cdot}$  was formed electrochemically to give a charge-transfer complex between the cryptophane  $2^{+\cdot}$  and anionic species.<sup>82</sup> Crystals of  $[\text{CHCl}_3@2^{+\cdot}][(\text{PF}_6^-)]$  were obtained by electrocrystallization in acetonitrile. The structure of the cryptophane moiety thus obtained is very close to that observed in the  $\text{CHCl}_3@2$  complex. Exchanging  $\text{CHCl}_3$  for  $\text{CH}_2\text{Cl}_2$  and using a larger anion, namely  $\text{Mo}_6\text{Br}_{14}^{2-}$  or  $\text{Re}_6\text{S}_5\text{Cl}_9^-$ , led to more complex structures involving radical cation complex  $\text{CH}_2\text{Cl}_2@2^{+\cdot}$ , anion, and solvent molecules (acetonitrile). With the divalent anion  $\text{Mo}_6\text{Br}_{14}^{2-}$ , a supramolecular assembly was formed with infinite sequences  $\{(\text{CH}_3\text{CN})_n[\text{CH}_2\text{Cl}_2@2^{+\cdot}][\text{Mo}_6\text{Br}_{14}^{2-}][\text{CH}_2\text{Cl}_2@2^{+\cdot}](\text{CH}_3\text{CN})_n\}$ . A discrete structure was obtained in the case of  $\{[\text{CH}_2\text{Cl}_2@2^{+\cdot}][\text{Re}_6\text{S}_5\text{Cl}_9^-]\}$ .<sup>83</sup>

The only example of solid-state structures reported for an *anti/syn* pair concerns cryptophane-C (**54**)<sup>84</sup> and cryptophane-D (**55**),<sup>85</sup> whose  $\text{CH}_2\text{Cl}_2$  inclusion complexes were analyzed (Figure 17). Interestingly,  $\text{CH}_2\text{Cl}_2@55$  spontaneously resolved to give the pure enantiomers ( $\text{CH}_2\text{Cl}_2@(+)-55$  was studied by X-ray diffraction), whereas  $\text{CH}_2\text{Cl}_2@54$  crystallizes in the centrosymmetric space group  $P2_1/n$ . The ethylenedioxy bridges adopt *agg* conformations in  $\text{CH}_2\text{Cl}_2@54$ , and are *ggg* in  $\text{CH}_2\text{Cl}_2@55$ . The  $\text{CH}_2$  group of the  $\text{CH}_2\text{Cl}_2$  entrapped molecule in  $\text{CH}_2\text{Cl}_2@55$  is oriented toward the cyclotribenzylene cap devoid of  $\text{OCH}_3$  groups,

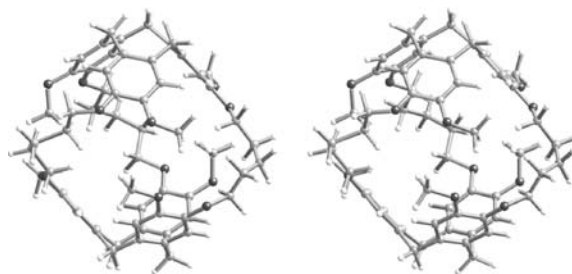


**Figure 18.** Stereoview of the X-ray molecular structure of cryptophane-O (**113**) (undefined disordered encapsulated species are omitted).

whereas the  $\text{CH}_2$  group faces the methoxylated CTV unit in  $\text{CH}_2\text{Cl}_2@54$ . In these two examples, the  $\text{CH}_2\text{Cl}_2$  molecule is tightly bound in the cavity with close contacts with the aromatic rings of the host.

Increasing the size of the cryptophane host may lead to more flexible molecules and favors disorder in the solid. For instance, cryptophane-O (**113**) exhibited the expected structure with ill-defined disordered guests probably because of the increased size of the cavity (Figure 18).<sup>32</sup>

## 6. Binding Properties of Cryptophanes

The description of guest complexation by cryptophane hosts was not immediately obvious. Indeed, it took a couple of years between the synthesis of the first cryptophane and characterization of the encapsulation of a guest inside the molecular cavity. NMR spectroscopy has proven to be the tool of choice to study the process of complexation in solution, but the solvent must also be considered as an efficient substrate that competes with the guest. The answer has been to use a bulky solvent molecule, which cannot enter the cavity of the cryptophanes. 1,1,2,2-Tetrachloroethane is now widely used for investigating the encapsulation, in organic solution, of suitable guests in the smallest cryptophanes-A (**1**), -E (**2**), and -C (**54**) and related ones.<sup>86</sup> Interestingly, cryptophanes are reasonably soluble in solvents such as  $\text{CHCl}_3$  or  $\text{CH}_2\text{Cl}_2$  that can enter the molecular cavity, whereas a bulky solvent such as 1,1,2,2-tetrachloroethane solubilizes the host only sparingly.

Since the first complexation experiments performed with cryptophane-A (**1**),<sup>52</sup> cryptophane-C (**54**),<sup>84,85,87</sup> or cryptophane-E (**2**),<sup>88</sup> the study of the binding properties of cryptophanes has been the subject of much attention. A large number of the investigations were done by chemists, and more recently by spectroscopists, who have disclosed the numerous advantages that these molecules offer for the study of the physical behavior of a single molecular species isolated in the confined space of a molecular cavity. Additional knowledge has also been gained from recent advances in solid-state NMR and vibrational spectroscopy as well as computational methods, which allow sensitive investigation of these systems both in the solid state and in solution. In this section, we wish to report only briefly on the early results, which have already been summarized in several review articles, and we will focus in the next section more particularly on physical aspects of the complexation (dynamics, studies in solid or mesophases). Section 8 will review aspects of chiral recognition by cryptophane hosts. Section 9 is devoted to the significant case of the xenon guest.



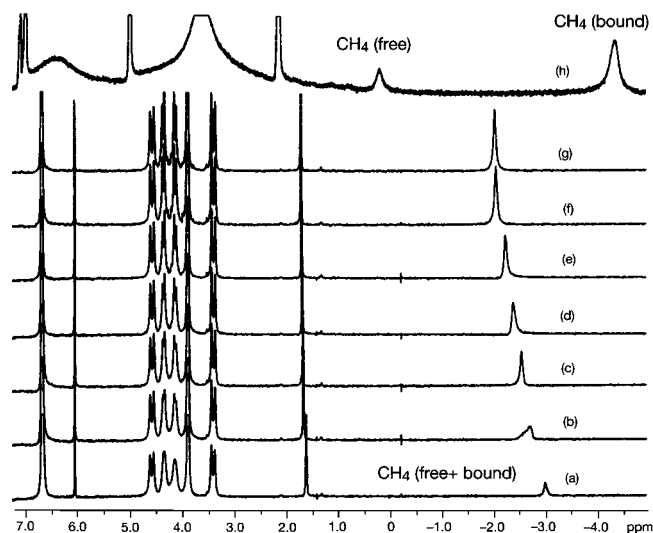


**Figure 19.**  $^1\text{H}$  NMR spectra (200 MHz,  $\text{C}_2\text{D}_2\text{Cl}_4$ , 298 K) of the  $\text{CH}_4$ @cryptophane-A **1** complex for an increasing molar ratio of guest/**1** from (a) 0.33 to (g) 1.35. (h) Spectrum at 199 K in  $\text{C}_2\text{D}_2\text{Cl}_4$ /toluene for a guest/**1** ratio = 0.9 (Reprinted from ref 9, Copyright 1993, with permission from Wiley-VCH).

### 6.1. Complexation of Small Neutral Molecules

Until the mid-1990s, these studies were mainly limited to small cryptophanes in solvents which did not compete with the guest under study. For instance, the first evidence of guest encapsulation was reported for cryptophanes-A (**1**), -C (**54**), and -E (**2**) with neutral molecules such as  $\text{CHCl}_3$ ,  $\text{CH}_2\text{Cl}_2$ ,  $\text{CHFCIBr}$ , or  $\text{CH}_4$ .<sup>14,15,62</sup> The complexation of methane by **1** was evidenced by  $^1\text{H}$  NMR experiments and was characterized by the high-field-shifted average signal of free and bound  $\text{CH}_4$  under fast exchange at 298 K (Figure 19).<sup>9</sup> The chiral discrimination of the two enantiomers of  $\text{CHFCIBr}$  by the enantioenriched *anti*-cryptophane-C (**54**) illustrates the unique behavior of these supramolecular systems (see section 8). More recently, the discovery of the binding of xenon in organic or aqueous solution by cryptophanes opened a new and fascinating field of investigation (see section 9).

The complexation of a nonpolar substrate by a cryptophane host depends mainly on the size of the guest with respect to the size of the cavity, and on the size of the portals through which the guest can enter and leave the cavity. The association is stabilized mainly through van der Waals forces. The structure and the symmetry of the guest, the electronic density of the aromatic rings of the host, and solvation effects are also important factors that may influence the formation of the complexes. All these parameters, however, are difficult to evaluate separately, but the knowledge of the guest size to cavity size ratio (occupancy factor) often provides an indication of an effective encapsulation process.<sup>89</sup> Figure 20 shows the stability curves for different complexes of cryptophane-E (**2**) and cryptophane-C (**54**), as a function of the size of the guest:  $\text{CH}_2\text{Cl}_2$  ( $V_{\text{vdw}} \approx 58 \text{ \AA}^3$ ) has better affinity for cryptophane-C (**54**) ( $V_{\text{vdw}}^{\text{cavity}} \approx 95 \text{ \AA}^3$ )<sup>90</sup> whereas  $\text{CHCl}_3$  ( $V_{\text{vdw}} \approx 72 \text{ \AA}^3$ ) is more suited for cryptophane-E (**2**) ( $V_{\text{vdw}}^{\text{cavity}} \approx 121 \text{ \AA}^3$ ), in good agreement with the 55% occupancy factor expected for an optimal binding process in solution.

Molecular dynamics and free-energy perturbation simulations of the guest@cryptophane-E (**2**) complexes, where the guest was  $\text{CH}_2\text{Cl}_2$ ,  $\text{CHCl}_3$ , or  $\text{CCl}_4$ , have been performed for the gas phase and in  $\text{CHCl}_3$  solution. Despite conformational rearrangement during the complexation process, the

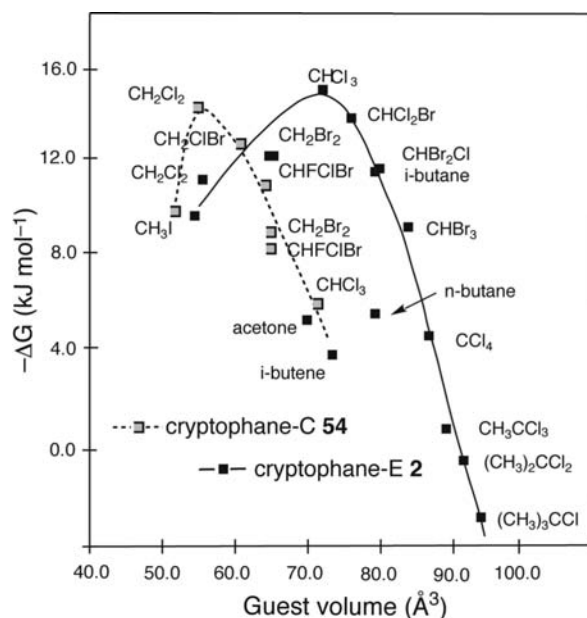


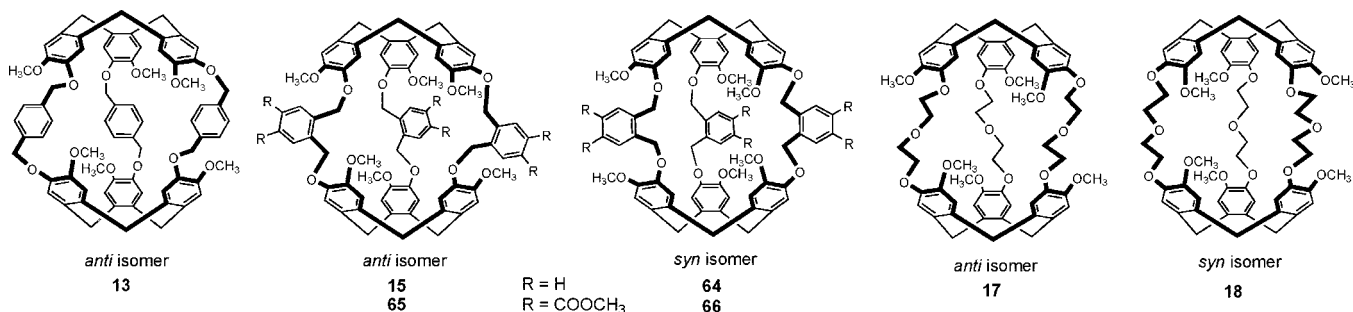
**Figure 20.** Free energy of association,  $\Delta G$ , for complexes of cryptophane-E (**2**) and -C (**54**) with neutral guests at 300 K in  $\text{C}_2\text{D}_2\text{Cl}_4$ .

host cavity is rather rigid and it appeared that  $\text{CHCl}_3$  is better complexed than  $\text{CH}_2\text{Cl}_2$ , in accordance with the experiment. In contrast, the calculation indicated an energetic preference for the  $\text{CCl}_4$ @**2** complex over a  $\text{CHCl}_3$ @**2** complex, a result inconsistent with experiment, where  $\text{CCl}_4$  shows no affinity for host **2**. This discrepancy was attributed to the difficulty to fit correctly the Van der Waals parameters of the Cl atom in the simulation procedure.<sup>91</sup>

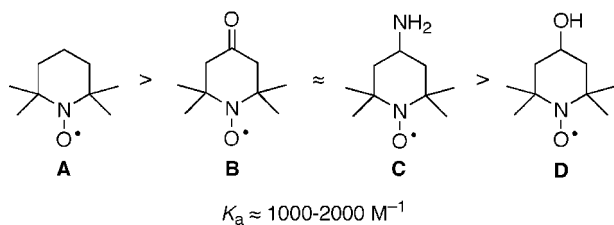
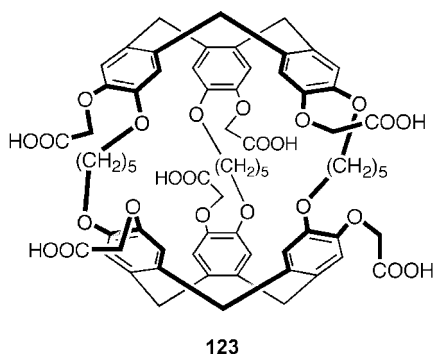
Akabori and co-workers investigated by  $^1\text{H}$  NMR spectroscopy the complexation of alkanes in the cavity of cryptophanes with xylylene or diethylenetrioxo linkers (Chart 5).<sup>35</sup> The efficiency of the encapsulation process is strongly dependent on whether the structure is *anti* or *syn* and on the substitution of the aromatic linkers. *syn*-Cryptophanes **64** and **66** form complexes with several methyl-substituted butane and pentane derivatives. Complexes were observed by  $^1\text{H}$  NMR spectroscopy under slow exchange conditions at 210 K, and free energies of complexation for **64** and **66** are given in Table 1. Similar investigations showed that *anti*-cryptophanes **13**, **15**, and **65** do not form complexes with these substrates, whereas cryptophanes **17** (*anti*) and **18** (*syn*), bearing diethylenetrioxo linkers, encapsulate efficiently some of them (Table 1). These experiments were run in  $\text{CD}_2\text{Cl}_2$ , a competitive solvent, which easily enters the cryptophane cavity. Therefore, only apparent binding constants were accessible.

Garel and co-workers reported an interesting EPR study on complexes of cryptophane **123** bearing six carboxylic acid groups with aminoxyl radicals (Figure 21). Cryptophane **123** binds readily, and reversibly, aminoxyl radicals **A–D** in water to form inclusion complexes.<sup>92</sup> EPR spectroscopy is particularly well adapted to study the exchange process, which is slow on the EPR time scale. The nitrogen hyperfine coupling of the radicals was lower in the complex than in the free state, due to the more hydrophobic environment of the  $\text{N}-\text{O}^\bullet$  group in the inner cavity compared to bulk water.

The same host **123** binds tetraalkyl derivatives  $\text{M}(\text{alk})_4$ , where  $\text{alk} = \text{CH}_3$  and  $\text{C}_2\text{H}_5$  and  $\text{M} = \text{Si}, \text{Ge}, \text{Sn},$  and  $\text{Pb}$ .<sup>93</sup> Inclusion of the guests was evident by the observation of the high-field-shifted  $^1\text{H}$  NMR signal of the alkyl group of

Chart 5. *anti*- and *syn*-Cryptophanes Studied by Akabori and Co-workersTable 1. Free Energy,  $\Delta G$  (kJ/mol), for Complexes of Alkanes with Cryptophanes 17, 18, 64, and 66 at 210 K in  $\text{CD}_2\text{Cl}_2$ 

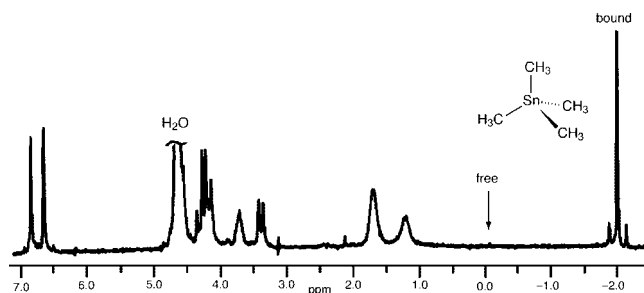
guest	17	18	64	66
2,2-dimethylbutane	-2.97	-3.01	-7.32	-8.16
3-methylpentane			-9.79	-9.25
2,3-dimethylbutane			-2.22	-1.67
3,3-dimethylpentane	-5.48	-5.36	-7.32	-7.36
3-ethylpentane			-7.32	-9.16
2,2,3-trimethylbutane	-6.57	-7.03		
2,2,3,3-tetramethylbutane	-6.15	-6.23		

Figure 21. Host **123** and guests **A–D** investigated by EPR spectroscopy.

the guest (Figure 22). Typical values are reported in Table 2. This host is also able to bind cationic organic guests such as tetraalkylammonium and -phosphonium (Table 2). The important topic of ammonium recognition by cryptophane hosts is more accurately developed in the following section.

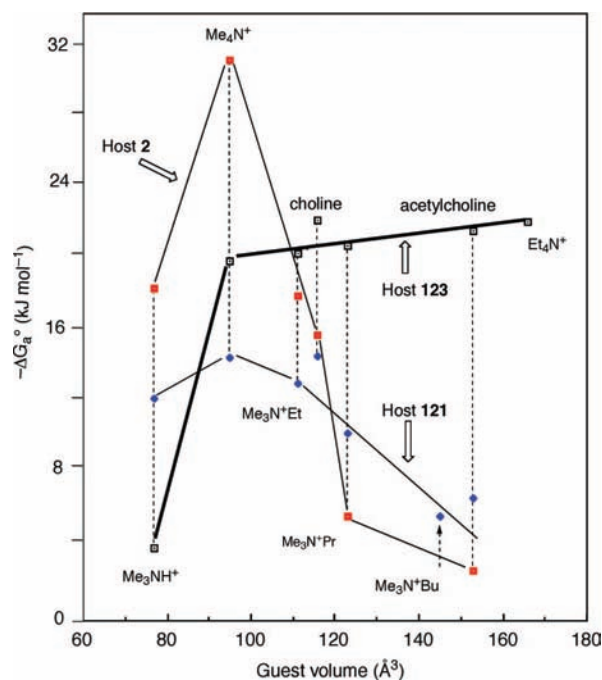
## 6.2. Complexation of Ammonium Guests

In addition to the efficient encapsulation of halomethanes and volatile organic compounds (VOCs), the cryptophanes are good candidates for the recognition of organic ammonium cations of suitable size. Generally, ammonium cations associate even more strongly than neutral guests, and this holds true for  $\text{C}_2\text{H}_2\text{Cl}_4$  and aqueous medium when water-soluble hosts are used. For instance, at 293 K, cryptophane-E (**2**) strongly binds tetramethylammonium with an unprecedented binding constant,  $K_a = 475000 \text{ M}^{-1}$ , and trimethylammonium with a significantly lower binding constant,  $K_a = 1600 \text{ M}^{-1}$ .<sup>36</sup> The water-soluble cryptophane-E-( $\text{OCH}_2\text{CO}_2\text{H}$ )<sub>6</sub> (**121**) and cryptophane-O-( $\text{OCH}_2\text{CO}_2\text{H}$ )<sub>6</sub> (**123**) easily

Figure 22.  $^1\text{H}$  NMR spectrum (200 MHz; 300 K) of a mixture of cryptophane **123** and  $\text{Sn}(\text{CH}_3)_4$  in  $\text{D}_2\text{O}$ - $\text{NaOD}$  (pH = 7).

encapsulate choline and acetylcholine, with an increase of the binding constants on going from cryptophane **121** to cryptophane **123** (Figure 23). This is a general trend for substrates in the size range  $\text{Me}_4\text{N}^+$  to  $\text{Et}_4\text{N}^+$  and acetylcholine, which makes cryptophane-O-( $\text{OCH}_2\text{CO}_2\text{H}$ )<sub>6</sub> (**123**) one of the best artificial water-soluble host for these substrates.

Several factors are involved in the association of ammonium guests; cation- $\pi$  interactions are assumed to be responsible for the stabilization of these complexes. However, other cation interactions, especially those with peripheral oxygen atoms, are likely to play a fundamental role in the

Figure 23. Free energy of association,  $\Delta G_a^\circ$ , at 300 K for complexes of cryptophanes **2**, **121**, and **123** with ammonium guests (Reprinted with permission from ref 10. Copyright 1993 American Chemical Society).



**Table 2.**  $^1\text{H}$  NMR Chemical Shifts (ppm) in  $\text{D}_2\text{O}-\text{NaOD}$  of Free ( $\delta_{\text{free}}$ )  $\text{M}(\text{CH}_3)_4$  and Bound ( $\delta_{\text{bound}}$ )  $\text{M}(\text{CH}_3)_4@123$  ( $\text{M} = \text{C}, \text{N}, \text{P}, \text{Si}, \text{Ge}, \text{Sn}, \text{Pb}$ )<sup>a</sup>

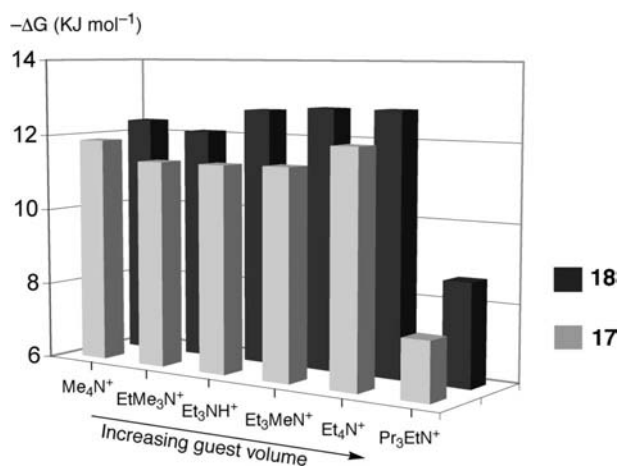
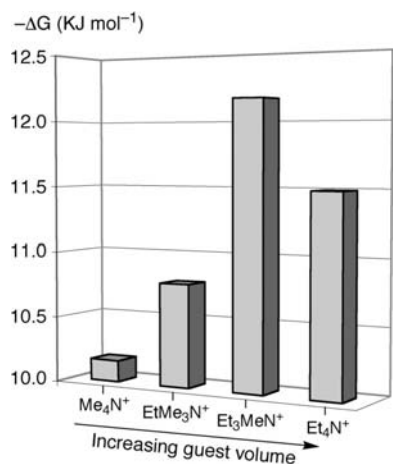
guest	$(\text{CH}_3)_4\text{C}$	$(\text{CH}_3)_4\text{N}^+$	$(\text{CH}_3)_4\text{P}^+$	$(\text{CH}_3)_4\text{Si}$	$(\text{CH}_3)_4\text{Ge}$	$(\text{CH}_3)_4\text{Sn}$	$(\text{CH}_3)_4\text{Pb}$
$\delta_{\text{free}}$	0.79	2.91	1.71	-0.12	-0.07	-0.07	0.39
$\delta_{\text{bound}}$	-1.50	0.52	-0.54	-2.20	-2.10	-2.00	-1.51
$\Delta\delta$	2.29	2.39	2.25	2.08	2.03	1.93	1.90

<sup>a</sup>  $\Delta\delta = \delta_{\text{free}} - \delta_{\text{bound}}$ .

**Table 3.** Kinetic Parameters for Association and Dissociation of  $\text{CHCl}_3$  and Ammonium Picrates in the Presence of Hosts **2** and **27** at 293 K in  $(\text{CDCl}_2)_2$  (Reproduced from Ref 36 (<http://dx.doi.org/10.1039/b211363e>) by Permission of The Royal Society of Chemistry)

guest	host	$k_a/(\text{M}^{-1} \text{s}^{-1})$	$k_d/\text{s}^{-1}$	$\Delta G_a^\ddagger/(\text{kJ mol}^{-1})$	$\Delta G_d^\ddagger/(\text{kJ mol}^{-1})$	$(t_{1/2})_\infty^a$
$\text{CHCl}_3$	<b>2</b>	760	$1.27^b$	55.6	71.2	0.55 s
	<b>27</b>	$1.16 \times 10^{-1}$	$4.88 \times 10^{-4}$	77.0	90.4	24 min
$(\text{CH}_3)_3\text{NH}^+$	<b>2</b>	76.6	$4.81 \times 10^{-2}$	61.9	79.2	14 s
	<b>27</b>	$2.32 \times 10^{-3}$	$1.99 \times 10^{-6}$	86.6	103.8	97 h
$(\text{CH}_3)_4\text{N}^+$	<b>2</b>	7.2	$1.49 \times 10^{-5}$	67.8	98.7	13 h
	<b>27</b>	$2.88 \times 10^{-3}$	$1.0 \times 10^{-8}$	85.4	116.3	792 days

<sup>a</sup> Half-life of the complex at infinite dilution. <sup>b</sup> Measured from line shape simulation of the free and complexed guest signals.

**Figure 24.** Free energy of association,  $\Delta G$  (210 K), for complexes of cryptophanes **17** and **18** with ammonium guests.**Figure 25.** Free energy of association,  $\Delta G$  (210 K), for complexes of cryptophane **13** with tetraalkylammonium guests.

stabilization of the complexes. McCammon and co-workers extensively investigated the binding dynamics of cryptophanes with ammonium salts through computational methods (see section 7.2).

Alternatively, Garcia et al. used an experimental approach to discriminate the main stabilizing contributions between the ammonium guests and cryptophanes.<sup>36</sup> Their approach consisted of the synthesis of the new cryptophane molecule

**27**, whose internal cavity size is similar to that of cryptophane-E (**2**) but where the six methoxy groups have been replaced by methylthio groups. This leads to a decrease of the negative charge density in the equatorial region of the host and also significantly decreases the size of the portals used by the guest molecule to access and escape from the cavity. When performing complexation experiments with chloroform, trimethylammonium picrate, or tetramethylammonium picrate, a drastic change of the binding properties of these guests was observed with host **27** with respect to cryptophane-E (**2**) in 1,1,2,2-tetrachloroethane-*d*<sub>2</sub>. Indeed, whereas the half-life time of the complex is about 0.55 s for chloroform in cryptophane-E (**2**), it reaches 24 min in cryptophane **27**. Even more impressive is the half-life time of 13 h for tetramethylammonium in **2**, which reaches 792 days in **27** (Table 3).

These results suggest that, with the use of appropriate substituents, cryptophanes may act as *carcerands*.<sup>94</sup> Determination of the thermodynamic parameters for these systems also suggests a change in the nature of the driving force as the guest changes. For instance, ammonium complexation by cryptophane is strongly entropy-driven, whereas chloroform complexation is enthalpy driven. In addition, these results shed light on the main stabilizing factors for encapsulation of ammonium salts. It was clearly demonstrated that ammonium salts interact also with the oxygen or sulfur atoms present in the structure. Thus, cation- $\pi$  interactions between guest and CTV units are not the only contribution to be considered for explaining the efficient complexation of ammonium salt by cryptophanes.

Akabori and co-workers have shown that hosts **17** and **18** in  $\text{CH}_2\text{Cl}_2$  extracted alkylammonium ions from water solution.<sup>34</sup> Better results were obtained with **18** and  $(\text{CH}_3)_4\text{N}^+$  ion (67.5% extracted). However, extraction efficiency drops dramatically with other cations:  $(\text{CH}_3)_4\text{N}^+ > (\text{CH}_3)_3\text{NH}^+ > (\text{CH}_3)_2\text{NH}_2^+ > \text{CH}_3\text{NH}_3^+ > \text{NH}_4^+$ . The same trend was observed with **17**, which extracts  $(\text{CH}_3)_4\text{N}^+$  moderately (17.8% extracted).  $^1\text{H}$  NMR experiments showed that the complexation of ammonium guests is under slow exchange conditions at the NMR time scale at 210 K in  $\text{CD}_2\text{Cl}_2/\text{CD}_3\text{OD}$  (9:1) solution. The apparent stability constants and thermodynamic parameters were estimated from the temperature dependence of the  $^1\text{H}$  NMR spectra. The relationship between the free energy of complexation and the volume of the ammonium guest demonstrates the somewhat low

selectivity, due to the size of the cavity, when compared for example to the case for cryptophane-E (**2**). A slightly higher stability of the complexes with the *syn*-isomer **18** was observed with regard to the case for the *anti*-isomer **17** (Figure 24).

The same experiments were performed with xylylene-bridged cryptophanes (see Chart 5).<sup>33</sup> The upfield shifts of the proton resonances of the  $\text{Et}_3\text{MeN}^+$ ,  $\text{Et}_4\text{N}^+$ ,  $\text{EtMe}_3\text{N}^+$ , and  $\text{Me}_4\text{N}^+$  ions were characteristic of their encapsulation by cryptophane **13**. Due to competition with the solvent ( $\text{CD}_2\text{Cl}_2/\text{CD}_3\text{OD}$ ; 9:1), only apparent stability constants were estimated, and these showed a higher selectivity for  $\text{Et}_3\text{MeN}^+$  (Figure 25). An interesting point was that the entropy values of the complexation process are positive for the small cations  $\text{Me}_4\text{N}^+$  and  $\text{EtMe}_3\text{N}^+$  and negative for the larger guests  $\text{Et}_3\text{MeN}^+$  and  $\text{Et}_4\text{N}^+$ . This difference was attributed to the more suitable size of the former cations for the cavity of **13**, which led to a favorable entropic contribution. The affinity of tetramethylammonium  $\text{Me}_4\text{N}^+$  for cryptophanes **15** (*anti*) and **66** (*syn*) has been reported, but no complex has been detected with *anti*-cryptophane **65**.

### 6.3. Complexation of Metal Cations

Until recently, the complexation of neutral molecules or ammonium ions by cryptophane hosts has been extensively studied. Curiously, the complexation of metal cations had not been observed until the investigations of Akabori and Weber. This could be a consequence of several factors, such as finding a suitable solvent for metal salts, which does not compete with the metal guest. In the first article published in 1996, Akabori and co-workers reported that dichloromethane solutions of cryptophanes **17** and **18**, bearing diethylenetrioxo linkers, are able to extract alkali metal ions from water.<sup>34</sup> Their extraction abilities favor the cesium cation, with better results for the *syn*-cryptophane **18** than for the *anti*-cryptophane **17**. More recently, Weber et al. synthesized the tailor-made cryptophane **10** with three *endo*-carboxylic acid groups for cation recognition. The *syn*-isomer **10**, an achiral molecule, extracts a number of different metal ions with a large affinity for  $\text{Ca}^{2+}$  and  $\text{Sr}^{2+}$  and almost no affinity for  $\text{Na}^+$ , following the sequence  $\text{Ca}^{2+} \sim \text{Sr}^{2+} > \text{Mg}^{2+} > \text{Ba}^{2+} > \text{Cs}^+ > \text{Na}^+$  (Figure 26).<sup>30</sup> The high affinity of **10** for  $\text{Ca}^{2+}$  and  $\text{Sr}^{2+}$  is in good agreement with their strong interaction with carboxylate anions and is a conse-

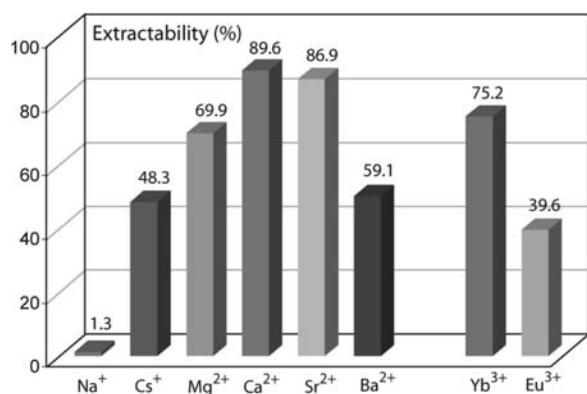


**Figure 26.** Extractability of metal ions with cryptophane **10**:  $[\text{M}(\text{NO}_3)_n] = 1 \times 10^{-4}$  M ( $\text{M} = \text{Na}, \text{Cs}, \text{Mg}, \text{Ca}, \text{Sr}, \text{Ba}$ ), pH 8.6 (TEA/HCl buffer);  $[\text{M}(\text{NO}_3)_3] = 1 \times 10^{-4}$  M ( $\text{M} = \text{Eu}, \text{Yb}$ ), pH 5.6 (MES/NaOH buffer);  $[\mathbf{10}] = 1 \times 10^{-3}$  M in  $\text{CHCl}_3$  (Reprinted from ref 30, Copyright 2003, with permission from Wiley-VCH).

quence of the preorganization of the host, in which the *endo*-oriented carboxylic acid functions favor the 1:1 complex formation. Furthermore, for the same reasons, the trivalent lanthanide ions  $\text{Yb}^{3+}$  and  $\text{Eu}^{3+}$  are also efficiently extracted by cryptophane **10**, whose binding properties are comparable to that of *spherand* hosts.<sup>95</sup>

### 6.4. Complexation of Anion Guests

The electron-rich molecular cap of the CTV units makes cryptophanes inappropriate for encapsulation of anionic species. However, Holman and co-workers modified cryptophane-E (**2**) by adding six  $[\text{Cp}^*\text{Ru}]$  moieties, thus giving rise to cryptophane **156** with an acidic internal cavity suitable for the encapsulation of anions such as  $\text{CF}_3\text{SO}_3^-$  and  $\text{SbF}_6^-$  (Figure 27).<sup>96</sup> To our knowledge, molecule **156** is the only example of a cryptophane derivative reported in the literature showing a high affinity for anionic species. As a consequence of the metalation, the volume of the molecular cavity in **156** is also slightly enlarged relative to that of cryptophane-E (**2**), thus favoring the complexation of large anionic guests. The enthalpy and entropy of activation of complexation for the  $[\text{CF}_3\text{SO}_3^- @ \mathbf{156}]^{5+}$  complex have been determined in  $\text{CD}_3\text{NO}_2$ , giving  $\Delta H^\ddagger = 73.2$  kJ mol<sup>-1</sup> and  $\Delta S^\ddagger = 8.4$  J K<sup>-1</sup> mol<sup>-1</sup> ( $\Delta G^\ddagger_{298\text{K}} = 75.2$  kJ mol<sup>-1</sup>). These values are significantly larger than those obtained for the  $\text{CHCl}_3 @ \mathbf{2}$  complex, as a consequence of the size of the anionic guest and an increase of the rigidity of the host upon metalation. Anions such as  $\text{PF}_6^-$  or  $\text{SbF}_6^-$  were found to compete with the triflate anion, whereas the binding of other anions seems less efficient depending on the size of the guest. For instance, halide or nitrate anions are not recognized by the cavity of **156** and larger anionic species such as  $\text{CH}_3\text{CH}_2\text{SO}_3^-$  showed smaller affinity than triflate.

## 7. Dynamics of the Guest in the Cryptophane Cavity

### 7.1. Investigations by NMR Spectroscopy

Particular attention has been devoted to the physical status and the behavior of a guest molecule in the confined space of the cryptophane cavity. For instance, Kowalewski and co-workers investigated the dynamics of reorientation of  $\text{CHCl}_3$  or  $\text{CH}_2\text{Cl}_2$  molecules inside the cavity of cryptophane-E (**2**). They first studied the kinetics of  $\text{CHCl}_3$  exchange between the complex and the bulk solution. Then, they performed an accurate measurement of the  $T_1$  carbon-13 relaxation time of the host and the guest and used the Lipari–Szabo model to interpret the tumbling motions of both molecules (Table 4). Similar values of the correlation times for the host (0.67 ns) and the bound guest  $\text{CHCl}_3$  (0.5 ns) have been reported by the authors, suggesting a strong dynamic coupling between the two partners. Thus, the  $\text{CHCl}_3 @ \mathbf{2}$  complex behaves as a unified system, on the time scale of molecular reorientation, with a strong anisotropic interaction between the CTV unit and the hydrogen of the encapsulated chloroform molecule.<sup>97</sup>

A different situation was observed with the  $\text{CH}_2\text{Cl}_2 @ \mathbf{2}$  complex. The approach described for the  $\text{CHCl}_3$  complex was applied to determine the correlation time of the encapsulated  $\text{CH}_2\text{Cl}_2$ . The drop in the correlation time of the bound  $\text{CH}_2\text{Cl}_2$  ( $\tau_c = 1.8$  ps) and the very short, but nonzero, motional parameter ( $S^2 = 0.02$ ) suggest that the reorientation dynamics of the bound  $\text{CH}_2\text{Cl}_2$  is only weakly

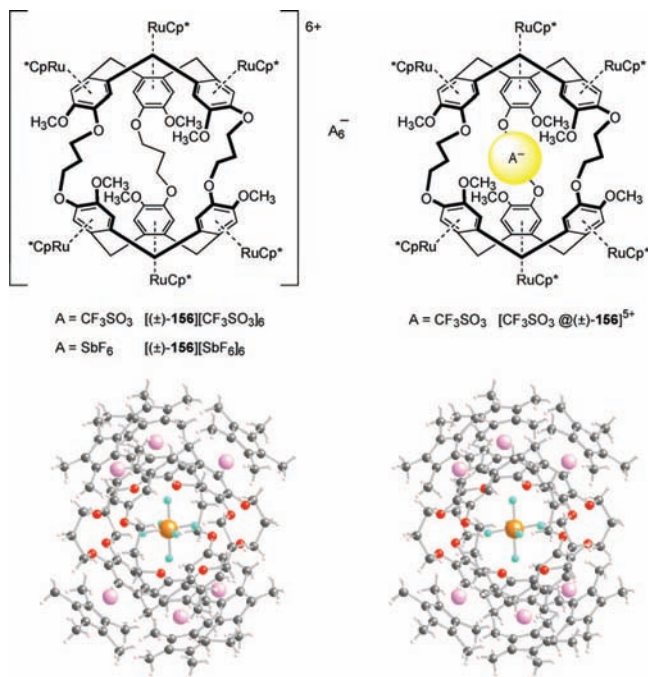


**Figure 27.** Anion complexation and stereoview of the X-ray structure of the inclusion complex  $\text{SbF}_6@156$ .

**Table 4.**  $^{13}\text{C}$  Longitudinal Relaxation Times,  $T_1$ , and Local Motional Parameters,  $S^2$  and  $\tau_e$ , Obtained from Lipari–Szabo Analysis of Relaxation Data of the Inclusion Complex  $\text{CHCl}_3@2^a$

carbon	$T_1$ (s) <sup>b</sup>	$S^2$	$\Delta S^2$ (%)	$\tau_e$ (ps)	$\Delta\tau_e$ (%)
ArCH <sub>2</sub>	0.148	0.79	6	56	55
OCH <sub>2</sub>	0.165	0.69	8	44	55
CCH <sub>2</sub> C	0.157	0.70	7	59	42
OCH <sub>3</sub>	0.589	0.065	12	15	13
bound $\text{CHCl}_3$	0.350 <sup>c</sup>	0.68	11	22	69

<sup>a</sup>  $\Delta S^2$  and  $\Delta\tau_e$  are the relative standard deviations of the parameter sets obtained from Monte Carlo simulation. <sup>b</sup> Measured at 14.1 T. <sup>c</sup> Free  $\text{CHCl}_3$ :  $T_1 = 11.9$  s.

**Table 5.**  $^{13}\text{C}$  Longitudinal Relaxation Times,  $T_1$ , and Local Motional Parameters,  $S^2$  and  $\tau_e$ , Obtained from the Analysis of the Relaxation Data of the Inclusion Complex  $\text{CH}_2\text{Cl}_2@2$  (Global Correlation Time  $\tau_M = 0.97$  ns)<sup>a</sup>

carbon	$T_1$ (s) <sup>b</sup>	$S^2$	$\Delta S^2$ (%)	$\tau_e$ (ps)	$\Delta\tau_e$ (%)
ArCH <sub>2</sub>	0.157	0.77	4	0.01	160
OCH <sub>2</sub>	0.167	0.72	5	8.8	104
CCH <sub>2</sub> C	0.159	0.76	4	0.01	194
bound $\text{CH}_2\text{Cl}_2$	4.02 <sup>c</sup>	0.02	16	1.8	58

<sup>a</sup>  $\Delta S^2$  and  $\Delta\tau_e$  are the relative standard deviations of the parameter sets obtained from Monte Carlo simulation. <sup>b</sup> Measured at 14.1 T. <sup>c</sup> Free  $\text{CH}_2\text{Cl}_2$ :  $T_1 = 10.3$  s.

coupled to the motion of the host. In other words, the molecular tumbling of the  $\text{CH}_2\text{Cl}_2$  molecule in the cavity of cryptophane-E **2** is significantly more pronounced than that of the chloroform guest (Table 5).<sup>98</sup> These experiments exemplify the importance of the size and symmetry of the guest in the binding properties of cryptophanes.

In the same article, the authors confirmed similar results in a preliminary study of the complexed cryptophane-E (**2**) in the solid state. They obtained very different  $^2\text{H}$  solid-state NMR spectra for deuterium labeled chloroform and dichloromethane. Each spectrum contains the contribution from the encapsulated guest as well as that of the interstitial  $\text{CDCl}_3$  or  $\text{CD}_2\text{Cl}_2$  molecules in the lattice. The encapsulated

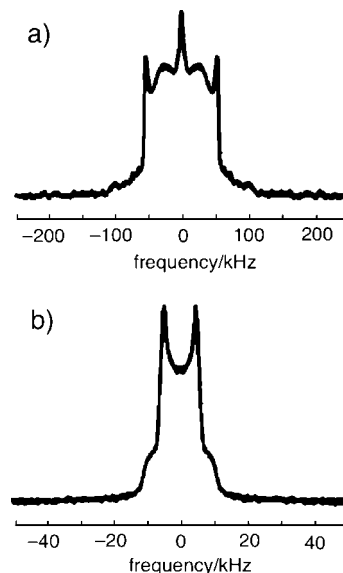


**Figure 28.**  $^2\text{H}$  solid state NMR spectra at 293 K of the inclusion complexes (a)  $\text{CDCl}_3@2$  and (b)  $\text{CD}_2\text{Cl}_2@2$  (Reprinted with permission from ref 86. Copyright 2002 American Chemical Society).

$\text{CDCl}_3$  exhibits a very broad signal, significantly larger than that obtained with  $\text{CD}_2\text{Cl}_2$ , indicating different tumbling motions of the guest within the host cavity (Figure 28).

This result is fully consistent with the observation made in the liquid state, where bound chloroform has a much more restricted motion than dichloromethane under the same experimental conditions. The large difference between the correlation times of the encapsulated  $\text{CHCl}_3$  measured in the solid state ( $\tau_e = 0.17$   $\mu\text{s}$ ) and in the liquid state ( $\tau_e = 22$  ps) was attributed to an increased rigidity of cryptophane-E (**2**) in the solid, which subsequently affects the mobility of the  $\text{CHCl}_3$  guest. In contrast, similar values of  $\tau_e$  were measured for the  $\text{CH}_2\text{Cl}_2$  guest in the solid state ( $\tau_e = 1.4$  ps at 283 K) and in the liquid state ( $\tau_e = 1.8$  ps at 273 K), suggesting a loosely bound complex. Such a difference probably arises from the smaller size of  $\text{CH}_2\text{Cl}_2$  vs  $\text{CHCl}_3$  and the lack of  $C_3$  symmetry in  $\text{CH}_2\text{Cl}_2$ . This has been further supported by a solid-state  $^{13}\text{C}$  NMR study of the chloromethane@cryptophane complexes using separated local-field NMR spectroscopy under magic angle spinning conditions (SLF MAS).<sup>99</sup> In these experiments, site resolved  $^1\text{H}$ – $^{13}\text{C}$  dipolar couplings in disordered inclusion complexes have been achieved, showing that the restricted motion of the engaged guests in the solid state is similar to that of the bound guests in solution (Figure 29). The orientations of the CH vectors in engaged  $\text{CHCl}_3$  and  $\text{CH}_2\text{Cl}_2$  are rather independent of the physical state of the system. It was also demonstrated that interstitial free  $\text{CHCl}_3$  molecules experience higher mobility with respect to their bound congeners.

Another interesting study was reported by Crassous and Hediger, who investigated the dynamics of chiral guests in the cavity of chiral *anti*-cryptophanes (see section 8.1). They studied the  $^{19}\text{F}$  relaxation rate of the free and bound  $\text{CHFClBr}$  molecules and considered the important contributions of chemical shift anisotropy (CSA) and dipolar coupling to the proton (DD) to measure the CSA-DD cross-correlated relaxation rates for both free and bound  $\text{CHFClBr}$ .<sup>100</sup> The determination of these parameters gave access to the correlation time  $\tau_c$  and the longitudinal relaxation time  $T_1$ . As observed previously for similar systems, especially with



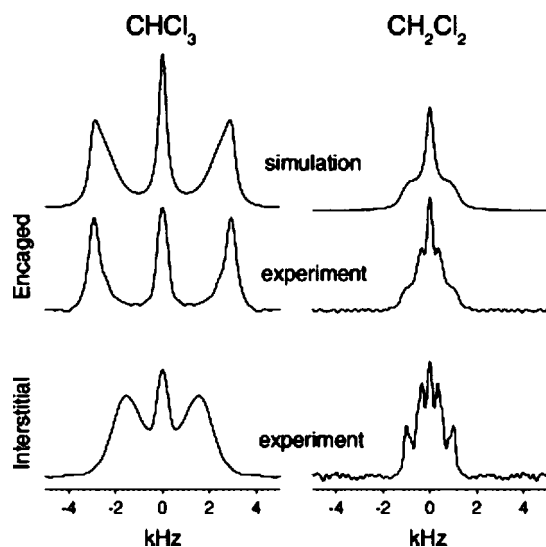


**Figure 29.** Site-resolved  $^1\text{H}$ - $^{13}\text{C}$  dipolar coupling from 2D-SLF MAS spectra of the  $\text{CHCl}_3@2$  and  $\text{CH}_2\text{Cl}_2@2$  complexes (Reprinted from ref 99a, Copyright 2004, with permission from Elsevier).

$\text{CHCl}_3$  as a guest, the authors reported a much shorter  $T_1$  relaxation time for the bound state, in accord with a more efficient relaxation process for the encaged substrate. Additionally, smaller values for  $\tau_c$  were found for both enantiomers of  $\text{CHFCIBr}$  trapped in the cavity of cryptophane-E- $(\text{SCH}_3)_6$  (**27**), suggesting a slowdown of the tumbling motion of the bound  $\text{CHFCIBr}$  ( $\tau_c = 0.62$  ns and  $\tau_c = 0.78$  ns for both diastereomeric complexes whose assignment was not reported) with respect to free  $\text{CHFCIBr}$  in solution ( $\tau_c = 0.27$  ns). These results were confirmed independently by measuring the tumbling correlation time  $\tau_c$  from the deuterium quadrupolar relaxation time  $T_q$  of deuterium labeled ( $\pm$ )- $\text{CDFCIBr}$  in the cavity of cryptophane **27**. These results are in good agreement with the conclusion reported previously by Kowalewski and co-workers with the  $\text{CH}_2\text{Cl}_2$  and  $\text{CHCl}_3@$ cryptophane complexes.

## 7.2. Computational Investigations

In a computational study of cryptophanes, published in 1996, McCammon and co-workers simulated the conformational behavior of the water soluble hexacarboxylic acid cryptophane-E **121** at the 20 ns scale, showing the importance of the fluctuations of the pore and cavity size on the binding of guests. Interestingly, it was also demonstrated that the pore size and fluctuations could affect the binding rates of large guests (i.e., guest radii larger than 1.6 Å in the case of host **121**), whereas for smaller guests (i.e., guest radii smaller than 1.6 Å) the rate constants were only diffusion controlled.<sup>101</sup> The nature of the guest molecule also plays an important role on the physical properties of the complex. McCammon, Kirchhoff, and co-workers examined by molecular dynamics simulation the physical behavior of the two nearly isomorphous guests neopentane and tetramethylammonium ion ( $\text{TMA}^+$ ) in the cavity of cryptophane **121** in water. They first compared the dynamics of the  $\text{TMA}^+@121$  complex with that of the free host including a water solvent molecule.<sup>102</sup> They showed that upon complexation the host becomes more rigid and, consequently, the release of the guest is more difficult, supporting the observed high affinity of  $\text{TMA}^+$  for host **121**. It must be underlined that the number of carboxylic acid and ionized carboxylate fragments also

contributes to the complexation process through Coulombic interactions. The authors showed that changing the nature of the guest influences the host–guest dynamics even though the structures of these complexes are rather similar. Compared to the previous case, the neopentane@**121** complex differs mainly by its charge; interaction of the guest with the carboxylate functions of the host in the case of  $\text{TMA}^+$  is prevalent but is inefficient with neopentane. For instance, it was noticed that despite their isomorphous structures, neopentane tumbles more freely in the cryptophane cavity than  $\text{TMA}^+$ . Semiquantitative data revealed that the overall average duration for the alignment of a guest  $\text{C}_3$  axis with the host  $\text{C}_3$  axis is significantly longer (3.2 ps) for  $\text{TMA}^+$  than for neopentane (1.2 ps). Additionally, the increased rate for guest tumbling of neopentane with respect to the  $\text{C}_2$  axis of the host is still faster than that for  $\text{TMA}^+$ , again suggesting a more hindered motion for the latter.<sup>103</sup>

These results emphasize that cryptophane hosts are particularly well suited for investigating physical phenomena that occur between weakly interacting molecules. Therefore, cryptophanes are useful models to study the different forces involved in the molecular recognition process with neutral or charged guests, as well as the host dependence on the guests' charge and symmetries. These host–guest interactions have been studied in various media and states of matter, such as organic or aqueous solutions, liquid or solid state, and even liquid-crystalline phases, as described in the following sections.

## 7.3. Host–Guest Complexes in the Solid: Raman Microspectrometry

Recently, Cavagnat et al. investigated chloroform@cryptophane complexes in the solid state by Raman microspectrometry.<sup>80</sup> Raman microspectrometry provides exceptional spatial resolution and extreme sensitivity that allow the study of micrometer scale solid samples such as single crystals of cryptophane complexes. Another feature is the possibility to use polarized light to gain information on the relative orientation of particular chemical bonds. Single crystals of  $\text{CDCl}_3@1$  complex have thus been investigated. Deuterium labeled chloroform gives bands outside the absorption domain of the cryptophane host and facilitates the interpretation of the relevant signals. With the rhomb crystals of  $\text{CDCl}_3@1$ , the most common crystalline form (see section 5.3), strong polarization effects were observed for the C–D stretching (Figure 30). Additionally, the main transitions due to the cryptophane host were assigned by means of computational methods, thus allowing the determination of the orientation of the guest with respect to the host. In this particular case, the  $\text{C}_3$  molecular axis of the complex is roughly parallel to the principal diagonal of the  $ac$  plane of the lattice, which strongly facilitates the interpretation of the experimental spectra. The C–D bond of the entrapped  $\text{CDCl}_3$  is clearly aligned with the  $\text{C}_3$  axis of the CTV unit. This result nicely confirms the observation made on the complex by NMR spectroscopy, both in the liquid and the solid state.

The situation is somewhat more complicated with the  $\text{CDCl}_3@2$  complex, since the molecular axis does not correspond to the crystal axis. The C–D stretching band is shifted toward low frequencies ( $2235\text{ cm}^{-1}$  compared to  $2245\text{ cm}^{-1}$  in  $\text{CDCl}_3@1$ ,  $2255\text{ cm}^{-1}$  for  $\text{CDCl}_3$  in the liquid phase, and  $2265\text{ cm}^{-1}$  for  $\text{CDCl}_3$  in the gas phase), suggesting a stronger interaction of the C–D bond with



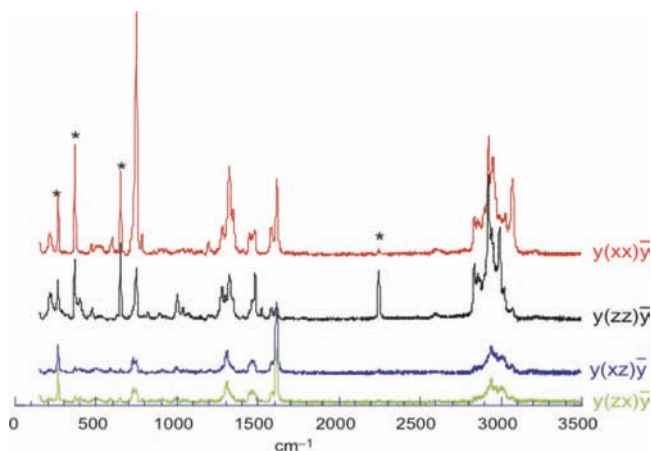


**Figure 30.**  $y(xx)\bar{y}$ ,  $y(zz)\bar{y}$ ,  $y(xz)\bar{y}$ , and  $y(zx)\bar{y}$  Raman spectra (see ref 80 for notation) of a rhomb crystal of the  $\text{CDCl}_3@1$  complex.  $\text{CDCl}_3$  bands are marked with an asterisk (Reprinted with permission from ref 80. Copyright 2004 American Chemical Society).

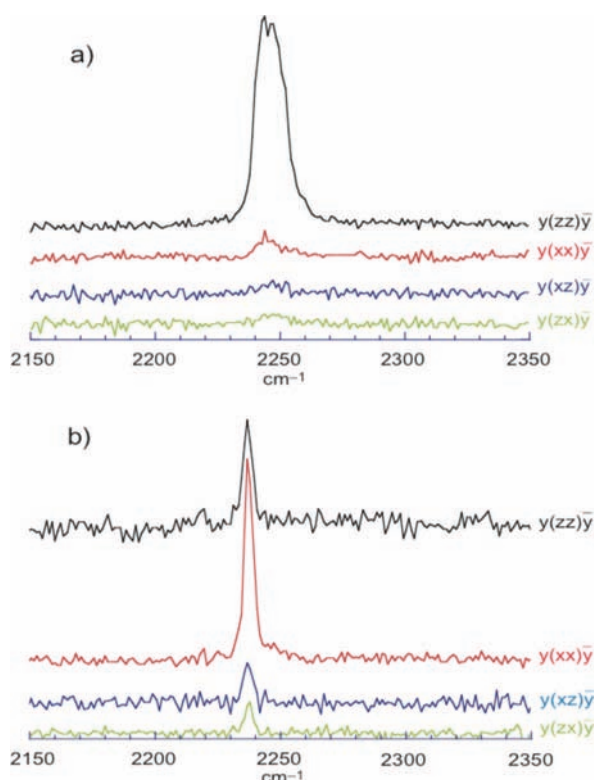


**Figure 31.**  $y(xx)\bar{y}$ ,  $y(zz)\bar{y}$ ,  $y(xz)\bar{y}$ , and  $y(zx)\bar{y}$  Raman spectra of (a) a rhomb crystal of the  $\text{CDCl}_3@1$  complex and (b) a crystal of the  $\text{CDCl}_3@2$  complex in the CD stretching region (Reprinted with permission from ref 80. Copyright 2004 American Chemical Society).

2 than with 1. The frequency dependence of the C–D bond stretching upon encapsulation also suggests that the molecules trapped in the cavities of cryptophanes are in a situation intermediate between the liquid state and the solid state. Additionally, a large difference of the width at half-height is observed between the two signals, which reflects the different dynamics of the chloroform guest in the two complexes (Figure 31). This again corroborates the previous conclusions obtained from NMR experiments.

Moreover, Raman microspectrometry can discriminate the structures of different  $\text{CHCl}_3@$ cryptophane solvates. X-ray diffraction studies have clearly identified a second crystalline form of the  $\text{CHCl}_3@1$  complex (rod crystals) with two

different chloroform molecules in the crystal unit. One  $\text{CHCl}_3$  is encaged within the cavity of the host, whereas the other occupies the interstitial space in the lattice, leading to two different signals in the Raman spectrum. Variable-temperature experiments showed that the interstitial chloroform molecule was sensitive to temperature and exhibited more mobility, whereas the encapsulated chloroform was not affected. This is a direct consequence of the different interactions experienced by the encaged and interstitial  $\text{CHCl}_3$  molecules.

## 7.4. Studies in Mesophases

The  $\text{CHCl}_3@1$  complex has also been investigated by  $^{13}\text{C}$  NMR in two nonchiral thermotropic nematic liquid crystals. This approach reported by Marjanska et al. allows the partial orientation of both host and guest molecules in the liquid crystal.<sup>104</sup> The preferential orientation of both molecules partially restores the dipolar coupling lost in isotropic medium and allows the study of the structure and the dynamics of host and guest molecules. For instance, when both  $^{13}\text{CHCl}_3$  and cryptophane-A (1) are dissolved in an aromatic (ZLI 1132) or an aliphatic (ZLI 1695) thermotropic nematic liquid crystal, a splitting of the bound and unbound  $^{13}\text{C}$ -labeled chloroform signal was observed (Figure 32). This splitting is much larger for the bound chloroform molecule than for the free one, irrespective of the liquid-crystalline solvent. Since dipolar couplings are partially responsible for this splitting, the knowledge of the magnitude and the sign of the dipole–dipole interaction factor  $D_{13\text{CH}}$  and of the scalar coupling factor  $J_{13\text{CH}}$  allows the determination of the order parameter  $S_{13\text{CH}}$  for both solutes. A significant enhancement

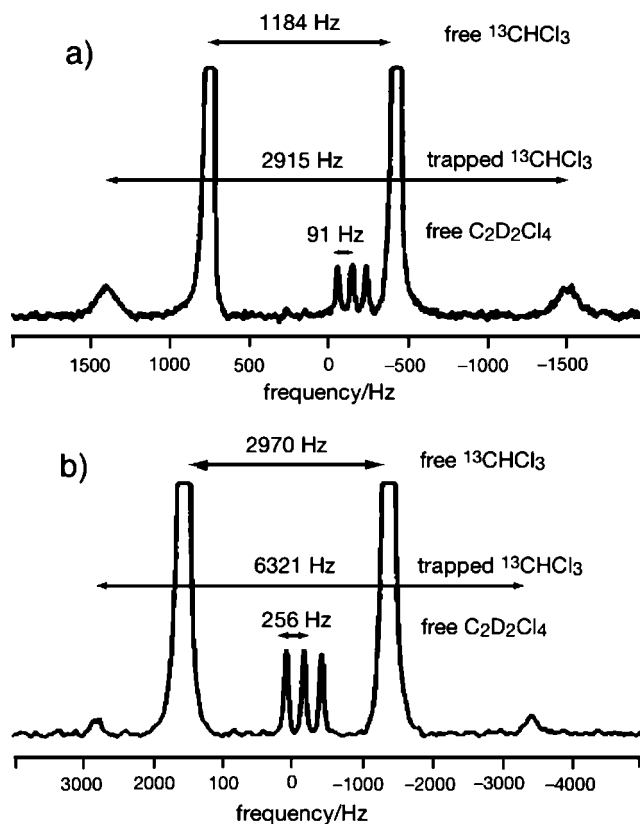


**Figure 32.**  $^{13}\text{C}$  NMR spectra of  $^{13}\text{C}$ -labeled chloroform dissolved in cryptophane-A (1)/ $\text{C}_2\text{D}_2\text{Cl}_4$ /ZLI 1695 (a) and in cryptophane-A (1)/ $\text{C}_2\text{D}_2\text{Cl}_4$ /ZLI 1132 (b) solutions at 298 K. Reprinted with permission from ref 104. Copyright 2003 American Chemical Society.

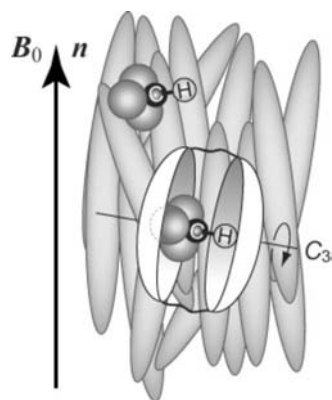


**Figure 33.** Schematic representation of the  $\text{CHCl}_3$ @cryptophane-A (**1**) complex oriented in a ZLI 1132 liquid crystal showing the average orientation of both free and bound chloroform (Reprinted from ref 105, Copyright 2006, with permission from Elsevier).

of the  $S_{13_{CH}}$  for the trapped  $^{13}\text{C}$ -labeled chloroform was observed with respect to the free chloroform molecule in the liquid crystals. For instance, in the ZLI 1695 liquid crystal, the parameter orders are 0.029 and 0.066 for the free and encapsulated chloroform, respectively. A higher degree of ordering was also observed for the free and trapped chloroform molecules when the temperature was decreased, with the latter being more sensitive to temperature effects. These results confirm the high degree of ordering and the restricted motion of the chloroform molecule entrapped within the cavity of the cryptophane with respect to the free guest dissolved in the liquid crystal.

This work was extended to the study of  $\text{CHCl}_3$ @**1** and  $\text{CHCl}_3$ @**151** (bis-cryptophane described in section 4.4) complexes in a nematic thermotropic liquid crystal (ZLI 1132) at different temperatures.<sup>105</sup> As previously observed by Goodson and co-workers, a larger  $^{13}\text{C}$ -H dipolar coupling was observed in both complexes for the encapsulated chloroform molecule vs the free guest. Variable temperature experiments led to the determination of the sign and magnitude of the order parameter  $S_{13_{CH}}$  of the C-H bond of the encapsulated chloroform. A significant enhancement of the order parameter was observed for the bound guests in  $\text{CHCl}_3$ @**1** and  $\text{CHCl}_3$ @**151**, which varies between  $-0.15$  and  $-0.08$ , respectively, when the temperature was changed from 283 to 304 K. These values are two times smaller (between  $-0.06$  and  $-0.05$ ) for the free guests in the same temperature range. Additionally, it was shown that the internal mobility of the guest is independent of the nature of the bulk solvent (isotropic or liquid crystal), thus suggesting a strong correlation between the molecular motion of the guest and the host. This assumption is corroborated by independent measurements performed by NMR spectroscopy in solution or in the solid state. Moreover, the data reported in this paper show that complexes both of cryptophane-A (**1**) and of bis-cryptophane **151** give fully consistent data and show an overall alignment of the complexes such that the 3-fold axis of the cryptophane lies roughly perpendicular to the liquid crystal director (Figure 33).

## 8. Chiral Discrimination

It is worth recalling that, originally, the first objective underlying the cryptophane project was to design a “tailor-made” host molecule in order to discriminate the two enantiomers of  $\text{CHFClBr}$ , one of the smallest chiral mol-

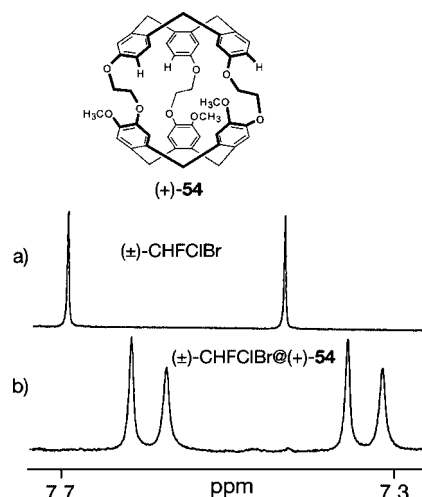


**Figure 34.** Enantioselective complexation of  $\text{CHFClBr}$  by enantioenriched cryptophane-C ((+)-**54**):  $^1\text{H}$  NMR spectra in  $\text{CDCl}_3$  at 332 K of (a)  $(\pm)\text{-CHFClBr}$  and (b)  $(\pm)\text{-CHFClBr}$  and enantioenriched (+)-**54**.

ecules. Indeed, this had been one of the first demonstrations of the complexation ability of a cryptophane by Collet and co-workers in 1985.<sup>87</sup> We will report herein on the main results on the matter, and we will develop further, in section 10, the latest advances in the field of chiral recognition by cryptophane hosts. Increasing interest in this topic is due to new strategies to obtain optically pure compounds, and also to recent investigations of their chiroptical properties. It also highlights future possible applications of these chiral hosts in e.g. the design of new materials for chiral HPLC stationary phases or catalytically active host-guest systems.

### 8.1. $\text{CHFClBr}$

Chiral cryptophane-C (**54**) is able to discriminate the two enantiomers of  $\text{CHFClBr}$ . When enantioenriched (+)-**54** is added to a racemic mixture of  $\text{CHFClBr}$  in organic solution, the  $^1\text{H}$  NMR spectrum displays two sets of doublets for the proton of  $\text{CHFClBr}$ , where the splitting is due to the scalar coupling with the fluorine atom (Figure 34).<sup>87</sup> These two doublets do not have the same intensity, suggesting different stability constants for the two diastereomeric complexes. In this case, from the  $^1\text{H}$  NMR spectra, the chiral discrimination energy has been estimated at  $\Delta\Delta G^\circ = 1.1 (\pm 5\%) \text{ kJ mol}^{-1}$  in favor of the (+)- $\text{CHFClBr}$ @(+)-**54** complex with respect to the (−)- $\text{CHFClBr}$ @(+)-**54** complex. This first example of chiral discrimination by cryptophanes later helped in the determination of the absolute configuration of  $\text{CHFClBr}$ . McCammon and co-workers used computational methods to support these experimental results. They came to the conclusion that (*R*)- $\text{CHFClBr}$ @(−)-**54** was more stable than (*S*)- $\text{CHFClBr}$ @(−)-**54**. The calculated energy difference  $[\Delta\Delta G^\circ]_{\text{calc}} \approx 1.51 \pm 1.4 \text{ kJ/mol}$  was in excellent agreement with the experimental value.<sup>11</sup> Together, the experiments and the computational approach led to the assignment of the absolute configurations (*R*)-(−) and (*S*)-(+) for  $\text{CHFClBr}$ . This result was in accord with an independent assignment based on a Raman optical activity investigation.<sup>106</sup>

In a recent study, Crassous and Hediger investigated the complexation of  $\text{CHFClBr}$  by the  $D_3$ -symmetrical hosts cryptophane-E (**2**) and cryptophane-E-( $\text{SCH}_3$ )<sub>6</sub> (**27**) using  $^1\text{H}$  and  $^{19}\text{F}$  NMR spectroscopy.<sup>100</sup> The reversible binding of  $(\pm)\text{-CHFClBr}$  by **2** and **27** was also demonstrated in the 500 MHz  $^1\text{H}$  NMR spectra, which displayed two upfield-shifted

doublets due to the  $^1\text{H}-^{19}\text{F}$  scalar coupling, for the two diastereomeric complexes and their corresponding mirror images under slow exchange conditions at the NMR time scale. In the  $^{19}\text{F}$  NMR spectrum of the cryptophane-E (**2**) complex, a single doublet was observed for the two equally shielded fluorines in both diastereomeric complexes. The situation is different with cryptophane **27**, for which the  $^{19}\text{F}$  spectrum shows two well resolved doublets upfield shifted respectively by 1.53 and 1.69 ppm with respect to the signal of free  $\text{CHFClBr}$ . This large chemical shift, observed for the two diastereomeric complexes, has been attributed to the different chemical environments experienced by the two enantiomers of  $\text{CHFClBr}$  in the chiral cavity of cryptophane-E-( $\text{SCH}_3$ )<sub>6</sub> (**27**). The association constants for the different host-guest systems were determined from the  $^1\text{H}$  NMR spectra and revealed almost no enantioselective recognition, as  $K_a$  is 100 and  $108\text{ M}^{-1}$  for the diastereomeric complexes of **2**, and a much lower  $K_a$  value of  $10\text{ M}^{-1}$  was found for both complexes of **27**.

## 8.2. CHFClI

Chiral halomethanes were also studied in an attempt to demonstrate parity violation effects at the molecular level.<sup>107</sup> The chiral cavity of the cryptophane host **27** was then used to determine the enantiomeric purity of (+) and (-) samples of  $\text{CHFClI}$ .<sup>55</sup> In  $\text{C}_2\text{D}_2\text{Cl}_4$  solution, (+)- $\text{CHFClI}$  and (-)- $\text{CHFClI}$  form diastereomeric complexes with ( $\pm$ )-**27**, which were characterized by  $^1\text{H}$ - and  $^{19}\text{F}$ -NMR spectroscopy. Interestingly, low enantioselective recognition was observed from the NMR data at 300 K. Binding constants were found to be  $37\text{ M}^{-1}$  for the (*R*)-(-)- $\text{CHFClI}@P$ -(-)-**27**/*S*-(+)- $\text{CHFClI}@M$ -(+)-**27** complexes and  $29\text{ M}^{-1}$  for the (*S*)-(+) - $\text{CHFClI}@P$ -(-)-**27**/*R*-(-) - $\text{CHFClI}@M$ -(+)-**27** complexes. Enantioenriched *M*-(+)-**27** and *P*-(-)-**27** were prepared from the resolved CTV precursor using the template method (see section 10.2.1). Cryptophane *P*-(-)-**27** was used as a chiral complexing agent and allowed measurement of the enantiomeric excess (*ee*) of (-)- $\text{CHFClI}$  samples by  $^{19}\text{F}$ -NMR spectroscopy (Figure 35), which was further confirmed by HPLC analysis.

## 9. Xenon in the Cryptophane Cavity

### 9.1. Xe@cryptophane Complexes

The complexation of noble gases such as helium, xenon, or even radon<sup>108</sup> by organic molecules in liquids or in the condensed phase represents a challenge for chemists, owing to the difficulties in designing suitable organic hosts to trap these elusive atoms. This field of research goes far beyond the fundamental study of supramolecular systems, since the noble gases helium<sup>109–111</sup> and xenon<sup>23–25</sup> are presently in advanced development for magnetic resonance imaging (MRI) and biomedical applications. However, only a few organic synthetic molecular receptors have been reported to bind xenon in solution. Cram, using *hemicarcerands*,<sup>112,113</sup> and Rebek, using self-assembled dimeric *tennis-ball capsules*,<sup>114,115</sup> reported results independently on the reversible capture of xenon in organic solution. The formation of the complexes were characterized by the high-field shift of the  $^{129}\text{Xe}$  NMR signal of the bound xenon, viz.  $\Delta\delta(^{129}\text{Xe}) = 101\text{ ppm}$  and  $19\text{ ppm}$  in the hemicarcerand and in the dimeric capsule, respectively. The affinity of xenon for the hemicarcerand host was estimated to be  $200\text{ M}^{-1}$  at 295–298

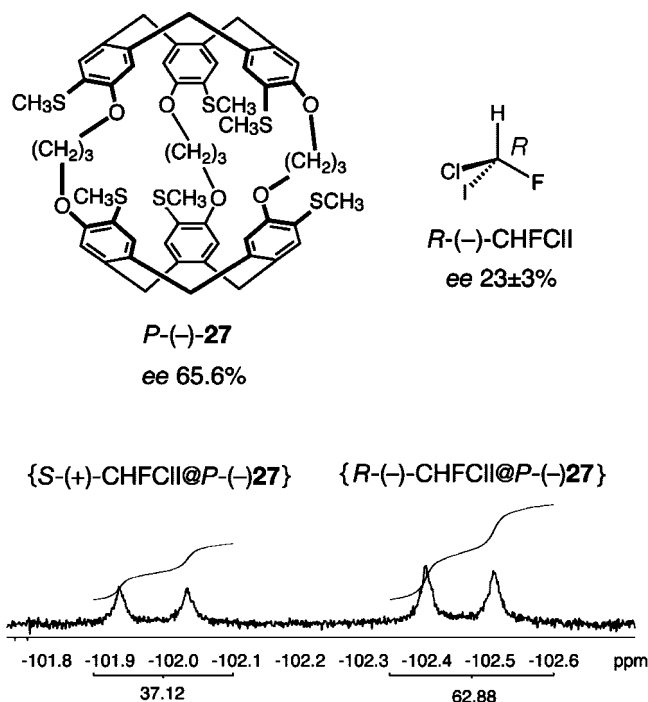


**Figure 35.** Enantiomeric excess determination of (-)- $\text{CHFClI}$  by  $^{19}\text{F}$ -NMR spectroscopy in  $\text{C}_2\text{D}_2\text{Cl}_4$  at 300 K using cryptophane (-)-**27** as a chiral complexing agent (Reproduced from ref 55 (<http://dx.doi.org/10.1039/b510675c>) by permission of The Royal Society of Chemistry).

K,<sup>112</sup> but no data were reported for the dimeric capsule. Bartik et al. reported the complexation of xenon in the apolar molecular cavity of  $\alpha$ -cyclodextrin in water. They observed a single resonance in the  $^{129}\text{Xe}$  NMR spectra, suggesting a fast exchange condition on the NMR time scale. From  $^{129}\text{Xe}$  NMR experiments, they determined the equilibrium constant,  $K_a$ , as  $22.9\text{ M}^{-1}$  at 298 K in water.<sup>116</sup> A similar result was then obtained by Bartik and co-workers, with xenon entrapped in the cavity of the *cucurbituril* host in aqueous solution. They reported an association constant  $K_a = 200\text{ M}^{-1}$  at 298 K and a strong high-field shift for the entrapped xenon,  $\Delta\delta(^{129}\text{Xe})$  of 68 ppm.<sup>117</sup> Bartik et al. were the first to demonstrate the formation of the  $\text{Xe}@1$  complex in 1,1,2,2-tetrachloroethane-*d*<sub>2</sub>.<sup>12</sup> At 278 K, the  $^{129}\text{Xe}$  NMR spectrum of the complex, in the presence of an excess of xenon, showed two well-separated signals (slow exchange conditions) at 229.5 and 62.3 ppm, attributed respectively to free xenon in solution and to xenon trapped in the cavity of cryptophane-A (**1**) (Figure 36).<sup>118</sup> The large chemical shift difference ( $\Delta\delta \approx 167\text{ ppm}$ ) is larger than the values reported by Cram and Rebek and is characteristic of a dramatic change of the environment of the xenon guest. This large effect was interpreted as due to van der Waals interactions between xenon and cryptophane-A (**1**) rather than as a consequence of the shielding effect of the aromatic rings. The stability of the  $\text{Xe}@1$  complex is characterized by a strong binding constant,  $K_a$ , of 3900 at 278 K, quite remarkable for the association of a gaseous neutral guest. This work led to further studies, which took advantage of the exceptional affinity of xenon for **1** in solution. Until very recently, cryptophane-A (**1**) was the best molecular host for xenon in organic solution (see note added in proof in section 14).



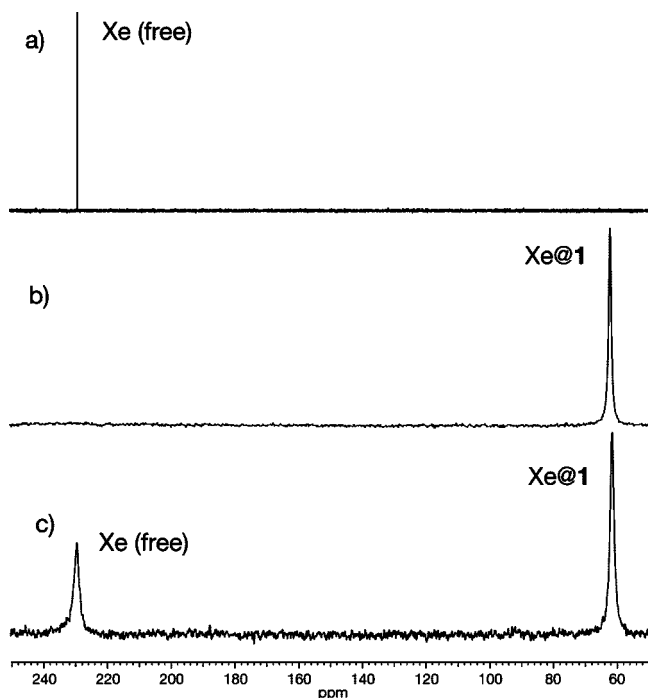


**Figure 36.**  $^{129}\text{Xe}$  NMR spectra in  $\text{C}_2\text{D}_2\text{Cl}_4$  at 278 K: (a) free xenon in solution; (b) xenon and cryptophane-A (**1**) ( $n_{\text{Xe}}/n_1 = 0.46$ ); (c) xenon and cryptophane-A (**1**) ( $n_{\text{Xe}}/n_1 = 2.12$ ) (Reprinted with permission from ref 12. Copyright 1998 American Chemical Society).

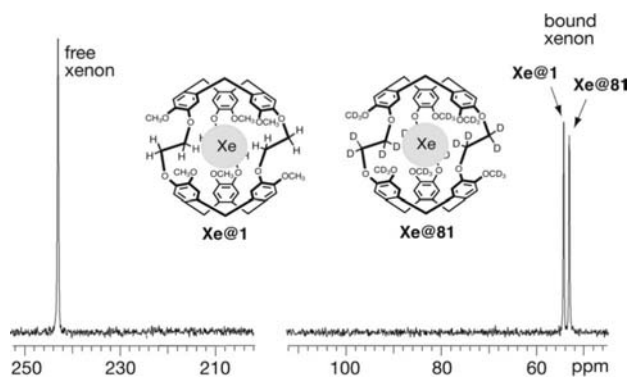


**Figure 37.**  $^{129}\text{Xe}$  NMR spectrum of a  $\sim 1:1$  mixture of cryptophanes **1** and **81**, and xenon ( $[^{129}\text{Xe}]/[\text{hosts}] \approx 2$ ), in  $\text{C}_2\text{D}_2\text{Cl}_4$  solution at 238 K. (Reprinted from ref 50, Copyright 2001, with permission from Wiley-VCH).

## 9.2. $^{129}\text{Xe}$ NMR Spectroscopy of Xe@Cryptophane Complexes

The large  $^{129}\text{Xe}$  NMR chemical shift effect observed in Xe@cryptophane complexes is due to the high polarizability of the xenon atom and how it is affected by its environment.<sup>119,120</sup> Therefore,  $^{129}\text{Xe}$  NMR spectroscopy can provide information on the chemical environment of the xenon guest and thus on the inner surface of the molecular cavity. To demonstrate this, Brotin et al. studied the encapsulation of xenon in a series of deuterium-labeled cryptophanes-A.<sup>50,121</sup> Cryptophane-A (**1**) and one of its labeled analogues were mixed together with xenon, and  $^{129}\text{Xe}$  NMR spectra were recorded. For example, when cryptophane-A-*d*<sub>30</sub> (**81**) was mixed with **1**, at low temperature, two well-resolved resonances were observed at low frequency, corresponding to xenon encapsulated in the cavity of each cryptophane (Figure 37). The high sensitivity of the xenon resonance led to the discrimina-

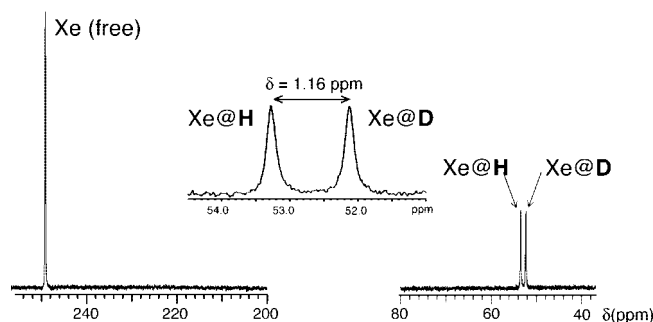


**Figure 38.**  $^{129}\text{Xe}$  NMR spectrum of bis-cryptophane **149** recorded at 228 K in  $\text{C}_2\text{D}_2\text{Cl}_4$ . **H** and **D** stand for the hydrogen- and deuterium-labeled cryptophane moieties (inset: enlarged spectrum of the two bound states. Reproduced from ref 66 (<http://dx.doi.org/10.1039/b312979a>) by permission of The Royal Society of Chemistry (RSC) on behalf of the Centre National de la Recherche Scientifique (CNRS)).

tion of both cryptophanes ( $\Delta\delta = 1.2$  ppm), differing only by their hydrogen or deuterium composition.

Similar experiments were also performed with differently labeled compounds and with the bis-cryptophane **149**.<sup>66</sup> For all labeled Xe@cryptophane[ $^2\text{H}_n$ ] complexes, the  $^{129}\text{Xe}$  resonance was high-field shifted with respect to the unlabeled host (Figure 38). A linear relationship between the  $^{129}\text{Xe}$  NMR resonance frequency and the degree of deuteration was observed at low temperature (238 K). The origin of this effect is intriguing but can be attributed to the vibrational modes of the cryptophane molecules, which differ with the degree of deuteration and induce a different polarization of the xenon atom. Even though this effect has not been clearly demonstrated by experiment, it is supported by the theoretical work of Sears and Jameson.<sup>122</sup>

The binding constants measured with cryptophane-A (**1**) and the larger cryptophane-E (**2**) clearly demonstrate that the size of the xenon guest ( $V_{\text{vdw}} \approx 42 \text{ \AA}^3$ ) fits the cavity of cryptophane-A (**1**) ( $V_{\text{vdw}} \approx 95 \text{ \AA}^3$ ) well, whereas cryptophane-E (**2**) ( $V_{\text{vdw}} \approx 121 \text{ \AA}^3$ ) binds xenon only moderately.<sup>123</sup> Brotin et al. synthesized the new  $\text{C}_2$ -symmetrical cryptophane-233 (**105**), cryptophane-223 (**106**), and cryptophane-224 (**107**), where the size of the internal cavity is modulated by the variation of the length of the linkers between the CTV units.<sup>58</sup> Cryptophanes **105** and **106** bind xenon efficiently, and different  $^{129}\text{Xe}$  NMR signals corresponding to free and bound xenon were observed at 293 K (Figure 39). High-field shifts of 21 and 9 ppm were observed for xenon bound to cryptophanes **105** and **106**, respectively, with respect to cryptophane **1**. Upon lowering the temperature, the signals are shifted further toward low frequencies, probably due to a modification of the internal dynamics of the cryptophanes. These additional examples again illustrate the exquisite sensitivity of the xenon NMR resonance with respect to its local surroundings. Sears and Jameson nicely supported these experimental results in their theoretical examination of the xenon chemical shift.<sup>122</sup> Whereas efficient binding of xenon was expected for cryptophane **106** ( $V_{\text{vdw}} \approx 102 \text{ \AA}^3$ ), the complexation by cryptophane **105** ( $V_{\text{vdw}} \approx 117 \text{ \AA}^3$ ) appears surprising, since the internal volume of its cavity is close to that of cryptophane-E (**2**), which is a poor receptor for xenon. On the other hand, cryptophane **107**, with an internal volume calculated as  $V_{\text{vdw}} \approx 110 \text{ \AA}^3$ , smaller than that of cryptophane **105**, does not trap xenon efficiently under the same experimental conditions (fast exchange condition on the NMR time scale). This could be the result of several



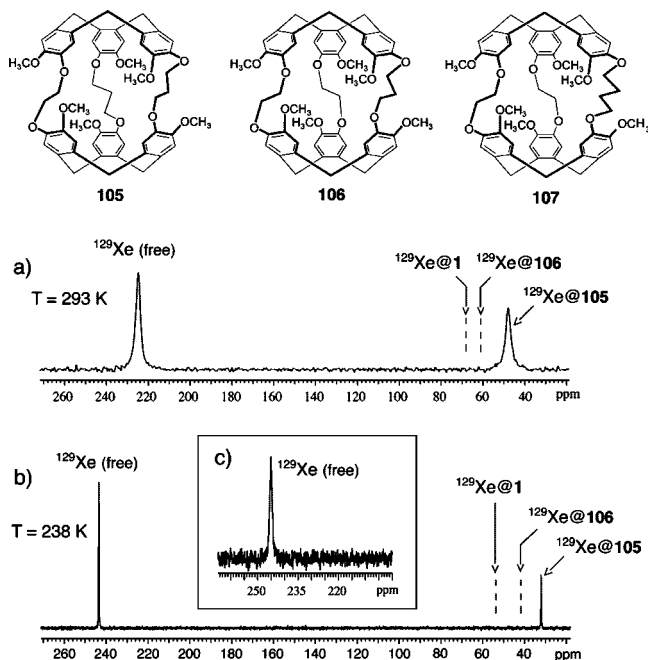


**Figure 39.**  $^{129}\text{Xe}$  NMR spectrum of the of  $\text{Xe}@105$  complex in  $\text{C}_2\text{D}_2\text{Cl}_4$ . The  $^{129}\text{Xe}$  NMR signals of xenon encapsulated in cryptophane-A (**1**) and cryptophane **106** are also shown for comparison: (a) 293 K; (b) 238 K. (c)  $^{129}\text{Xe}$  NMR spectrum of a solution containing cryptophane **107** in  $\text{C}_2\text{D}_2\text{Cl}_4$  solution at 233 K (Reprinted from ref 58, Copyright 2003, with permission from Wiley-VCH).

factors: a competition between xenon encapsulation and self-complexation of part of the  $-\text{O}(\text{CH}_2)_4\text{O}-$  linker, the effect of the symmetry on the shape of the molecular cavity for xenon recognition, the size of the portals that allow xenon to enter and leave the cavity, or a nonoptimal modeling of the different structures, from which the volumes of the cavities are determined. The binding constants were measured from competition experiments and are estimated as  $K_a = 800$  and  $2800 \text{ M}^{-1}$  for **105** and **106**, respectively.

Interestingly, the xenon guest experiences the chirality of *anti* cryptophane-A (**1**). In solution and in the presence of a chiral chemical shift reagent (CSR), Bartik et al. observed by  $^{129}\text{Xe}$  NMR spectroscopy a splitting of the resonance of the bound xenon into two well-resolved signals corresponding to xenon in both diastereotopic  $\text{Xe}@1/\text{CSR}$  supermolecules.<sup>124,125</sup> This is the first example of a *chiralized* xenon atom trapped in the cavity of a chiral host molecule. The term *chiralization* was thus preferred to the term polarization to describe more accurately the effect of the electronic interactions of xenon with the chiral environment. A theoretical approach to the magnetic shielding of xenon in a chiral environment has been reported by Jameson et al.<sup>126</sup>

### 9.3. Dynamics of Xenon Encapsulation

The dynamics of the xenon exchange process between different sites were studied using variable temperature 1D-EXSY experiments. Using  $^{129}\text{Xe}$  1D-EXSY NMR of an equimolar mixture of cryptophane-A (**1**) and deuterated cryptophane **81** in solution, Brotin et al. investigated the exchange dynamics between the three available sites for xenon: labeled cryptophane- $[\text{2-}^2\text{H}]$  **81**, cryptophane- $[\text{1-}^1\text{H}]$  **1**, and solvent (Figure 40).<sup>50</sup> From these experiments, it was possible to determine the whole set of kinetic constants and to conclude that the process involving the direct exchange

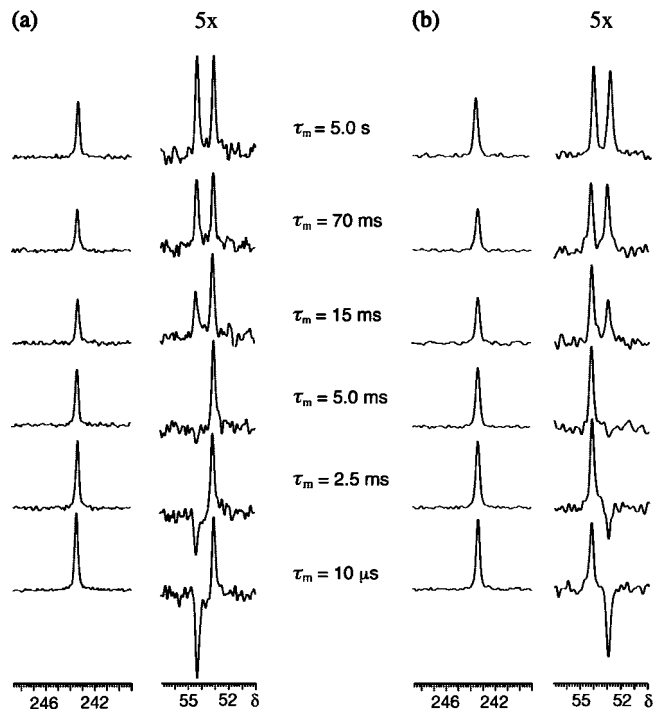


**Figure 40.** Evolution of the magnetization ( $^{129}\text{Xe}$ ) of the three sites (1D-EXSY experiments at 238 K) as a function of the mixing time,  $\tau_m$ : (a) after selective excitation of the peak corresponding to  $\text{Xe}@1$ ; (b) after selective excitation of the peak corresponding to  $\text{Xe}@105$  (Reprinted from ref 50, Copyright 2001, with permission from Wiley-VCH).

of xenon by collision between cryptophanes was negligible and that the main mechanism involved the capture and the release of xenon from the solution and into it. Similar conclusions were obtained from 2D-EXSY experiments.<sup>121</sup> Additionally, the activation energy  $E_a = 37.5 \text{ kJ mol}^{-1}$  for the decomplexation process of cryptophane-A (**1**) and its deuterated analog **81** was determined from 1D-EXSY experiments at different temperatures, thus leading to an activation enthalpy for decomplexation  $\Delta H^\ddagger = 35.5 \text{ kJ mol}^{-1}$  and an activation entropy for decomplexation  $\Delta S^\ddagger = -60 \text{ J K}^{-1} \text{ mol}^{-1}$ . Similar experiments were performed with cryptophane **105** ( $E_a = 34.8 \text{ kJ mol}^{-1}$ ) and cryptophane **106** ( $E_a = 35 \text{ kJ mol}^{-1}$ ). However, the results are more difficult to analyze for cryptophanes with  $\text{C}_2$ -symmetry, since xenon may pass through two portals with different sizes.

### 9.4. Laser-Polarized Xenon and Cryptophanes

The previous section was related to the  $\text{Xe}@$ cryptophane complexes, whose developments toward biological applications have already been underlined. One of the most significant problems for biological applications arises from factors such as poor water solubility of hosts and moderate natural abundance of  $^{129}\text{Xe}$ , which make conventional NMR experiments very restrictive. Thus, the association of hyperpolarized xenon and cryptophane is very promising, and the current principal research in this field is reported below.

The use of laser-polarized (LP), or hyperpolarized, xenon is of increasing interest in chemistry, biology, and medicine due to the extraordinary properties of this gas and its use in magnetic resonance imaging (MRI) and biomedical applications.<sup>23–25,127</sup> The large nuclear spin polarization of  $^{129}\text{Xe}$  allows the fast detection of xenon gas dissolved in water or biological media in a few seconds. NMR spectra are obtained with excellent resolution and a signal-to-noise ratio enhanced

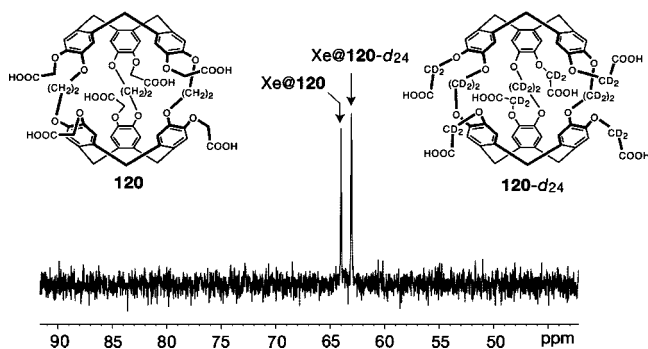


**Figure 41.** Laser-polarized  $^{129}\text{Xe}$  NMR spectrum of an equimolar mixture of cryptophanes **120** and **120- $d_{24}$**  in  $\text{D}_2\text{O}$  at 293 K (xenon pressure 110 kPa) (Reprinted with permission from ref 64. Copyright 2006 American Chemical Society).

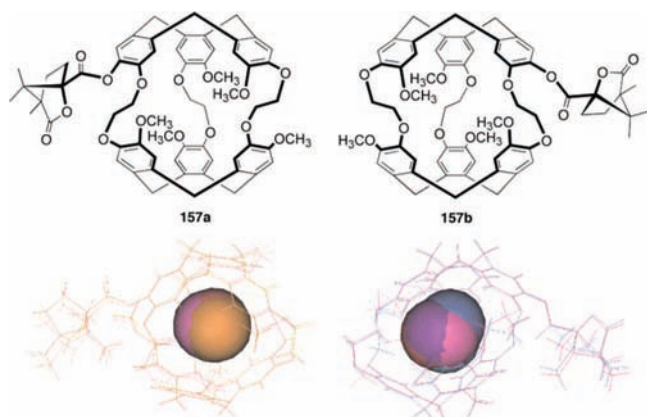


**Figure 42.** Superimposition of five low-energy structures of  $\text{Xe}@157\text{a}$  (left) and  $\text{Xe}@157\text{b}$  (right) complexes. The xenon atoms in the cavities are represented by their Van der Waals spheres (Reprinted with permission from ref 128. Copyright 2004 American Chemical Society).

by 4 orders of magnitude. For example, LP  $^{129}\text{Xe}$ -NMR spectra of  $\text{Xe}@$ cryptophane **120** and **120- $d_{24}$**  complexes have been obtained in a few minutes, whereas a conventional  $^{129}\text{Xe}$  NMR experiment requires larger amounts of the compound and an acquisition time of several hours (Figure 41).<sup>64</sup>

#### 9.4.1. Laser-Polarized Xenon in Cryptophane Complexes

Recently, Huber et al. reported on the importance of the stereospecificity of cryptophane derivatives for xenon binding and hence on the need for optically pure cryptophane hosts for the design of cryptophane-based biosensors. Indeed, while studying the interaction of xenon with cryptophane diastereomers **157a** and **157b**, they noticed an important  $^{129}\text{Xe}$  NMR chemical shift difference of approximately 7 ppm between  $\text{Xe}@157\text{a}$  and  $\text{Xe}@157\text{b}$ , associated with the different binding properties of each compound. This result was attributed to the relative orientation of the camphanic moiety in the two diastereomeric structures of the cryptophane. Consequently, xenon binds more efficiently to cryptophane **157b** ( $K_a = 3200 \text{ M}^{-1}$ ) than to cryptophane **157a** ( $K_a = 2000 \text{ M}^{-1}$ ).<sup>128</sup> A complete analysis of a whole set of 1D and 2D-NMR experiments and molecular modeling performed on both molecules showed that the (–)-camphanate moiety interacts more strongly with the (+)-cryptophane skeleton, leading to a more rigid structure (Figure 42). Furthermore, off-resonance ROESY experiments allowed a description of the

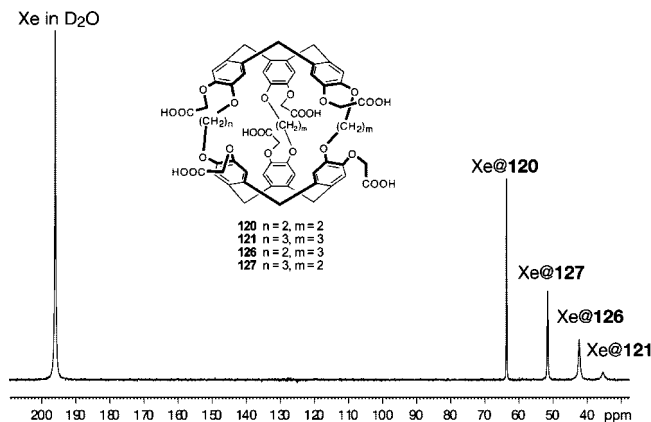


**Figure 43.** LP  $^{129}\text{Xe}$  NMR spectrum in  $\text{D}_2\text{O}$  solution of a mixture of cryptophanes **120** (0.74 mM), **121** (0.69 mM), **126** (0.69 mM), and **127** (0.50 mM) at 289 K (Reprinted with permission from ref 64. Copyright 2006 American Chemical Society).

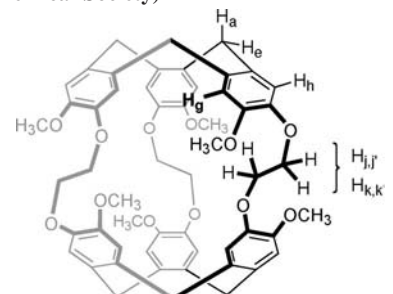
dynamics on the nanosecond time scale. The internal dynamics of the (+)-cryptophane(–)-camphanate system were found to be more appropriate to accommodate xenon whereas the other diastereomer (–)-cryptophane(–)-camphanate showed more rapid internal dynamics that are less favorable for encapsulating xenon. Ruiz et al. first reported evidence that the diastereomeric splitting of xenon chemical shifts depends on the number of asymmetric centers on the cryptophane host.<sup>129</sup>

The physical properties of the water-soluble cryptophanes **120**, **121**, **126**, and **127** toward xenon encapsulation were recently investigated. When mixed together in water solution, each cryptophane exhibits a distinct signal whose frequency decreases with the size of the internal cavity, as previously observed with their parent cryptophanes **1**, **2**, **105**, and **106**, respectively, in 1,1,2,2-tetrachloroethane- $d_2$  (Figure 43).<sup>64</sup> Moreover, these compounds exhibit a larger binding constant in water than their parent compounds in organic solution. This can be seen as a direct consequence of the hydrophobic character of the xenon guest. For instance, xenon binds to cryptophane **120** in water with a binding constant  $K_a$  of  $6800 \text{ M}^{-1}$ . Cryptophane **121**, the water-soluble congener of **2**, also exhibits a much higher binding constant,  $K_a = 1000 \text{ M}^{-1}$ , in water than **2** in organic solvent. The precise measurement of the binding constant for **120**, however, was found to be more complicated due to the presence of an unexpected *out-saddle* conformer unable to complex xenon. The work of Huber et al. also demonstrated that  $^{129}\text{Xe}$  NMR spectra of cryptophane complexes with concentrations as low as  $1 \mu\text{M}$  could be obtained in a few seconds with good signal-to-noise ratio using the laser-polarized  $^{129}\text{Xe}$  NMR technique.<sup>64</sup> This demonstrates the possibility to design efficient cryptophane-based biosensors for the *in vitro* or *in vivo* MRI detection of biological molecular targets.

#### 9.4.2. Probing the Molecular Cavity of Cryptophane

The ability to obtain  $^{129}\text{Xe}$  NMR spectra in aqueous solution with high resolution is one of the main advantages of this technique. The ability of laser-polarized xenon to transfer its polarization efficiently to surrounding nuclei is another important characteristic of the hyperpolarized gas. A subsequent increase of the signal of the neighboring protons is expected and obtained through the SPINOE experiment (spin polarization induced nuclear Overhauser

**Table 6. Spin Lattice Relaxation Times, SPINOE Enhancements, Relative H–Xe Cross-Relaxation Rates, and Calculated Relative Values for a Gauche Conformation of the OCH<sub>2</sub>CH<sub>2</sub>O Linker, for the Various Protons of Cryptophane 1 (Reprinted with Permission from Ref 131. Copyright 1999 American Chemical Society)**



proton	type	$T_1^H$ (s)	SPINOE (%)	$\sigma_{\text{HXe}}^b / \sigma_{\text{H}_{\text{gh}}}^b \text{Xe}$	$\langle r_{\text{HXe}}^{-6} \rangle^b / \langle r_{\text{H}_{\text{gh}}}^{-6} \text{Xe} \rangle^b$
aromatic	H <sub>g</sub> , H <sub>h</sub>	0.80	11.0	(1.00)	(1.00)
axial	H <sub>a</sub>	0.27	3.0	0.47	0.3–0.4
linker	H <sub>j</sub> , H <sub>j'</sub>	0.36	5.2	0.67	0.3
linker	H <sub>k</sub> , H <sub>k'</sub>	0.41	13.0	1.55	1.5–1.8
methoxy	CH <sub>3</sub>	0.83	2.6	0.23	0.1–0.3
equatorial	H <sub>e</sub>	0.35	2.7	0.35	0.3–0.4

effect).<sup>130</sup> It is particularly important for probing molecular regions such as the internal cavity of the cryptophane host. Indeed, since  $^1\text{H}$ – $^{129}\text{Xe}$  cross relaxation rates decrease quickly as a function of  $1/r_{\text{HXe}}^6$ , the knowledge of these parameters for all the involved protons gives information on the spatial arrangement of the protons. Luhmer et al. performed SPINOE experiments on a solution of cryptophane-A and laser-polarized xenon in 1,1,2,2-tetrachloroethane-*d*<sub>2</sub>. They first observed a significant decrease of the longitudinal relaxation time  $T_1$  of the xenon trapped in the cavity of cryptophane-A (**1**) ( $T_1 = 16$  s), with respect to xenon gas dissolved in the solvent ( $T_1$  several hundreds of seconds).<sup>131</sup> The significant decrease of  $T_1$  for the encapsulated guest is characteristic of efficient polarization transfer between xenon and protons of the host. This was supported by SPINOE experiments and by measurements of the cross relaxation rate  $\sigma_{\text{HXe}}$  for all protons in cryptophane-A (**1**) (Table 6). Interestingly, they determined different values for the protons of the linkers and noticed that the cross relaxation rate between xenon and aromatic protons was dominant. Then, by comparing their data with molecular models, they were able to assign the *gauche* conformation to the three linkers (Figure 44). The *anti*-conformation of the linkers would have led to similar cross relaxation rates  $\sigma_{\text{HXe}}$  for the protons of the –OCH<sub>2</sub>CH<sub>2</sub>O– bridges. This situation is different from that observed in the solid with a CHCl<sub>3</sub> guest, since X-ray crystallography shows that the *anti*-conformation seems to be dominant when a CHCl<sub>3</sub> molecule is trapped inside the cavity of cryptophane **1**. However, the large difference in affinity for xenon (20 times greater than that for CHCl<sub>3</sub>) and its symmetry, size, and spherical shape are likely important factors that affect the conformation of the host.

Desvaux et al. performed similar experiments with cryptophane **105** and developed new SPIROE-NMR sequences, in which intramolecular homonuclear spin-diffusion is quenched.<sup>132</sup> As an example, the SPIROE sequence applied to Xe@**105** shows that redistribution of the magnetization between protons of the cryptophane has been quenched. The signals for the resonance of the protons interacting only weakly with xenon are absent. The SPIROE spectrum is quite

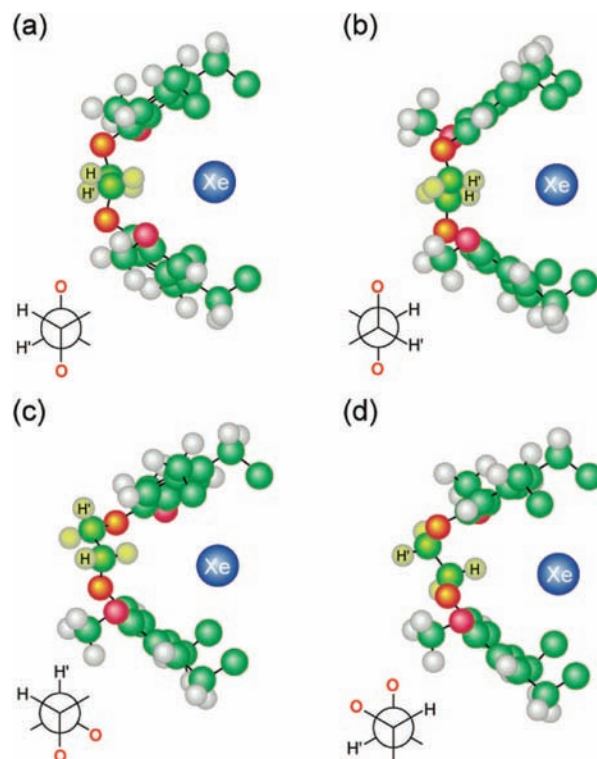


**Figure 44.** Minimum energy structures of cryptophane-A (**1**) with included xenon for the various conformations of the displayed spacer bridge. The atoms of the cyclotrimeratrylene subunits are at similar positions in each view; the molecule is slightly rotated such that the spacer bridge is clearly visible. In (a) and (b), the linkers are in an *anti* conformation. In (c) and (d), the linkers are in a *gauche* conformation (Reprinted with permission from ref 131. Copyright 1999 American Chemical Society).

different from that of the SPINOE experiment, where efficient intramolecular redistribution of the magnetization occurs after xenon has transferred its magnetization (Figure 45). Therefore, SPIROE experiments promise to be of great importance for quantifying interactions and determining the average distances between xenon and neighboring protons. Recently, the same group reported the use of a 2D-SPIROE-TOCSY sequence to assign the protons of cryptophane **157b**.<sup>133</sup> Cross-peaks in the 2D-SPIROE-TOCSY spectrum gave information about the connectivity between protons through scalar coupling. This leads therefore to a simplification of the SPINOE peaks through 2D NMR spectroscopy. These investigations show that the development of specific NMR sequences is closely associated to the design of cryptophane molecules for probing and mapping hydrophobic cavities.

#### 9.4.3. “Functionalized” Xenon

The binding of xenon in aqueous media is of prime importance for any application in biological sciences and in particular for MRI applications. Pines and co-workers were the first to investigate the synthesis and binding properties of a water-soluble xenon-cryptophane biosensor.<sup>68</sup> The functionalized cryptophane-A **141** bearing hydrophilic moieties (amino acids) and a biotin recognition site was designed to self-associate to the avidin protein with a large binding constant. Although cryptophane **141** is only sparingly soluble in water (300  $\mu\text{M}$ ), the authors were able to record in a few seconds the laser-polarized  $^{129}\text{Xe}$ -NMR spectrum of the Xe@**141** complex with a good signal-to-noise ratio. The



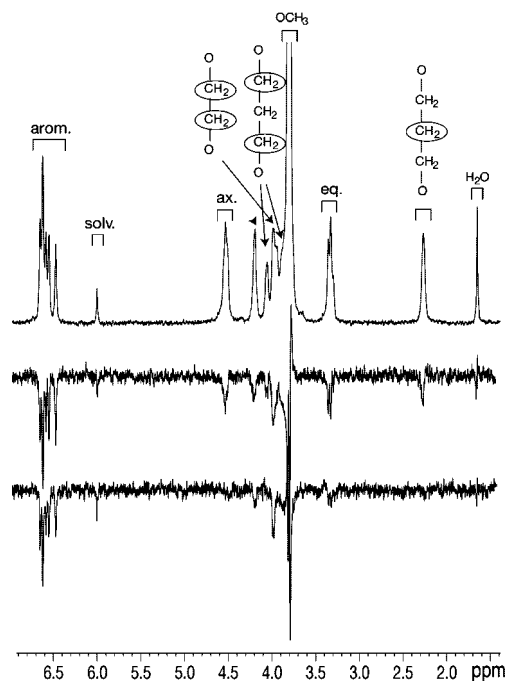


**Figure 45.** 500 MHz  $^1\text{H}$  NMR spectrum of cryptophane **105** (top) and SPINOE (middle) and SPIROE (bottom) subspectra (Reprinted from ref 132, Copyright 2003, with permission from Wiley-VCH).

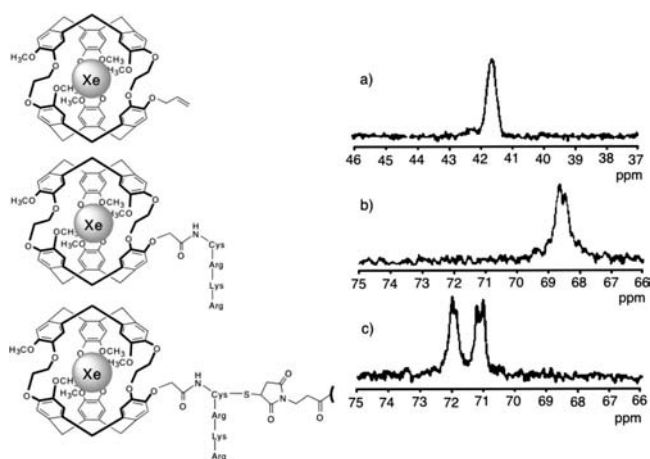


**Figure 46.** Detection of cage diastereomers by laser-polarized xenon NMR. (a) Cryptophane **128** in 25% toluene/75% tetrachloroethane; (b) after substitution by a single-enantiomer peptide chain (**140**); (c) after addition of a biotin linker (**141**) (Reprinted with permission from ref 68b. Copyright 2004 American Chemical Society).

main goal of their approach was to demonstrate that the  $^{129}\text{Xe}$  chemical shift was sensitive enough to distinguish between the free Xe@**141** complex and the complex bound to the avidin protein. The free Xe@cryptophane **141** complex displays four distinct resonances, which were interpreted as a consequence of the diastereotopic environment due to the chiral centers in the ligand and leading to a mixture of the *RLR*, *RLL*, *LLR*, and *LLL* chiral combinations [cryptophane•L-amino acids•biotin linker]. The band widths were mainly related to the exchange dynamics between the different sites (Figure 46).

When the avidin protein was added to the solution of Xe@**141**, a dramatic change, which was dependent on the concentration of avidin, was observed on the  $^{129}\text{Xe}$ -NMR spectrum. Addition of a small excess of protein led to the

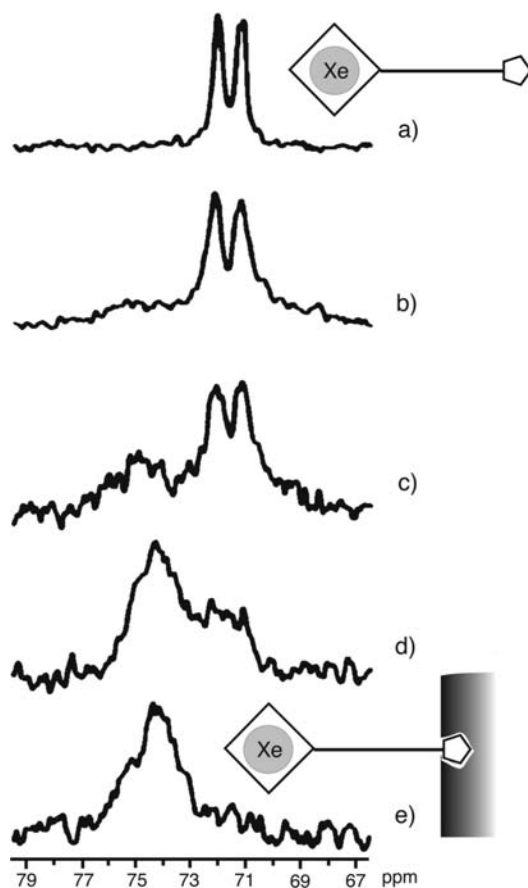


**Figure 47.** LP  $^{129}\text{Xe}$  NMR spectra of the functionalized xenon biosensor Xe@**141** in the presence of different relative amounts of avidin: (a) 0%, (b) 10%, (c) 20%, (d) 60%, (e) 120% (Reprinted with permission from ref 68b. Copyright 2004 American Chemical Society).

disappearance of the four sharp peaks and gave rise to a broad signal shifted toward higher frequency by about 2 ppm (Figure 47). This signal has been firmly attributed to the binding of the Xe@cryptophane complex to avidin. The broadening of the signal appears as a consequence of the distribution of diastereomeric shifts. The multiplicity of the signals arising from the diastereomeric mixtures is not desirable, as it complicates the xenon spectra by increasing the number of peaks and consequently decreases their intensity. So it is obvious that the design of enantiopure ligands will become a necessity and thus justifies the efforts which are made to synthesize enantiopure cryptophanes. On the other hand, a theoretical approach has been proposed to assign the diastereomeric Xe NMR chemical shifts in cryptophane-based biosensors.

Jameson et al. recently used quantum mechanical calculations to predict the diastereomeric Xe chemical shifts observed in different diastereomeric Xe@**1**-based biosensors arising from the introduction of chiral substituents on the cryptophane host.<sup>134</sup> Even though their assumptions do not allow a quantitative estimation of the splitting of the Xe NMR signals between the different diastereomers, the authors have observed a clear correspondence between the measured chemical shift differences and the calculated shielding differences. As expected, the effect on the diastereomeric splitting decreases with an increase of the distance of the encapsulated xenon to the stereogenic centers. From their calculations, it was thus possible to assign each peak observed in the xenon spectrum. The following order *LLL*,

*LLR*, *RLL*, and *RLR* of decreasing chemical shifts was thus obtained for compound **141** and related biosensors, where *L(R)* refers to the left-handed (right-handed) enantiomer of the cryptophane host and of the stereogenic centers as defined above.

This work has been recently extended to the study of new Xe@cryptophane sensors using cryptophanes **142–145** in solution in the presence of avidin protein.<sup>69</sup> The study of these new complexes and their interaction with avidin emphasizes the importance of the linker for obtaining enhanced discrimination between the free and bound complexes in solution. Thus, the characteristics (length, flexibility) of the linkers connecting the cryptophane to the biotin moiety appear to be of crucial importance to obtain sufficient resolution for the two expected <sup>129</sup>Xe NMR signals. For instance, a short linker connecting the cryptophane and the biotin moiety was found to be inappropriate for efficient biosensor applications, as it increases the contact between the cryptophane and the surface of the protein. As a consequence, the line width of the bound biosensor increases with respect to a decrease in linker length, whereas the chemical shift difference increases as well. A rigid linker strongly reduces the molecular motion of the cryptophane moiety, which then cannot be decoupled from that of the protein. An increase of the line width of the bound biosensor is observed as well. In contrast, a flexible linker enables the cage to rapidly reorient and gives rise to a sharp <sup>129</sup>Xe NMR signal for the bound biosensor. The work reported by Lowery et al. suggests some of the molecular parameters required to prepare efficient biosensors for future MRI applications. Other parameters such as the deuteration of the cryptophane molecule or the need for optically pure cryptophanes are also discussed. The use of the latter decreases the number of diastereomers formed in solution, and more facile interpretation of the xenon spectra is thus expected.

In a recent article, Dmochowski et al. developed an enzyme-responsive xenon biosensor based on a peptide–cryptophane-A conjugate. They synthesized a monofunctionalized cryptophanol protected with a propargyl group that can be further coupled to a tryptophan-containing peptide moiety, chosen for its known overexpression and extracellular localization in many tumors. Using tryptophan fluorescence and <sup>129</sup>Xe NMR spectroscopy, the authors were able to follow the enzymatic cleavage of the tryptophan-containing peptide.<sup>135</sup>

The recent progress made in hyperpolarization techniques for the production of xenon with high polarization (yield of ~50% can be expected) under continuous flow conditions suggests the possibility to develop in the near future biosensors at low concentration for NMR imaging. For instance, Hilty et al. demonstrated the feasibility of this approach for the detection of the Xe@**142**·avidin complex in solution.<sup>136</sup> Even though further progress is necessary in order to use such complexes for *in vivo* applications, the authors claim that the sensitivity could be increased by a factor of 1000 by optimizing the xenon polarizer and the biosensor and by the use of isotopically enriched xenon. They suggest the design of biosensors that do not suffer broadening of the xenon line after complexation and the design of sensors bearing several xenon-binding cryptophanes. Deuteration of the cryptophane host also appears as an option by increasing the longitudinal relaxation of xenon. These improvements in sensitivity would enable the detection of a 100 nM sample in an optimized NMR coil.

From the above suggestions, Han et al. proposed a new method for the quasi-continuous delivery of polarized <sup>129</sup>Xe to the biosensor in solution. This *bubble mode* delivery was tested with the Xe@**142** biosensor in the nanomolar concentration range. This approach can be adapted for the detection of xenon in heterogeneous samples as well as in *in vivo* experiments.<sup>137</sup> Mynar et al. introduced the use of dendritic structures to increase the signal-to-noise ratio without requiring the synthesis of optically pure cryptophanes.<sup>138</sup> Their work is based on the use of water-soluble dendritic structures bearing a biotin moiety and capable of incorporating several monofunctionalized cryptophanes **139** to obtain an easily detected NMR signal of the biosensor-bound complex. In these examples, the attachment of the cryptophanes to the dendritic structure is not required, since the cohesion between cryptophane and dendrimer is the result of the electrostatic interaction between the carboxylic acid of the cryptophane moieties and the numerous amido groups present inside the dendritic structure. The authors demonstrated that up to 11 cryptophanes could be encapsulated in the dendrimer matrix, thus leading to a significant improvement of the sensitivity without altering the line width. Undoubtedly, the pioneering work of the Pines group illustrates the potential use of cryptophane biosensors for *in vitro* or *in vivo* MRI applications.<sup>139</sup>

## 10. Syntheses and Chiroptical Properties of Optically Pure Cryptophanes

### 10.1. Optical Resolution of CTVs and Cryptophanes

As mentioned previously, the different routes used to synthesize cryptophanes usually lead to the formation of a main compound identified as the *anti* isomer or to a mixture of *anti* and *syn* isomers. When the substituents on both CTV units are identical, the *syn* compounds are generally achiral, whereas the *anti* compounds are chiral and obtained as racemic mixtures. A separation step is thus required to isolate the two enantiomers of the *anti*-racemate. Independent of the study of their chiroptical properties, the separation of the enantiomers is crucial for applications in biosensing and chiral recognition. Separation by crystallization is a difficult task due to the spherical shape of the molecules, which favors the formation of solid solutions, leading to unfavorable conditions for optical resolution.<sup>140</sup> In order to overcome this problem, several methods which present both advantages and disadvantages have been proposed and are discussed in the next section.

#### 10.1.1. Optical Resolution Using Chiral HPLC

The first attempt to resolve cryptophanes was proposed by Collet and co-workers, who used a chiral-stationary-phase HPLC column (chiralpak OT+).<sup>141</sup> This stationary phase is made of an optically active polymer having a stable helical conformation that is coated on silica gel. The authors separated the enantiomers of a series of cryptophanes and CTV derivatives (Figure 48), and under well defined conditions the column was particularly efficient (at 288 K) to discriminate the two enantiomers of cryptophane-A (**1**) and cryptophane-E (**2**). Larger cryptophanes such as *anti*-cryptophane-M (**112**), bearing three -O(CH<sub>2</sub>)<sub>4</sub>O- linkers, and cryptophane-I (**158**), containing olefinic linkers, have been efficiently resolved under the same experimental conditions.

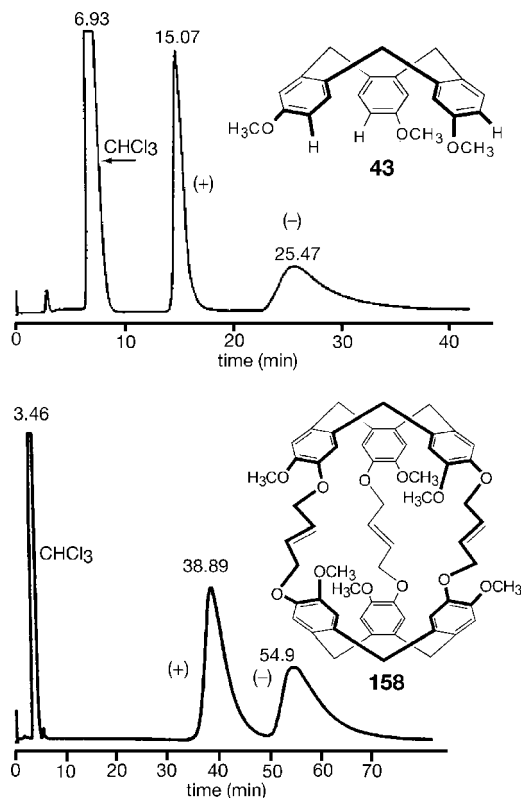


**Figure 48.** Chromatographic resolution of CTV ( $\pm$ )-**43** and cryptophane ( $\pm$ )-**158** (for conditions see Table 7) (Reproduced with permission from ref 141. Copyright 1989 The Chemical Society of Japan).

**Table 7.** Analysis of  $D_3$  and  $C_{3h}$  Cryptophanes on Chiralpak-OT(+) at 288 K<sup>a</sup>

compd	symmetry	bridges	retn time/min		$\alpha^b$
<b>1</b>	$D_3$	O(CH <sub>2</sub> ) <sub>2</sub> O	22.1(+)	30.0(-)	1.43
<b>2</b>	$D_3$	O(CH <sub>2</sub> ) <sub>3</sub> O	27.4(+)	37.6(-)	1.42
<b>152</b>	$C_{3h}$	O(CH <sub>2</sub> ) <sub>3</sub> O	36.0		
<b>112</b>	$D_3$	O(CH <sub>2</sub> ) <sub>4</sub> O	30.3	75.3 <sup>c</sup>	2.67
<b>158</b>	$D_3$	OCH <sub>2</sub> CH=CHCH <sub>2</sub> O	38.9(+)	54.9(-)	1.45

<sup>a</sup> Column 250 mm  $\times$  4.6 mm i.d.; methanol 1.0 mL min<sup>-1</sup>; UV detection at 230 nm. <sup>b</sup> Separation factor (defined as  $(t_2 - t_0)/(t_1 - t_0)$ , where  $t_2$  is the retention time of the slowest enantiomer and  $t_0$  that of a nonretained solute). <sup>c</sup> Absolute configuration unknown.

As expected, the achiral  $C_{3h}$  isomer **152** showed a single peak (Table 7).<sup>141</sup> So far, no interpretation of the results based on a discrimination mechanism between the stationary phase and the CTVs or the cryptophanes has been proposed. Despite the satisfactory results obtained, the low stability of this phase leads to a drop of its efficiency over time and thus appears of little use to isolate a large amount of cryptophanes.

Recently, Soulard et al. used a Regis (*S,S*) Whelk-O1 column for the separation of the two enantiomers of the  $D_3$ -symmetrical cryptophane **27**.<sup>55</sup> Similarly, enantiomers of **2** were efficiently separated by the Whelk-O1 column (Figure 49).

However, the success of the HPLC separation depends on the cryptophane itself, on strictly controlled experimental conditions (mainly temperature), and on the quality and stability of the chiral phase. Other limiting factors, such as the high cost of semipreparative or preparative chiral phases and of HPLC-grade solvents, often restrict their use to analytical work such as the determination of enantiomeric

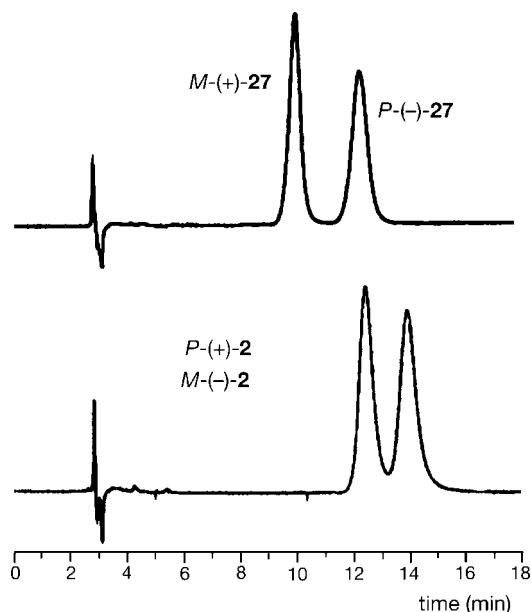


**Figure 49.** Chromatographic resolution of ( $\pm$ )-**27** and ( $\pm$ )-**2** (conditions: Whelk-O1 (*S,S*), 298 K, hexane/THF 6:4, 1 mL/min, UV 254 nm).

excesses. To overcome the problems arising from these different factors, new phases or new techniques are required. We will now describe two synthetic routes which have been proposed for the resolution of cryptophanes. The first route is based on the resolution of the CTV precursors, whereas the second one involves the separation of cryptophane diastereomers.

### 10.1.2. Resolution of CTVs

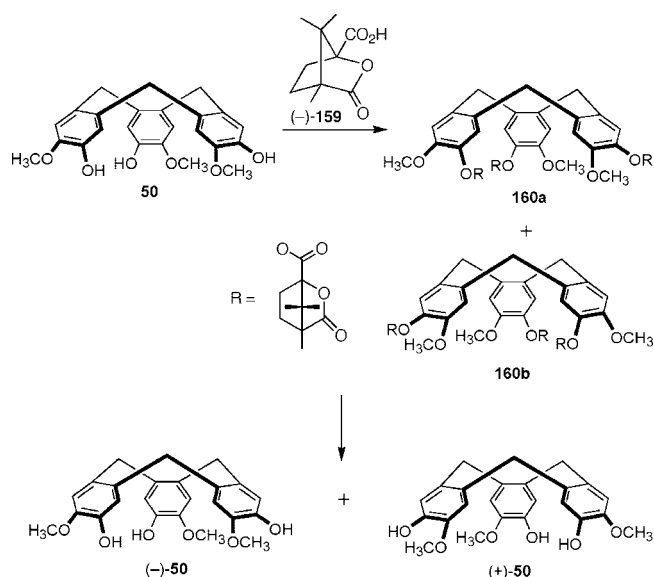
The cyclotrimeratrylene (CTV) structure in its *crown* conformation ( $C_3$  symmetry) is chiral when each aromatic ring bears two different substituents. The inversion barrier for racemization is low ( $\Delta G^\ddagger \approx 110$ – $115$  kJ/mol) but is sufficient, however, to allow the separation of the two enantiomers at room temperature. First attaching a chiral moiety on the CTV affords two diastereomers which can be separated by column chromatography or crystallization. For instance, compound **50** was resolved by using (*1S*)-(-)-camphanic acid (-)-**159** to give diastereomers **160a** and **160b**. The separation of **160a–b** was achieved by chromatography followed by crystallization. Hydrolysis of the ester groups gave rise to the resolved cyclotriguaiacylene derivatives (+)-**50** and (-)-**50** (Scheme 24).<sup>51</sup> Compared to HPLC separation, this approach rapidly supplies sizable amounts of enantiopure CTV derivatives.

Similar routes using different chiral reagents have been developed. For example, *R*-(+)-2-phenoxypropionic acid reacts with CTV ( $\pm$ )-**52** to give diastereomers *M*-*RRR*-(+)-**161a** and *P*-*RRR*-(+)-**161b**, which leads, after chromatographic separation and reduction, to the pure enantiomers (+)-**52** and (-)-**52**.<sup>51</sup> The cyclotrimerization of the benzyl derivative *S*-(-)-**162** obtained from 2-bromopropionic acid and thiovanillin, followed by an esterification step, gave diastereomers *P*-*SSS*-(-)-**163a** and *M*-*SSS*-(-)-**163b**. Raney-Ni desulfuration of *P*-*SSS*-(-)-**163a** and *M*-*SSS*-(-)-**163b** gave *M*-(+)-**43** and *P*-(-)-**43**, which are starting compounds for the preparation of the resolved cryptophane-C (**54**) (Scheme 25).<sup>142</sup>

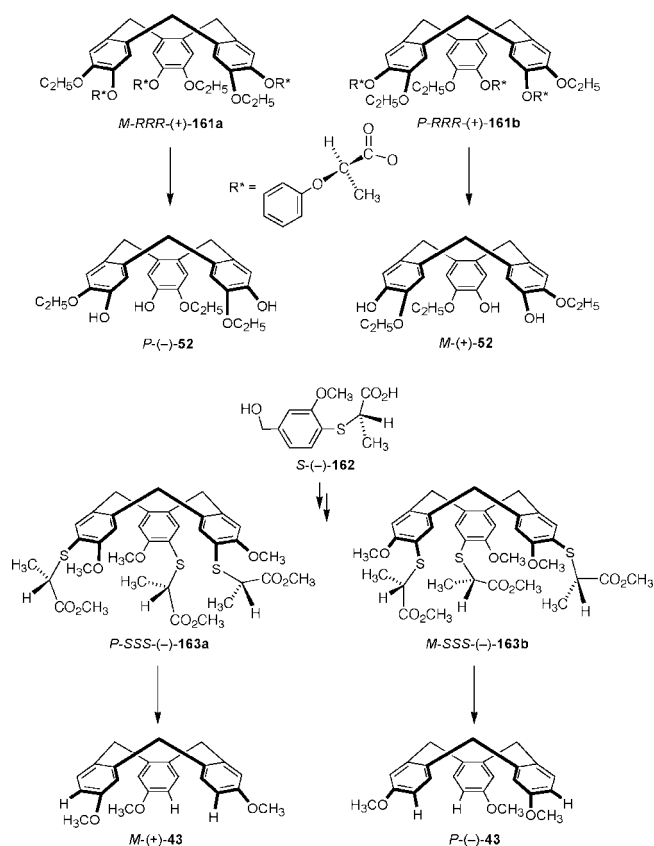
The *R*-(+)-2-(4-chlorophenoxy)propionic acid *R*-(+)-**164** has also been used successfully for the optical resolution of



Scheme 24

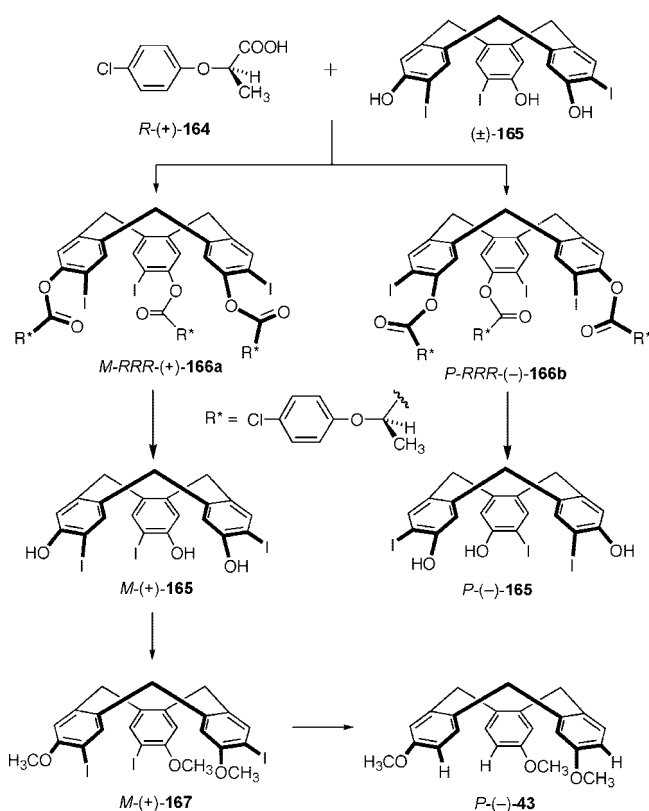


Scheme 25



cyclotriveratrylene derivatives. The reaction of the iodine containing CTV ( $\pm$ )-**165** with *R*-(+)-**164** gave rise to the two diastereomers *M*-RRR-(+)-**166a** and *P*-RRR(-)-**166b**, which were efficiently separated by column chromatography on silica gel. Then hydrolysis under mild conditions afforded the two enantiomers *M*-(+)-**165** and *P*-(-)-**165**, respectively, in low yield. Compound *M*-(+)-**165** was then allowed to react with methyl iodide at room temperature to afford compound *M*-(+)-**167**. Subsequent reaction with  $\text{LiAlH}_4$  at  $0^\circ\text{C}$  gave the enantioenriched derivative *P*-(-)-**43** (Scheme 26).<sup>70</sup>

Scheme 26



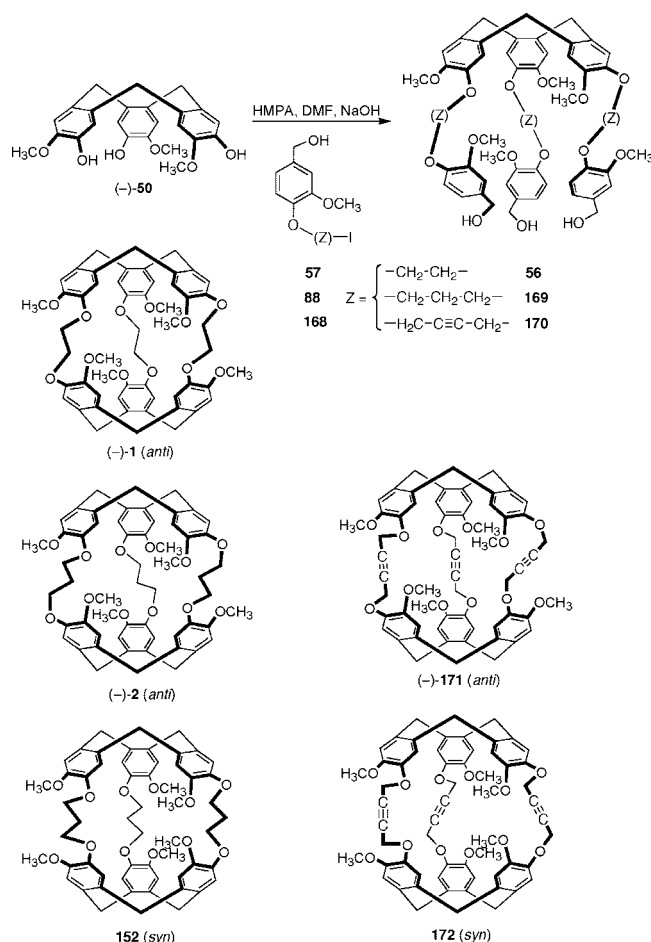
Obviously, the different procedures described above allow the production of fair amounts of enantioenriched cyclotriveratrylene derivatives with good enantiomeric excess (*ee*). Thus, even though it requires great care to avoid racemization of the CTV backbone, the optical resolution of CTVs appears as a very attractive way to synthesize enantioenriched cryptophanes. This approach, summarized in section 10.2.1, has been widely used by Collet and co-workers to investigate the chiroptical properties of cryptophanes (presented later in this section) and chiral recognition phenomena (see section 8).

## 10.2. Syntheses of Optically Pure Cryptophanes

### 10.2.1. From Enantiopure CTVs

Optically pure CTVs have been used as a platform to prepare chiral cryptophanes. As mentioned above, the drawback of this method is the need for mild experimental conditions to avoid inversion of the CTV, which causes racemization and a drop in the expected *ee*, when the reactions are performed above room temperature. For instance, the chiral precursor **56** of cryptophane-A (**1**) was prepared at room temperature from cyclotriguaiacylene ( $-$ )-**50** and iodo derivative **57**, in an aqueous mixture of DMF, HMPA, and sodium hydroxide (Scheme 27). Although the subsequent cyclization reaction was run in formic acid solution (1 mM) at higher temperature ( $60$ – $95^\circ\text{C}$ ), enantioenriched cryptophane ( $-$ )-**1** was obtained with good yield. Similarly, reaction of ( $-$ )-**50** with derivatives **88** and **168** furnished the cryptophane precursors **169** and **170**, respectively. The final cyclization step in formic acid gave rise to the optically resolved ( $-$ )-cryptophane-E (( $-$ )-**2**) and ( $-$ )-cryptophane-G (( $-$ )-**171**), respectively. In the two latter cases, the achiral meso isomers syn-cryptophane-F (**152**) and

## Scheme 27



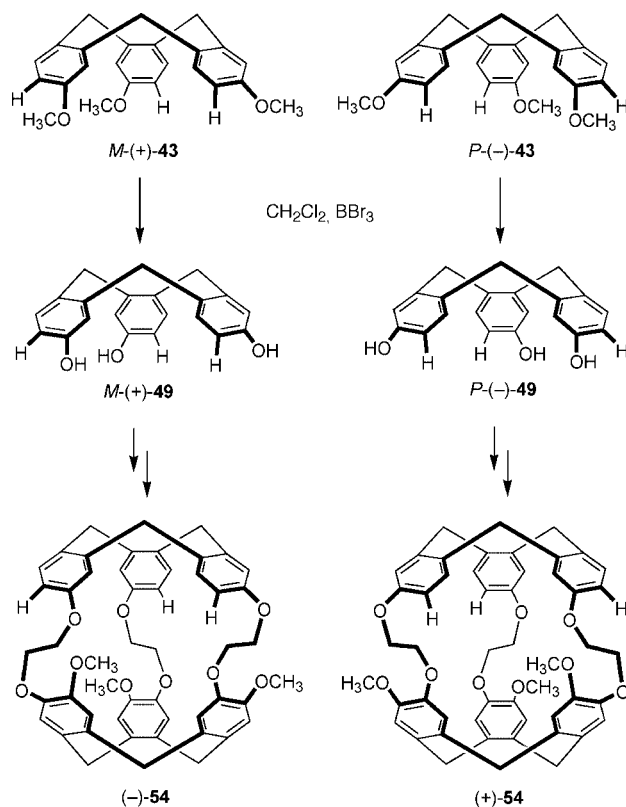
syn-cryptophane-H (**172**) were also obtained and characterized (Scheme 27).<sup>143</sup>

Enantioenriched cryptophane-C (**54**) was also prepared by following this method starting from the optically pure C<sub>3</sub>-cyclotriphenylene **49** (Scheme 28).<sup>142</sup> Several other resolved cryptophanes were synthesized from their chiral cyclotriphenylene precursors such as M-(+)-**27** and P-(−)-**27** with methylthio substituents,<sup>55</sup> and hosts bearing three ethylenic bridges in the case of the anticryptophane **158** (see Figure 48).<sup>144</sup> The resolved cryptophanes thus obtained have *ee* ≈ 90–95%. However, one has to keep in mind that partial racemization of the CTV platform still remains the main drawback with regard to the resolution of more elaborate molecules, which will have to be obtained by means of other efficient procedures.

## 10.2.2. From Cryptophanol

From the simple idea that diastereomers are often more easily separable than enantiomers, Brotin and co-workers proposed a novel approach for the optical resolution of cryptophanes based on the preparation of cryptophane diastereomers. It was important to develop a method that could give rise to optically active cryptophanes with very high enantiomeric excess, *ee* = 99–100%, which cannot be reached with the procedures described above because of the low energy barrier for racemization of the CTV backbone. The condensation of the racemic cryptophanol ( $\pm$ )-**129** described in section 4.2, with optically pure (−)-camphanic acid, led to the two expected diastereomers with excellent yields. The two compounds were separated by crystallization

## Scheme 28



from toluene to give pure (−)-**157a** and (+)-**157b** with a diastereomeric excess (*de*) of 98–100%, as determined by <sup>1</sup>H NMR spectroscopy in CDCl<sub>3</sub> (Scheme 29). The diastereomers were easily characterized by <sup>1</sup>H NMR (Figure 50). The cleavage of the ester group afforded (−)-**129** and (+)-**129**, respectively, with *ee* values close to 100%. This approach provides sizable amounts of enantiopure cryptophanol that can be used in further reactions to design new host molecules without the risk of racemization and loss of optical activity.<sup>145</sup>

This strategy was applied to the synthesis of the two enantiomers (+)-**1** and (−)-**1** of cryptophane-A, which were obtained by reacting (+)-**129** and (−)-**129** with methyl iodide, respectively. The C<sub>1</sub>-symmetrical enantiopure cryp-

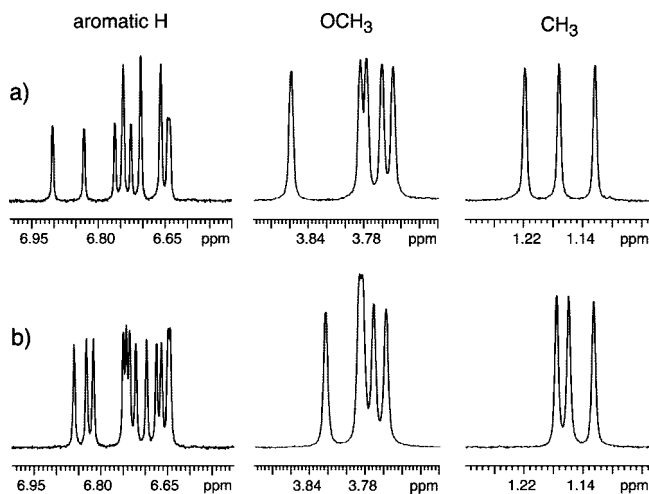
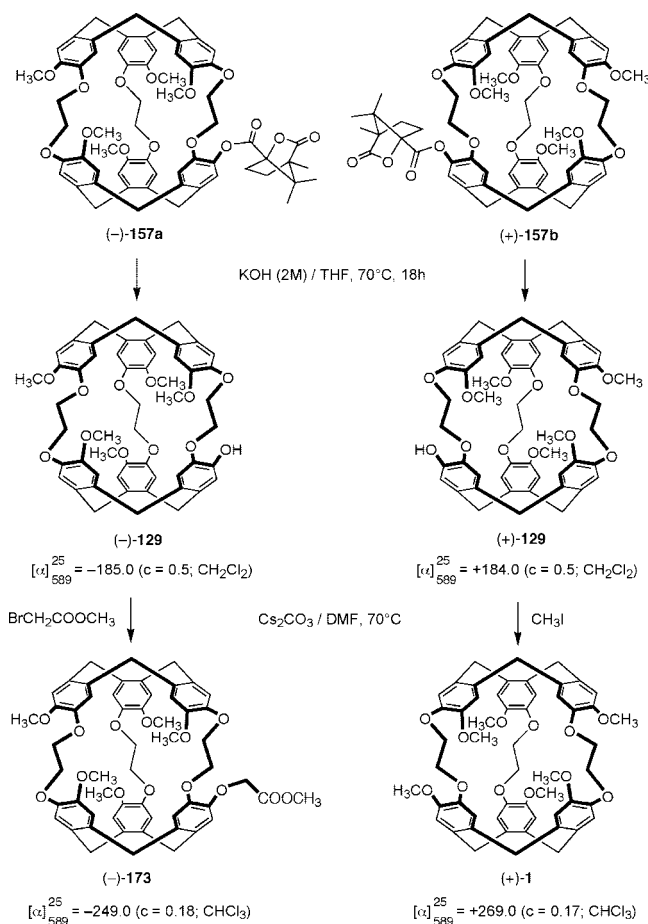


**Figure 50.** Portions of the 500 MHz <sup>1</sup>H NMR spectra of diastereomers (−)-**157a** (a) and (+)-**157b** (b) in CDCl<sub>3</sub> at 293 K (Reprinted from ref 145, Copyright 2003, with permission from Wiley-VCH).

## Scheme 29



tophane (-)-173 has also been obtained by reacting (-)-129 with methyl bromoacetate at 80 °C in DMF (Scheme 29). The racemate (±)-173 has been used for the design of cryptophane-based biosensors (section 4.3), and the resolved host is thus of particular importance for future MRI applications (see section 9.4.3).

### 10.3. Electronic Circular Dichroism (ECD) Spectra of Resolved Cryptophanes

#### 10.3.1. ECD of CTVs

Chiral cryptophanes represent a class of molecules whose chiroptical properties have been investigated by electronic circular dichroism (ECD). Indeed, they are made up of six aromatic rings in a unique rigid structure that makes these compounds interesting for studying the effects of multiple chromophores interacting within the same molecular framework. In a preliminary study, Gottarelli and Collet pioneered this work by studying the ECD spectra of a series of chiral cyclotrimeratrylene compounds. They demonstrated that a simple model derived from the excitonic coupling between the three aromatic rings could be used to predict the sign of the Cotton effect for the two forbidden transitions, B<sub>1u</sub> (<sup>1</sup>L<sub>a</sub>) and B<sub>2u</sub> (<sup>1</sup>L<sub>b</sub>), of the benzene chromophores. Using the Kuhn–Kirkwood model,<sup>146–149</sup> they showed that the sign of the ECD signals for the B<sub>1u</sub> and B<sub>2u</sub> transitions is strongly dependent on the relative intensity of the spectroscopic moments (*sm*) of the two benzylic substituents R<sup>1</sup> and R<sup>2</sup> (R<sup>1</sup> ≠ R<sup>2</sup>).<sup>150</sup> The two substituents affect the polarization angle of both the B<sub>1u</sub> and the B<sub>2u</sub> transitions. For CTVs having C<sub>3</sub>-symmetry, the use of the Kuhn–Kirkwood model

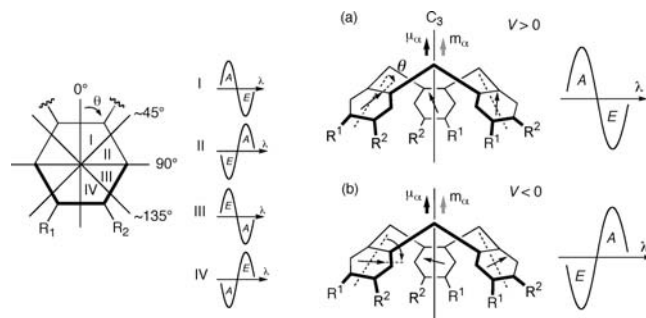


**Figure 51.** In-phase coupling of the B<sub>2u</sub> transition dipoles ( $sm(R^2) > sm(R^1)$ ). Only the A component is shown on the CTV structure. (a)  $0 < \theta < \sim 45^\circ$ , repulsive Coulombic interaction ( $V > 0$ ); (b)  $\sim 45^\circ < \theta < 90^\circ$ , attractive Coulombic interaction ( $V < 0$ ). The two E components can be obtained by changing the direction of one or two arrows shown for the A state on the CTV molecules.

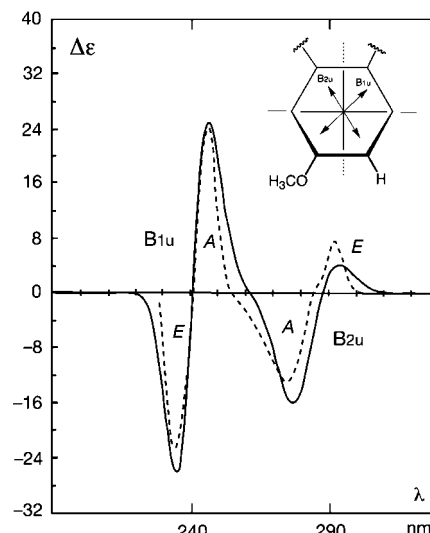


**Figure 52.** Calculated (—) and experimental (---) ECD spectra of *P*-(-)-43 (Reprinted from ref 13, Copyright 1987, with permission from Elsevier).

leads to the conclusion that each B<sub>1u</sub> and B<sub>2u</sub> transition is a combination of three components: one A component polarized along the C<sub>3</sub> axis of the CTV and two degenerate E components polarized perpendicular to the C<sub>3</sub> axis of the CTV. Two bands with opposite sign usually characterize the excitonic coupling for each B<sub>2u</sub> and B<sub>1u</sub> transition of chiral CTV derivatives. The signs of these bands are related to the nature of the substituents R<sup>1</sup> and R<sup>2</sup> (Figure 51). Simple rules that depend only on the deviation angles  $\theta$  of both the B<sub>1u</sub> and B<sub>2u</sub> transitions caused by the two substituents were then deduced to explain the excitonic coupling observed in the ECD spectra of chiral CTV compounds.<sup>51</sup> For instance, it was shown that a change of sign for the two bands is expected when the deviation angle  $\theta$ , depicted in Figure 51, reaches the *magic angles*  $\theta = 0, 45^\circ, 90^\circ$ , and  $135^\circ$ .

An example is given below with CTV *P*-(-)-43 bearing three methoxy groups at the R<sup>1</sup> position and with three hydrogen atoms at the R<sup>2</sup> position. In this example, the methoxy group possesses a much larger spectroscopic moment  $sm = 31$  (cm M)<sup>-1/2</sup> than that of the hydrogen atom ( $sm = 0$ ), thus leading to a strong deviation of the angle ( $\sim -38^\circ$ ) of the transition dipole moment for both the B<sub>1u</sub> and the B<sub>2u</sub> transitions, as reported in Figure 52.<sup>151</sup> The A component appears therefore at higher energy for the B<sub>2u</sub> transition and at lower energy for the B<sub>1u</sub> transition. A



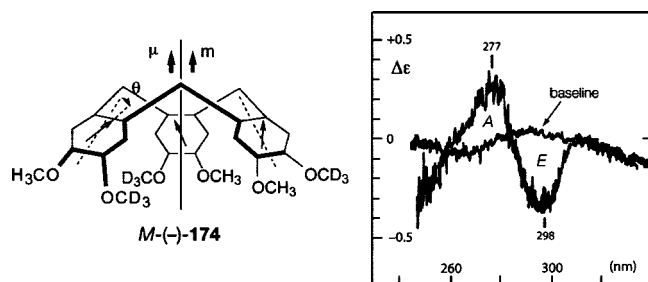


**Figure 53.** ECD spectrum of *M*(-)-**174** (Reprinted with permission from ref 152. Copyright 1981 American Chemical Society).

simulated spectrum confirms the reversal of the sign of both the *A* and *E* components for the two transitions.

It was shown by the same authors that even very small Cotton effects could be observed with CTV compounds. For instance, isotopic substitution is able to induce small ECD signals. This was nicely exemplified with the deuterium-labeled CTV *M*(-)-**174**, which exhibits two bands with opposite signs for the  $B_{2u}$  transition. The knowledge of the absolute configuration of this derivative permitted the authors to demonstrate that the  $OCD_3$  moiety possesses a slightly larger spectroscopic moment (due to conformational effects) than its congener  $OCH_3$  (Figure 53).<sup>152</sup>

### 10.3.2. ECD of $D_3$ -Symmetrical Cryptophanes

Collet and Gottarelli followed a similar approach to interpret the ECD spectra of cryptophanes with  $D_3$ -symmetry.<sup>143</sup> However, the situation is somewhat more complicated, since each  $B_{1u}$  ( $^1L_a$ ) or  $B_{2u}$  ( $^1L_b$ ) transition of the benzene rings splits into several components according to the molecular symmetry. Using the Kuhn–Kirkwood coupled exciton model to calculate the intensity and the sign of each transition, they demonstrated that the  $^1L_a$  and  $^1L_b$  forbidden transitions could be interpreted as the sum of three components with different polarization states (one  $A_2$  and two nondegenerate *E* components), resulting from the electric dipole–dipole interaction between the chromophores. The *A* and *E* components do not necessarily have the same sign or even the same energy. In contrast to the CTV derivatives with  $C_3$ -symmetry, the presence of two nondegenerate *E* components with different signs and different intensities now leads to more complicated ECD spectra for  $D_3$ -symmetrical cryptophanes. As a result, their respective transition energy and intensity may lead to very different ECD spectra depending on the substitution. As previously observed for the CTV derivatives, it was noticed experimentally that the sign of these transitions is also strongly dependent on the nature of the substituents  $R^1$  and  $R^2$  on the six benzene rings. Additionally, the observed Cotton effect is mainly governed by the polarization angles of the transition induced by the substituents, just as for the CTV derivatives. The knowledge of the polarization angle of the two forbidden transitions, that is to say the knowledge of the respective spectroscopic moment for the two substituents (for a  $D_3$ -symmetrical cryptophane) is in most cases sufficient to predict the sign of the Cotton effect of the two  $B_{1u}$  and  $B_{2u}$  transitions. Additional factors, such as the conformation of the linkers or the presence of solvent molecules inside the cavity of cryptophane derivatives, were also found to affect the experimental ECD signals.

Canceill et al. reported the ECD spectra of several partially resolved cryptophanes (*ee* = 90–95%) with known absolute

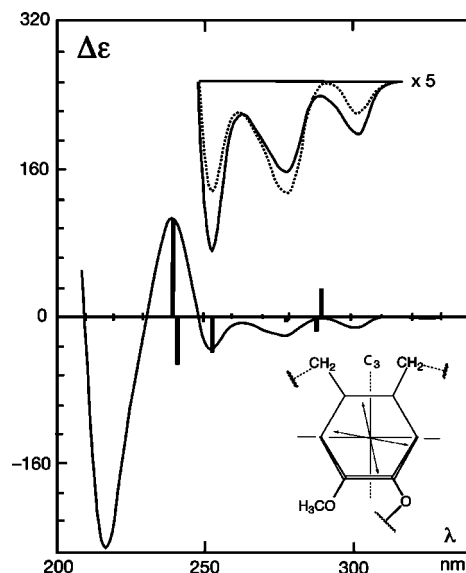


**Figure 54.** ECD spectrum of (–)-cryptophane-A ((–)-**1**) in dioxane; the inset shows the complex  $CHCl_3@(-)-1$  in dioxane (solid line) and dioxane/ $CHCl_3$  (8:2) (dotted line). The bars represent the calculated components of the  $B_{1u}$  and  $B_{2u}$  transitions; length and direction reflect the intensity and the sign of these components, respectively. Reprinted with permission from ref 143. Copyright 1987 American Chemical Society.

configuration.<sup>143</sup> They found, in most cases, a good agreement between the experimental and the theoretical ECD spectra, suggesting that the excitonic model based on the Kuhn–Kirkwood excitonic mechanism can be used, in a first approximation, to accurately describe the ECD spectra of cryptophanes. In addition, this model gave satisfactory results irrespective of the nature of the bridges connecting the two CTV units. An example is given with the ECD spectrum of the optically pure (–)-cryptophane-A ((–)-**1**) (Figure 54). It was shown that for this molecule the Kuhn–Kirkwood model predicts correctly the sign of the Cotton effect for the  $B_{1u}$  transition.<sup>143</sup> However, the prediction of the Cotton effect for the  $B_{2u}$  transition is more difficult, in this case, due to the difficulty of estimating the splitting and the relative energy between the two nondegenerate *E* components. For compound (–)-**1**, this splitting is expected to be very small. The ECD spectrum of (–)-**1** also nicely demonstrates that a large Cotton effect can be expected when two similar substituents (methoxy and alkoxy groups) are attached to the cryptophane backbone. In other words, a small deviation angle of the polarization for the two transitions  $B_{1u}$  and  $B_{2u}$  can induce a large Cotton effect in cryptophane derivatives.

Only a few enantioenriched or optically pure cryptophanes have been synthesized in order to investigate their chiroptical properties. Thus, the determination of the absolute configuration of these derivatives by means of ECD spectroscopy is still questionable. Nevertheless, it is observed experimentally with the few examples reported so far in the literature that the nature of the substituents affects more strongly the  $B_{2u}$  transition (at lower energy) than the  $B_{1u}$  transition. For instance, both the intensity and the energy of each component of the  $B_{2u}$  transition are strongly affected by the nature of the substituents  $R^1$  and  $R^2$ , thus leading to characteristic ECD signals for that transition. In contrast, the  $B_{1u}$  transition is much less affected, and consequently, the sign of the Cotton effect remains unchanged, leading to a confident determination of the absolute configuration for these compounds. Of course, further investigation with new optically pure

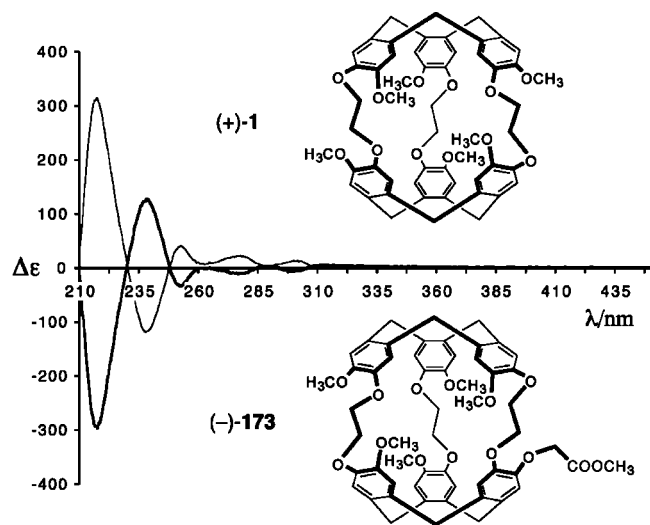


**Figure 55.** ECD spectra of cryptophanes (+)-**1** and (-)-**173** in 1,4-dioxane, showing the similarities between the two compounds. Reprinted from ref 145, Copyright 2003, with permission from Wiley-VCH.

cryptophanes with  $D_3$ -symmetry would test these assumptions. Additionally, in section 10.4 we will show that other techniques such as VCD spectroscopy give access to an unambiguous determination of the absolute configuration of cryptophane derivatives.

### 10.3.3. ECD of $C_1$ -Symmetrical Cryptophanes

Most of the work reported in the literature is focused on the synthesis and the chiroptical properties of the  $D_3$ -symmetrical cryptophane hosts, with the exception of the  $C_3$ -symmetrical cryptophane-C **54**, which discriminates the two enantiomers of CHFCIBr (see section 8). Thus, little is known about the chiroptical properties of cryptophanes of lower symmetry, as the synthesis of the enantiopure molecules is still a difficult challenge. Only the two optically pure monofunctionalized cryptophanes **129** and **173** have been investigated so far. Such compounds are expected to exhibit large differences in their ECD spectra compared to that of  $D_3$ -symmetrical cryptophanes. In this case, each Cotton band observed for the two forbidden transitions is now a combination of six nondegenerated components with different intensities and polarizations, which may not necessarily be parallel or perpendicular to the pseudo- $C_3$  axis of the CTV units. This situation is thus clearly different from that observed with cryptophane-A (**1**), where each  $^1L_a$  and  $^1L_b$  band can be described as the sum of three components each polarized perpendicular or parallel to the pseudo- $C_3$  axis of the two CTV units. The cases of the chiral monofunctionalized cryptophanes (-)-**173**, (-)-**129**, and (+)-**129** show that the molecular symmetry is not the only factor needed to induce a large change in the ECD spectra with respect to **1**. For instance, compound (-)-**173** in dioxane exhibits an ECD spectrum very similar, but with opposite sign, to that of (+)-**1**, as the  $sm$  of the  $OCH_2COOCH_3$  moiety is expected to be similar to that of the  $OCH_3$  group (Figure 55).<sup>145</sup> In this example, the symmetry breaking is not sufficient to induce a significant change in the ECD spectrum of (-)-**173** with respect to **1**.

Similarly, the two enantiomers of cryptophanol **129** exhibit very similar ECD spectra to that observed for the two enantiomers of cryptophane-A (**1**) under the same experimental conditions (Figure 56).<sup>145</sup> Although the OH group

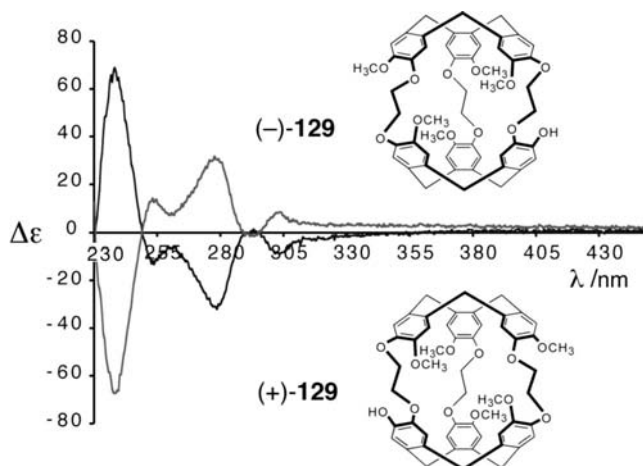


**Figure 56.** ECD spectra of the enantiomers of cryptophanol (-)-**129** and (+)-**129** in  $CHCl_3$ . Reprinted from ref 145, Copyright 2003, with permission from Wiley-VCH.

possesses a slightly higher spectroscopic moment,  $sm = 34$   $(cm M)^{-1/2}$ , than the  $OCH_3$  group,<sup>150</sup> with regard to the  $^1L_b$  transition, the difference is expected to be small. These results suggest that the model used by Collet et al. to interpret the ECD spectra of  $D_3$ -symmetrical cryptophanes can be applied in a first approximation to interpret the ECD spectra of cryptophanes **129** and **173**. However, a different situation should be considered when monofunctionalized cryptophanes bear substituents with different  $sm$  values. For instance, exchanging one  $OCH_3$  group for a strong electron-withdrawing or electron-donating group could induce larger modifications of the ECD spectra with respect to that of **1**. Obviously, the investigation of the chiroptical properties of more complex cryptophanes gives a strong impulse to further develop novel syntheses of enantiopure compounds.

To conclude this section, it is important to emphasize that the understanding of the optical properties of cryptophanes goes beyond a simple description of their photophysical properties. These molecules can serve as model compounds for interpreting the chiroptical properties of supramolecular systems having multiple interacting chromophores.

## 10.4. VCD of Cryptophane Hosts

The recent progress made in the chemistry of cryptophanes, and in particular the development of a novel approach giving access to sizable amounts of optically pure cryptophanes with  $D_3$ - or  $C_1$ -symmetry, opens new possibilities for the study of these systems by modern spectroscopic techniques. At present, vibrational circular dichroism (VCD) spectroscopy, when combined with *ab initio* calculations at the DFT level, appears to be the method of choice to determine unambiguously the absolute configuration of molecular systems.<sup>153–155</sup> This technique also gives more reliable results than the more conventional electronic circular dichroism spectroscopy when the conformation of the molecule is known. The use of a sophisticated *ab initio* quantum calculation to predict the experimental spectrum, from a selected low-energy configuration of the molecule, appears however as the main limitation of this method, since these calculations are tremendously time demanding as the size of the molecule increases. Despite this limitation, it is now possible to predict, with sufficient accuracy, the IR and VCD spectra of quite large organic molecules possessing up to approximately 100 atoms, due to recently developed

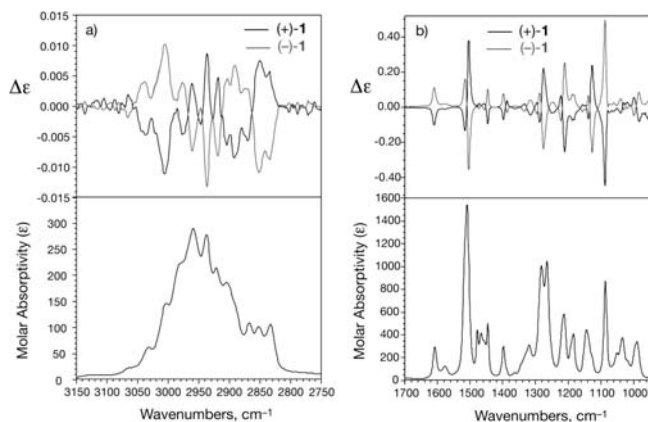


**Figure 57.** Experimental IR (lower frame) and VCD (upper frame) spectra of (+)-**1** (black line) and (-)-**1** (red line) in  $\text{CDCl}_3$  for the (a)  $3150\text{--}2750\text{ cm}^{-1}$  region and the (b)  $1700\text{--}950\text{ cm}^{-1}$  region. Reprinted with permission from ref 156. Copyright 2006 American Chemical Society.

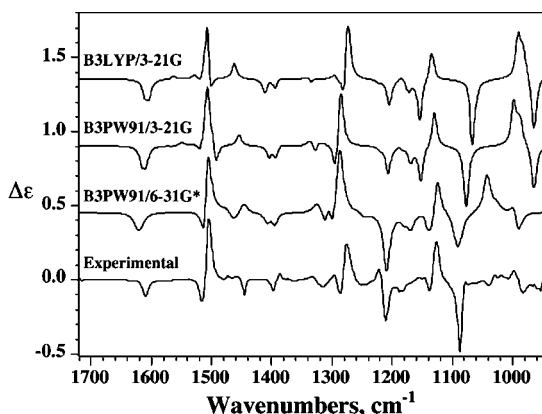


**Figure 58.** Experimental and calculated VCD spectra of (+)-cryptophane-A (**1**) (calculated for the *all-trans* conformer using three different levels). Reprinted with permission from ref 156. Copyright 2006 American Chemical Society.

computational methods and the increased power of computers. Recently, Brotin et al. published a VCD spectroscopic study of both enantiomers of cryptophane-A (**1**) (120 atoms) combined with a prediction of their experimental IR and VCD spectra by DFT calculations (Figure 57).<sup>156</sup>

As mentioned previously in this review, cryptophane-A (**1**) has no chiral center but possesses  $D_3$ -symmetry. This introduces complexity, since the calculation must be performed on the whole structure. Despite the size of cryptophane-A (**1**), a fairly reasonable agreement was found between theoretical and experimental spectra (Figure 58). Although better agreement was found using the B3PW91 functional with the 6-31G\* basis set, a small basis set such as 3-21G led to the correct prediction of the absolute configuration of the molecules.<sup>156</sup>

The results reported by Brotin et al. show that a comparison between theoretical and experimental spectra allows the determination of the absolute configuration of cryptophane-A (**1**) and gives useful information on the conformation of the alkyl chains connecting the two CTV units of the cryptophane. Indeed, the three linkers can adopt a *gauche* or a *trans* conformation (see section 5.3). It is noteworthy that the predicted VCD spectra also depend strongly on the presence or lack of an encapsulated guest inside the host cavity. The effect of encapsulation greatly influences the relative energy of the different conformations, and very

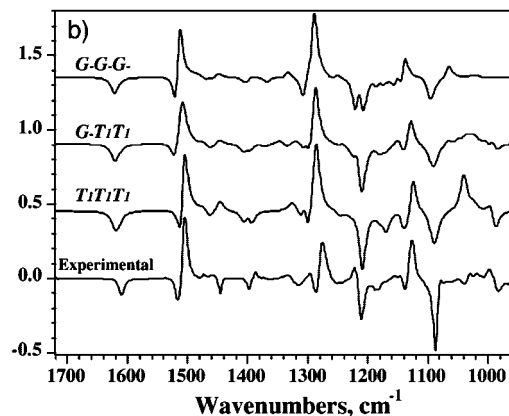
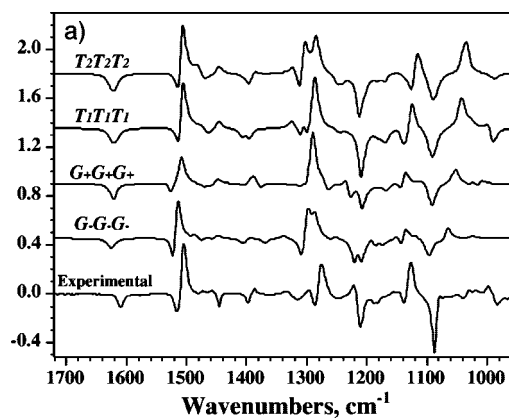


**Figure 59.** Comparison of experimental and calculated VCD spectra of (a) (+)-cryptophane-A ((+)-**1**) and (b) the  $\text{CHCl}_3@$ (+)-**1** complex. Calculated spectra at the B3PW91/6-31G\* level for different conformers. Reprinted with permission from ref 156. Copyright 2006 American Chemical Society.

different results were obtained depending on whether the gas-phase calculations were performed on the free host or on the  $\text{CHCl}_3$ -bound complex. As an example, the calculation shows that the *gauche* conformation has a lower energy than the *anti* conformation for the empty cryptophane whereas the conformational stability is reversed when the simulation is performed on the  $\text{CHCl}_3@$ cryptophane-A (**1**) complex (Figure 59). Additionally, better agreement between the experimental and the predicted spectra is observed when the *all-anti* (*aaa*) or the *gauche-anti-anti* (*gaa*) conformation of the linkers is considered. This result suggests a predominance of the *anti* conformation over the *gauche* conformation of the alkyl chains in **1**. This is corroborated by X-ray crystallography studies that show a preference for the *anti* conformation.

## 11. Conclusion—The Future of Cryptophanes

In this review we have reported the most important steps in the evolution of the chemistry of the cryptophanes, and we also note that the most exciting works are concerned with their chiroptical and binding properties. This is particularly well exemplified by the development of the xenon-based biosensors, which in our opinion is the most highlighted aspect of cryptophanes covered in the past decade. This is due, on one hand, to the exceptional characteristics of the xenon atom and its use in medical diagnostics and, on the other hand, to the great affinity of the xenon atom for certain cryptophanes. Consequently, a current challenge is the realization of supramolecular biosensors for the selective recognition of biological targets and their use in MRI in



combination with laser-polarized xenon. This topic will likely be developed extensively in the near future. The recognition of volatile organic compounds (VOCs) has been the subject of recent investigations for the detection of methane, where cryptophanes are either included in a polymeric support<sup>157</sup> or deposited on surfaces to form Langmuir–Blodgett layers.<sup>158</sup> Another example is a cryptophane-coated sensor using a quartz microbalance (QMB) sensitive to ammonia.<sup>159</sup> Other devices using cryptophanes are likely to develop in the field of environmental chemistry.

Like the *carceplexes*, the cryptophanes offer a unique environment to investigate the physical behavior of small molecules confined in the cavity of a molecular host. The emergence of new spectroscopic techniques and computational methods is also responsible for these activities. For example, Raman microspectrometry, IR, and VCD spectroscopy have been used to extract information about the cryptophane and their complexes. We must add the use of dielectric spectroscopy, which was very recently used to study the guest tumbling in the inner cavity of cryptophane-A (**1**) in molecular crystals.<sup>160</sup>

As mentioned throughout this review, the main advances in the understanding of the physical chemistry of cryptophanes are intimately connected to the development of new strategies for the synthesis of functionalized cryptophanes and for their optical resolution. The chemistry of cryptophane can be adapted to many objectives belonging to different fields of research. An interesting approach will be the functionalization of the inner space of the cryptophane cavity to construct chemical nanoreactors, as for example in novel structures such as hemicyptophanes, for which innovative work is starting to appear in the literature. Hemicyptophanes are molecular containers that share many similarities with cryptophanes, since they consist of a CTV moiety connected to an organic group of  $C_3$ -symmetry with three tentacles whose nature and length can be varied. These hosts may provide efficient and selective systems for chemical transformations when a catalytic site is included in the structure.<sup>161</sup>

Recent developments in cryptophane chemistry, and in particular the ability to selectively functionalize cryptophanes, considerably increased the interest of the scientific community in these host molecules. Methods of producing cryptophane-based materials are envisioned, and some groups are developing new strategies to construct mono- or multi-layer systems, as well as solid materials, using *polymeric*<sup>162</sup> or *dendritic* cryptophanes. Collaborative efforts among chemists, biochemists, spectroscopists, and theoreticians will ensure the successful development of future cryptophane-based structures and devices, increasing the impact of cryptophanes in biological and medical sciences as well as in nanosciences.

## 12. Dedication

This review is a tribute to the memory of Prof. André Collet, who originally designed and then developed for 18 years the chemistry of cryptophanes. His contribution is essential and is without doubt at the origin of many investigations in the fields of host–guest chemistry, biosensing, and chiral discrimination.

## 13. Acknowledgments

We are indebted to Dr. P. Berthault, Dr. J. Crassous, Prof. B. Goodson, Prof. T. Holman, and Prof. C. Roussel for their

help in providing figures and schemes as well as communicating some prospective ideas in forthcoming investigations on cryptophane hosts. Dr. K. Chaffee, Dr. H. Fogarty, and Dr. S. Karlen are greatly acknowledged for their invaluable critical reading of the manuscript.

## 14. Note Added in Proof

Since the submission of this review, several papers have appeared dealing with the chemistry of cryptophane derivatives and the study of their binding properties. Recent works relevant to the formation of cryptophane-like structures and nanocages by self-assembly of CTV derivatives have been reported.<sup>163</sup> Additional articles on the encapsulation and detection of gases by cryptophane hosts have been published.<sup>164</sup> The characterization and the chiroptical properties of enantiopure cryptophanes were investigated further.<sup>165</sup> Clearly, the future of cryptophanes appears in the exciting developments of xenon-based biosensors for applications in magnetic resonance imaging (MRI) using hyperpolarized xenon gas.<sup>166</sup>

## 15. References

- (1) Cram, D. J.; Cram, J. M. *Container Molecules and their guests Monographs in Supramolecular Chemistry*; Stoddart, J. F., Eds. The Royal Society of Chemistry: Thomas Graham House, Science Park, Cambridge, U.K., 1994.
- (2) Frömring, K. H. In *Comprehensive Supramolecular Chemistry*; Atwood, J. L., Lehn, J.-M., Davies, J. E. D., MacNicol, D. D., Vögtle, F., Eds.; Elsevier: Amsterdam, 1996; Vol. 10, p 445.
- (3) Rudkevitch, D. M.; Leontiev, A. V. *Aust. J. Chem.* **2004**, *57*, 713.
- (4) Vriezema, D. M.; Comellas Aragonès, M.; Elemans, J. A. A. W.; Cornelissen, J. J. L. M.; Rowan, A. E.; Nolte, R. J. M. *Chem. Rev.* **2005**, *105*, 1445.
- (5) Sanders, J. K. M. *Chem.—Eur. J.* **1998**, *4*, 1378.
- (6) Pluth, M. D.; Bergman, R. G.; Raymond, K. N. *Science* **2007**, *316*, 85.
- (7) The name cryptophane was introduced by A. Collet to designate this new class of molecules, recalling the cyclophane structure and the presence of an inner cavity.
- (8) Gabard, J.; Collet, A. *J. Chem. Soc. Chem. Commun.* **1981**, 1137.
- (9) Garel, L.; Dutasta, J.-P.; Collet, A. *Angew. Chem. Int. Ed. Engl.* **1993**, *32*, 1169.
- (10) Garel, L.; Lozach, B.; Dutasta, J.-P.; Collet, A. *J. Am. Chem. Soc.* **1993**, *115*, 11652.
- (11) Costante-Crassous, J.; Marone, T. J.; Briggs, J. M.; McCammon, J. A.; Collet, A. *J. Am. Chem. Soc.* **1997**, *119*, 3818.
- (12) Bartik, K.; Luhmer, M.; Dutasta, J.-P.; Collet, A.; Reisse, J. *J. Am. Chem. Soc.* **1998**, *120*, 784.
- (13) Collet, A. *Tetrahedron* **1987**, *43*, 5725.
- (14) Collet, A.; Dutasta, J.-P.; Lozach, B.; Canceill, J. *Top. Curr. Chem.* **1993**, *165*, 103.
- (15) Collet, A.; Dutasta, J.-P.; Lozach, B. In *Advances in Supramolecular Chemistry* Gokel, G. W., Eds.; JAI Press Inc.: 1993; Vol. 3, p 1.
- (16) Collet, A. In *Comprehensive Supramolecular Chemistry*; Atwood, J. L., Lehn, J.-M., Davies, J. E. D., MacNicol, D. D., Vögtle, F., Eds.; Elsevier: Amsterdam, 1996; Vol. 2, p 325.
- (17) Holman, K. T. In *Encyclopedia of Supramolecular Chemistry*; Atwood, J., Eds.; Marcel Dekker Inc.: 2004; p 340.
- (18) See ref 1, Chapter 10.
- (19) Jasat, A.; Sherman, J. C. *Chem. Rev.* **1999**, *99*, 931.
- (20) Rebeck, J., Jr. *Chem. Soc. Rev.* **1996**, 255.
- (21) Caulder, D. L.; Raymond, K. N. *Acc. Chem. Res.* **1999**, *32*, 975.
- (22) Fujita, M.; Umemoto, K.; Yoshizawa, M.; Fujita, N.; Kusakawa, T.; Biradha, K. *Chem. Commun.* **2001**, 509.
- (23) Goodson, B. M. *J. Magn. Reson.* **2002**, *155*, 157.
- (24) Cherubini, A.; Bifone, A. *Prog. Nucl. Magn. Reson. Spectrosc.* **2003**, *42*, 1.
- (25) Oros, A.-M.; Shah, N. *J. Phys. Med. Biol.* **2004**, R105.
- (26) Collet, A.; Gabard, J. *J. Org. Chem.* **1980**, *45*, 5400.
- (27) Zimmermann, H.; Tolstoy, P.; Limbach, H.-H.; Poupko, R.; Luz, Z. *J. Phys. Chem. B* **2004**, *108*, 18772.
- (28) For example, the systematic name for cryptophane-E (**2**) is 3,23-(epoxypropanoxy)-6,9:26,29-dietheno-7,38:18,27-dimethano-15,19:35,39-dimetheno-11H,19H,31H,39H-dibenzo[k,c<sub>1</sub>][1,5,19,23]tetra-

- oxacyclohexatriacontin-5,12,13,20,25,32,33,40-octahydro-2,16,22,36,43,52-hexamethoxy-(±).
- (29) In the direct method, the use of dissymmetrical bis(benzyl alcohol) derivatives would lead to untractable mixtures of cryptophane compounds.
- (30) Roesky, C. E. O.; Weber, E.; Rambusch, T.; Stephan, H.; Gloe, K.; Czugler, M. *Chem.—Eur. J.* **2003**, *9*, 1104.
- (31) Mough, S. T.; Goeltz, J. C.; Holman, K. T. *Angew. Chem.* **2004**, *43*, 5631.
- (32) Garcia, C.; Aubry, A.; Collet, A. *Bull. Soc. Chim. Fr.* **1996**, *133*, 853.
- (33) Miura, M.; Yuzawa, S.; Takeda, Mi.; Takeda, Ma.; Habata, Y.; Tanase, T.; Akabori, S. *Supramol. Chem.* **1996**, *8*, 53.
- (34) Akabori, S.; Miura, M.; Takeda, M.; Yuzawa, S.; Habata, Y.; Ishii, T. *Supramol. Chem.* **1996**, *7*, 187.
- (35) Akabori, S.; Takeda, M.; Miura, M. *Supramol. Chem.* **1999**, *10*, 253.
- (36) Garcia, C.; Humilière, D.; Riva, N.; Collet, A.; Dutasta, J.-P. *Org. Biomol. Chem.* **2003**, *1*, 2207.
- (37) (a) Newman, M. S.; Karnes, H. A. *J. Org. Chem.* **1966**, *31*, 3980. (b) Kwart, K.; Evans, E. R. *J. Org. Chem.* **1966**, *31*, 410. (c) Rahman, L. K. A.; Scrowston, R. M. *J. Chem. Soc., Perkin Trans. 1* **1983**, 2973.
- (38) Garcia, C.; Andraud, C.; Collet, A. *Supramol. Chem.* **1992**, *1*, 31.
- (39) Cram, D. J.; Tanner, M. E.; Keipert, S. J.; Knobler, C. B. *J. Am. Chem. Soc.* **1991**, *113*, 8909.
- (40) Garcia, C.; Malthête, J.; Collet, A. *Bull. Soc. Chim. Fr.* **1993**, *130*, 93.
- (41) Canceill, J.; Gabard, J.; Collet, A. *J. Chem. Soc., Chem. Commun.* **1983**, 122.
- (42) Brotin, T.; Roy, V.; Dutasta, J.-P. *J. Org. Chem.* **2005**, *70*, 6187.
- (43) Scott, J. L.; MacFarlane, D. R.; Raston, C. L.; Mei Teoh, C. *Green Chem.* **2000**, *2*, 123.
- (44) Humilière, D. Doctorat thesis, École Normale Supérieure de Lyon, France, 2002.
- (45) Thomas, R. M.; Mohan, G. H.; Iyengar, D. S. *Tetrahedron Lett.* **1997**, *38*, 4721.
- (46) Bohle, D. S.; Stasko, D. J. *Inorg. Chem.* **2000**, *39*, 5768.
- (47) (a) Sumbly, C. J.; Hardie, M. J. *Angew. Chem., Int. Ed.* **2005**, *44*, 6395. (b) Sumbly, C. J.; Fisher, J.; Prior, T. J.; Hardie, M. J. *Chem.—Eur. J.* **2006**, *12*, 2945.
- (48) Canceill, J.; Collet, A. *New J. Chem.* **1986**, *10*, 17.
- (49) Canceill, J.; Collet, A. *J. Chem. Soc., Chem. Commun.* **1983**, 1145.
- (50) Brotin, T.; Devic, T.; Lesage, A.; Emsley, L.; Collet, A. *Chem.—Eur. J.* **2001**, *7*, 1561.
- (51) Canceill, J.; Collet, A.; Gabard, J.; Gottarelli, G.; Spada, G. P. *J. Am. Chem. Soc.* **1985**, *107*, 1299.
- (52) Canceill, J.; Lacombe, L.; Collet, A. *C. R. Acad. Sci. Paris, Sér. II* **1984**, *298*, 39.
- (53) Zhong, Z.; Ikeda, A.; Shinkai, S.; Sakamoto, S.; Yamaguchi, K. *Org. Lett.* **2001**, *3*, 1085.
- (54) Lee, S. B.; Hong, J.-I. *Tetrahedron Lett.* **1996**, 8501.
- (55) Soulard, P.; Asselin, P.; Cuisset, A.; Aviles Moreno, J. R.; Huet, T. R.; Petitprez, D.; Demaison, J.; Freedman, T. B.; Cao, X.; Nafie, L. A.; Crassous, J. *Phys. Chem. Phys.* **2006**, *8*, 79.
- (56) (a) Chauvet, J.-P.; Gambut, L.; Seauve, A.; Garcia, C.; Collet, A. *C. R. Acad. Sci. Paris, Sér. II* **1994**, *318*, 771. (b) Gambut, L.; Chauvet, J.-P.; Garcia, C.; Berge, B.; Renault, A.; Rivière, S.; Meunier, J.; Collet, A. *Langmuir* **1996**, *12*, 5407.
- (57) Gosse, I.; Chauvet, J.-P.; Dutasta, J.-P. *New J. Chem.* **2005**, *29*, 1549.
- (58) Brotin, T.; Dutasta, J.-P. *Eur. J. Org. Chem.* **2003**, 973.
- (59) A convenient nomenclature was used for this series of cryptophanes, where -223, -233, and -224 refer to the number of CH<sub>2</sub> groups in the alkyl linkers.
- (60) Canceill, J.; Lacombe, L.; Collet, A. *J. Chem. Soc., Chem. Commun.* **1987**, 219.
- (61) For the formation of PPh<sub>2</sub>Li or dealkylation reactions of alkyl aryl ethers, see: (a) Mann, F. G.; Pragnell, M. J. *J. Chem. Soc.* **1965**, 4120. (b) Vedejs, E.; Fuchs, P. L. *J. Am. Chem. Soc.* **1973**, *95*, 822. (c) Ashby, E. C.; Gurumurthy, R.; Riddlehuber, R. W. *J. Org. Chem.* **1993**, *58*, 5832. (d) Vériot, G.; Collet, A. *Acros Org. Acta* **1995**, *1*, 40.
- (62) Collet, A.; Dutasta, J.-P.; Lozach, B. *Bull. Soc. Chim. Belg.* **1990**, *99*, 617.
- (63) Lozach, B. Doctorat thesis, University of Lyon, France, 1991.
- (64) Huber, G.; Brotin, T.; Dubois, L.; Desvaux, H.; Dutasta, J.-P.; Berthault, P. *J. Am. Chem. Soc.* **2006**, *128*, 6239.
- (65) Darzac, M.; Brotin, T.; Bouchu, D.; Dutasta, J.-P. *Chem. Commun.* **2002**, 48.
- (66) Darzac, M.; Brotin, T.; Rousset-Arzel, L.; Bouchu, D.; Dutasta, J.-P. *New J. Chem.* **2004**, *28*, 502.
- (67) Zang, H. X.; Guibé, F.; Balavoine, G. *Tetrahedron Lett.* **1988**, *29*, 619.
- (68) (a) Spence, M. M.; Rubin, S. M.; Dimitrov, I. E.; Ruiz, E. J.; Wemmer, D. E.; Pines, A.; Yao, S. Q.; Tian, F.; Schultz, P. G. *Proc. Natl. Acad. Sci. U.S.A.* **2001**, *98*, 10654. (b) Spence, M. M.; Ruiz, E. J.; Rubin, S. M.; Lowery, T. J.; Wemmer, N.; Schultz, P. G.; Wemmer, D. E.; Pines, A. *J. Am. Chem. Soc.* **2004**, *126*, 15287.
- (69) Lowery, T. J.; Garcia, S.; Chavez, L.; Ruiz, E. J.; Wu, T.; Brotin, T.; Dutasta, J.-P.; King, D. S.; Schultz, P. G.; Pines, A.; Wemmer, D. E. *ChemBioChem* **2006**, *7*, 65.
- (70) Garcia, C.; Collet, A. *Bull. Soc. Chim. Fr.* **1995**, *132*, 52.
- (71) For the use of the P and M descriptors for the CTVs, see: Collet, A.; Gabard, J.; Jacques, J.; Cesario, M.; Guilhem, J.; Pascard, C. *J. Chem. Soc., Perkin Trans. 1* **1981**, 1630.
- (72) (a) Tellenbröcker, J.; Kuck, D. *Angew. Chem., Int. Ed.* **1999**, *38*, 919. (b) Harig, M.; Neumann, B.; Stammli, H.-G.; Kuck, D. *Eur. J. Org. Chem.* **2004**, 2381.
- (73) (a) Kuck, D. *Chem. Rev.* **2006**, *106*, 4885. (b) Kuck, D. *Pure Appl. Chem.* **2006**, *78*, 749.
- (74) (a) Irico, A.; Vincenti, M.; Dalcanale, E. *Chem.—Eur. J.* **2001**, *7*, 2034. (b) Ventola, E.; Vainotialo, P.; Suman, M.; Dalcanale, E. *J. Am. Chem. Soc. Mass Spectrom.* **2006**, *17*, 213. (c) Baytkin, B.; Baytekin, H. T.; Schalley, C. A. *Org. Biomol. Chem.* **2006**, *4*, 2825.
- (75) Brotin, T.; Darzac, M.; Forest, D.; Becchi, M.; Dutasta, J.-P. *J. Mass Spectrom.* **2001**, *36*, 1092.
- (76) (a) In non-degassed solution, the presence of dissolved gas (O<sub>2</sub>, N<sub>2</sub>) or water molecules inside the cryptophane cavities cannot be excluded. The presence of dissolved oxygen can increase even more the broadening of the signals (see, for instance: (b) Tanner, M. E.; Knobler, C. B.; Cram, D. J. *J. Org. Chem.* **1992**, *57*, 40.
- (77) Garel, L. Doctorat thesis, University of Lyon, France, 1995.
- (78) At the time of this work, the possibility to have an out-saddle conformer was not considered. In the light of recent results and the lack of variable temperature NMR experiments, the out-saddle conformer cannot be excluded for inv-113 instead of the in-out conformer. The value of the activation energy, close to that reported in ref 31 supports this assumption.
- (79) Le Letty, M. Doctorat thesis, École Normale Supérieure de Lyon, France, 1997.
- (80) Cavagnat, D.; Brotin, T.; Bruneel, J.-L.; Dutasta, J.-P.; Thozet, A.; Perrin, M.; Guillaume, F. *J. Phys. Chem. B* **2004**, *108*, 5572.
- (81) Canceill, J.; Cesario, M.; Collet, A.; Guilhem, J.; Lacombe, L.; Lozach, B.; Pascard, C. *Angew. Chem., Int. Ed. Engl.* **1989**, *28*, 1246.
- (82) Renault, A.; Talham, D.; Canceill, J.; Batail, P.; Collet, A.; Lajzerowicz, J. *Angew. Chem., Int. Ed. Engl.* **1989**, *28*, 1249.
- (83) Renault, A.; Lajzerowicz, J.; Batail, P.; Coulon, C. *Bull. Soc. Chim. Fr.* **1993**, *130*, 740.
- (84) Canceill, J.; Cesario, M.; Collet, A.; Guilhem, J.; Pascard, C. *J. Chem. Soc., Chem. Commun.* **1985**, 361.
- (85) Canceill, J.; Cesario, M.; Collet, A.; Guilhem, J.; Riche, C.; Pascard, C. *J. Chem. Soc., Chem. Commun.* **1986**, 339.
- (86) 1,1,2,2-Tetrachloroethane-d<sub>2</sub> is a quite acidic solvent but was preferred to hexachloroacetone due to its higher stability (see ref 39).
- (87) Canceill, J.; Lacombe, L.; Collet, A. *J. Am. Chem. Soc.* **1985**, *107*, 6993.
- (88) Canceill, J.; Lacombe, L.; Collet, A. *J. Am. Chem. Soc.* **1986**, *108*, 4230.
- (89) Mecozzi, S.; Rebek, J., Jr. *Chem.—Eur. J.* **1998**, *4*, 1016.
- (90) This value was deduced from the previous one reported for cryptophane-A (**1**) as estimated with the program GRASP (see ref 89). A smaller value (81.5 Å<sup>3</sup>), determined with the molecular modeling software PCMODEL, was reported earlier (see ref 9).
- (91) Varnek, A.; Helissen, S.; Wipff, G.; Collet, A. *J. Comput. Chem.* **1998**, *19*, 820.
- (92) Garel, L.; Vezin, H.; Dutasta, J.-P.; Collet, A. *Chem. Commun.* **1996**, 719.
- (93) Garel, L.; Dutasta, J.-P.; Collet, A. *New J. Chem.* **1996**, *20*, 1265.
- (94) Cram, D. J.; Karbach, S.; Kim, Y. H.; Baczynskyj, L.; Marti, K.; Sampson, R. M.; Kallemeyn, G. *J. Am. Chem. Soc.* **1988**, *110*, 2554.
- (95) Cram, D. J.; Kaneda, T.; Helgeson, R. C.; Brown, S. B.; Knobler, C. B.; Maverick, E.; Trueblood, K. N. *J. Am. Chem. Soc.* **1985**, *107*, 3645.
- (96) Fairchild, R. M.; Holman, K. T. *J. Am. Chem. Soc.* **2005**, *127*, 16364.
- (97) Lang, J.; Dechter, J. J.; Effemey, M.; Kowalewski, J. *J. Am. Chem. Soc.* **2001**, *123*, 7852.
- (98) Tosner, Z.; Lang, J.; Sandström, D.; Petrov, O.; Kowalewski, J. *J. Phys. Chem. A* **2002**, *106*, 8870.
- (99) (a) Tosner, Z.; Petrov, O.; Dvinskikh, S. V.; Kowalewski, J.; Sandström, D. *Chem. Phys. Lett.* **2004**, *388*, 208. (b) Petrov, O.; Tosner, Z.; Csöreg, I.; Kowalewski, J.; Sandström, D. *J. Phys. Chem. A* **2005**, *109*, 4442.
- (100) Crassous, J.; Hediger, S. *J. Phys. Chem. A* **2003**, *107*, 10233.
- (101) Kirchhoff, P. D.; Bass, M. B.; Hanks, B. A.; Briggs, J. M.; Collet, A.; McCammon, J. A. *J. Am. Chem. Soc.* **1996**, *118*, 3237.



- (102) Kirchoff, P. D.; Dutasta, J.-P.; Collet, A.; McCammon, J. A. *J. Am. Chem. Soc.* **1997**, *119*, 8015.
- (103) Kirchoff, P. D.; Dutasta, J.-P.; Collet, A.; McCammon, J. A. *J. Am. Chem. Soc.* **1999**, *121*, 381.
- (104) Marjanska, M.; Goodson, B. M.; Castiglione, F.; Pines, A. *J. Phys. Chem. B* **2003**, *107*, 12558.
- (105) Chaffee, K. E.; Marjanska, M.; Goodson, B. M. *Solid State Nucl. Magn. Reson.* **2006**, *29*, 104.
- (106) Costante, J.; Hecht, L.; Polavarapu, P. L.; Collet, A.; Barron, L. D. *Angew. Chem., Int. Ed. Engl.* **1997**, *36*, 885.
- (107) Crassous, J.; Chardonnet, C.; Saue, T.; Schwerdtfeger, P. *Org. Biomol. Chem.* **2005**, *3*, 2218.
- (108) It is interesting to note that, according to the occupancy factor defined by Rebek Jr. (see section 6.1), radon is probably the ideal guest for cryptophane-A, and development of radon sensors based on cryptophane-A should be seriously considered, taking into account its radioactive properties.
- (109) Gast, K. K.; Eberle, B.; Schmiedeskamp, J.; Kauczor, H. U. *Acad. Radiol.* **2003**, *10*, 1119.
- (110) Leawoods, J. C.; Yablonskiy, D. A.; Saam, B. T.; Gierada, D. S.; Conradi, M. S. *Concepts Magn. Reson.* **2001**, *13*, 277.
- (111) Möller, H. E.; Chen, X. J.; Saam, B. T.; Hagspiel, K. D.; Johnson, G. A.; Altes, T. A.; de Lange, E. E.; Kauczor, H. U. *Magn. Reson. Med.* **2002**, *47*, 1029.
- (112) Cram, D. J.; Tanner, M. E.; Knobler, C. B. *J. Am. Chem. Soc.* **1991**, *113*, 7717.
- (113) Robbins, T. A.; Knobler, C. B.; Bellew, D. R.; Cram, D. J. *J. Am. Chem. Soc.* **1994**, *116*, 111.
- (114) Branda, N.; Grotzfeld, R. M.; Valdés, C.; Rebek, J., Jr. *J. Am. Chem. Soc.* **1995**, *117*, 85.
- (115) Valdés, C.; Spitz, U. P.; Toledo, L. M.; Kubik, S. W.; Rebek, J., Jr. *J. Am. Chem. Soc.* **1995**, *117*, 12733.
- (116) Bartik, K.; Luhmer, M.; Heyes, S. J.; Ottinger, R.; Reisse, J. *J. Magn. Reson.* **1995**, *109*, 164.
- (117) El Haouaj, M.; Luhmer, M.; Ko, Y.-H.; Kim, K.; Bartik, K. *J. Chem. Soc., Perkin Trans. 2* **2001**, 804.
- (118) <sup>129</sup>Xe chemical shifts were referenced to the resonance frequency of pure xenon gas extrapolated to zero pressure.
- (119) Reisse, J. *Nouv. J. Chim.* **1986**, *10*, 665.
- (120) Raftery, D. *Annu. Rep. NMR Spectrosc.* **2006**, *57*, 205.
- (121) Brotin, T.; Lesage, A.; Emsley, L.; Collet, A. *J. Am. Chem. Soc.* **2000**, *122*, 1171.
- (122) Sears, D. N.; Jameson, C. J. *J. Chem. Phys.* **2003**, *119*, 12231.
- (123) Bartik, K.; Luhmer, M.; Reisse, J. Private communication.
- (124) Bartik, K.; El Haouaj, M.; Luhmer, M.; Collet, A.; Reisse, J. *ChemPhysChem* **2000**, *4*, 221.
- (125) Bartik, K.; Luhmer, M.; Collet, A.; Reisse, J. *Chirality* **2001**, *13*, 2.
- (126) (a) Sears, D.; Jameson, C.; Harris, R. A. *J. Chem. Phys.* **2003**, *119*, 2685. (b) **2003**, *119*, 2691. (c) **2003**, *119*, 2694. (d) **2004**, *120*, 3277.
- (127) Bartik, K.; Choquet, P.; Constantinesco, A.; Duhamel, G.; Fraissard, J.; Hyacinthe, J.-N.; Jokisaari, J.; Locci, E.; Lowery, T. J.; Luhmer, M.; Meersmann, T.; Moudrakovski, I. L.; Pavlovskaya, G. E.; Pierce, K. L.; Pines, A.; Ripmeester, J. A.; Telkki, V.-V.; Veeman, W. S. *L'actualité Chim.* **2005**, *287*, 16.
- (128) Huber, J. G.; Dubois, L.; Desvieux, H.; Dutasta, J.-P.; Brotin, T.; Berthault, P. *J. Phys. Chem. A* **2004**, *108*, 9608.
- (129) Ruiz, E. J.; Spence, M. M.; Rubin, S. M.; Wemmer, D. E.; Pines, A.; Winssinger, N.; Tian, F.; Yao, S. Q.; Schultz, P. G. Presented at the 43rd Experimental NMR Conference, Asilomar, CA, April 14–19, 2002.
- (130) Song, Y.-Q. *Concepts Magn. Reson.* **2000**, *12*, 6.
- (131) Luhmer, M.; Goodson, B. M.; Song, Y.-Q.; Laws, D. D.; Kaiser, L.; Cyrier, M. C.; Pines, A. *J. Am. Chem. Soc.* **1999**, *121*, 3502.
- (132) Desvieux, H.; Huber, J. G.; Brotin, T.; Dutasta, J.-P.; Berthault, P. *ChemPhysChem* **2003**, *4*, 384.
- (133) Dubois, L.; Berthault, P.; Huber, J. G.; Desvieux, H. C. R. *Phys.* **2004**, *5*, 305.
- (134) Ruiz, E. J.; Sears, D. N.; Pines, A.; Jameson, C. J. *J. Am. Chem. Soc.* **2006**, *128*, 16980.
- (135) Wei, Q.; Seward, G. K.; Hill, P. A.; Patton, B.; Dimitrov, I. E.; Kuzma, N. N.; Dmochowski, I. J. *J. Am. Chem. Soc.* **2006**, *128*, 13274.
- (136) Hilty, C.; Lowery, T. J.; Wemmer, D. E.; Pines, A. *Angew. Chem., Int. Ed.* **2006**, *45*, 70.
- (137) Han, S.-I.; Garcia, S.; Lowery, T. J.; Ruiz, E. J.; Seeley, J. A.; Chavez, L.; King, D. S.; Wemmer, D. E.; Pines, A. *Anal. Chem.* **2005**, *77*, 4008.
- (138) Mynar, J. L.; Lowery, T. J.; Wemmer, D. E.; Pines, A.; Fréchet, J. M. J. *J. Am. Chem. Soc.* **2006**, *128*, 6334.
- (139) Schröder, L.; Lowery, T. J.; Hilty, C.; Wemmer, D. E.; Pines, A. *Science* **2006**, *314*, 446.
- (140) Jacques, J.; Collet, A.; Wilen, S. H. *Enantiomers, racemates and resolutions*; Krieger Publishing Company: Malabar, FL, 1991; pp 32–166.
- (141) Tambuté, A.; Canceill, J.; Collet, A. *Bull. Chem. Soc. Jpn.* **1989**, *62*, 1390.
- (142) Costante, J.; Garcia, C.; Collet, A. *Chirality* **1997**, *9*, 446.
- (143) Canceill, J.; Collet, A.; Gottarelli, G.; Palmieri, P. *J. Am. Chem. Soc.* **1987**, *109*, 6454.
- (144) Gabard, J.; Canceill, J.; Collet, A. *Tetrahedron* **1987**, *43*, 4531.
- (145) Brotin, T.; Barbe, R.; Darzac, M.; Dutasta, J.-P. *Chem.—Eur. J.* **2003**, *9*, 5784.
- (146) Kuhn, W. *Trans. Faraday Soc.* **1930**, *26*, 293.
- (147) Kirkwood, J. G. *J. Chem. Phys.* **1937**, *5*, 479.
- (148) Schellman, J. A. *Acc. Chem. Res.* **1968**, *1*, 144.
- (149) Harada, N.; Nakanishi, K. *Circular Dichroic Spectroscopy: Exciton Coupling in Organic Stereochemistry*; University Science Books: Mill Valley, CA, 1983.
- (150) The spectroscopic moments are empirical parameters, which have been introduced to quantify the influence of the substituents on the absorption intensities in aromatic compounds. See, for instance: (a) Platt, J. R. *J. Chem. Phys.* **1951**, *19*, 263. (b) Sagiv, J. *Tetrahedron* **1977**, *33*, 2303. (c) **1977**, *33*, 2315.
- (151) Collet, A.; Gottarelli, G. *Croat. Chem. Acta* **1989**, *62*, 279.
- (152) Collet, A.; Gottarelli, G. *J. Am. Chem. Soc.* **1981**, *103*, 5912.
- (153) Stephens, P. J. In *Computational Medicinal Chemistry for Drug Discovery*; Bultinck, P., de Winter, H., Langenaecker, W., Tollenaere, J., Eds.; Dekker: New York, 2003; pp 699–725.
- (154) Freedman, T. B.; Cao, X.; Dukor, R. K.; Nafie, L. A. *Chirality* **2003**, *15*, 743, and references therein.
- (155) Stephens, P. J.; Delvin, F. J. *Chirality* **2000**, *12*, 172.
- (156) Brotin, T.; Cavagnat, D.; Dutasta, J.-P.; Buffeteau, T. *J. Am. Chem. Soc.* **2006**, *128*, 5533.
- (157) Benounis, M.; Jaffrezic-Renault, N.; Dutasta, J.-P.; Cherif, K.; Abdelghani, A. *Sens. Actuators, B* **2005**, *107*, 32.
- (158) Souteyrand, E.; Nicolas, D.; Martin, J.-R.; Chauvet, J.-P.; Perez, H. *Sens. Actuators, B* **1996**, *33*, 182.
- (159) Schramm, U.; Roesky, C. E. O.; Winter, S.; Rechenbach, T.; Boeker, P.; Schulze Lammers, P.; Weber, E.; Bargon, J. *Sens. Actuators, B* **1999**, *57*, 233.
- (160) Winston, E.; Horansky, R.; Myers, M.; Price, J.; Vacek, J. 2006 APS March meeting, Abstract Q1.00019.
- (161) Gautier, A.; Mulatier, J.-C.; Crassous, J.; Dutasta, J.-P. *Org. Lett.* **2005**, *7*, 1207.
- (162) Mough, S. T.; Holman, K. T. *Chem. Commun.* **2008**, 1407.
- (163) (a) Huerta, E.; Cequier, E.; De Mendoza, J. *Chem. Commun.* **2007**, 5016. (b) Westcott, A.; Fischer, J.; Harding, L.; Rizkallah, P.; Hardie, M. J. *J. Am. Chem. Soc.* **2008**, *130*, 2950. (c) Xu, D.; Warmuth, R. *J. Am. Chem. Soc.* **2008**, *130*, 7520. (d) Harel, E.; Schroder, L.; Xu, S. *Annu. Rev. Anal. Chem.*, in press.
- (164) (a) Rudkevich, D. M. *Eur. J. Org. Chem.* **2007**, 3255. (b) Rudkevich, D. *Prog. Inorg. Chem.* **2007**, *55*, 205. (c) Benounis, M.; Aka-Ngnui, T.; Jaffrezic, N.; Dutasta, J.-P. *Sens. Actuators, A* **2008**, *141*, 76.
- (165) (a) Gomez, E. D.; Brotin, T.; Duddeck, H. *Tetrahedron: Asymmetry* **2007**, *18*, 2155. (b) Cavagnat, D.; Buffeteau, T.; Brotin, T. *J. Org. Chem.* **2008**, *73*, 66.
- (166) (a) Hill, P. A.; Wei, Q.; Eckenhoff, R. G.; Dmochowski, I. J. *J. Am. Chem. Soc.* **2007**, *129*, 9262. (b) Roy, V.; Brotin, T.; Dutasta, J.-P.; Charles, M. H.; Delair, T.; Mallet, F.; Huber, G.; Desvieux, H.; Boulard, Y.; Berthault, P. *ChemPhysChem* **2007**, *8*, 2082. (c) Fogarty, H.; Berthault, P.; Huber, G.; Desvieux, H.; Dutasta, J.-P. *J. Am. Chem. Soc.* **2007**, *129*, 10332. (d) Schröder, L.; Chavez, L.; Meldrum, T.; Smith, M.; Lowery, T. J.; Wemmer, D. E.; Pines, A. *Angew. Chem., Int. Ed.* **2008**, *47*, 4316. (e) Aaron, J. A.; Chambers, J. M.; Jude, K. M.; Di Costanzo, L.; Dmochowski, I. J.; Christianson, D. W. *J. Am. Chem. Soc.* **2008**, *130*, 6942.